PREFACE

This compilation of fifteen contributions to the Fourteenth International Cosmic Ray Conference to be held August 15-29, 1975 in Munich, West Germany, is the result of several collaborations among scientists at Applied Physics Laboratory and scientists at other institutions. The scientists and institutions involved are (in alphabetical order):

Air Force Cambridge Research Laboratories

M. A. Shea and D. F. Smart

American Science and Engineering, Inc.

A. S. Krieger and J. T. Nolte

Applied Physics Laboratory, The Johns Hopkins University

C. O. Bostrom, R. E. Gold, J. W. Kohl, S. M. Krimigis, E. C. Roelof and E. T. Sarris

Massachusetts Institute of Technology

A. J. Lazarus and J. D. Sullivan

National Oceanic and Atmospheric Administration

P. S. McIntosh and D. J. Williams

University of Calgary

D. Venkatesan

University of Iowa

W. M. Cronyn and S. D. Shawhan

University of Kansas

T. P. Armstrong and G. Chen

We all wish to express our appreciation to the following people at Applied Physics Laboratory whose exceptional efforts produced this document:

Joyce Hainley and Barbara Northrop, typing and editing

Jack Mothershead
Karen Runkles
Ruth Pordy
Daryl George
Douglas Gillette
Lee Roberts
Joan Williams

Illustrations

Gary Cardinal
Joyce VanElls
Deborah Wallace

Xeroxing

Cal Floyd
James Reel
David Sussman
William Hampton
Ronald Rooney
Frances Pettit

Photography Lab

William Wills
Wilbert Miles
Charles Merson
Dan Tatarewicz
Charles Jakeman
Howard Collier
Richard Clark
Sara Warden
Russell Wise

Printing

CONTRIBUTIONS TO THE 14TH INTERNATIONAL COSMIC RAY CONFERENCE

August 15-29, 1975 Munich, West Germany

THE QUIET-TIME LOW ENERGY SPECTRUM IN THE VICINITY OF EARTH — SP 2.2-7
S. M. Krimigis, J. W. Kohl and T. P. Armstrong

OBSERVATIONS OF QUIET-TIME INTERPLANETARY ELECTRON ENHANCEMENTS OF JOVIAN ORIGIN — SP 2.2-2
S. M. Krimigis, E. T. Sarris and T. P. Armstrong

SCATTER-FREE COLLIMATED CONVECTION AND COSMIC-RAY TRANSPORT AT 1 AU — SP 5.1-1
E. C. Roelof

MATHEMATICAL FORMULATION OF SCATTER-FREE PROPAGATION OF SOLAR COSMIC RAYS — SP 5.1-2
J. T. Nolte and E. C. Roelof

RELATION OF LARGE-SCALE CORONAL X-RAY STRUCTURE AND COSMIC RAYS: 1. SOURCES OF SOLAR WIND STREAMS AS DEFINED BY X-RAY EMISSION AND Hα ABSORBTION FEATURES — SP 4-4
A. S. Krieger, J. T. Nolte, P. S. McIntosh, J. D. Sullivan R. E. Gold and E. C. Roelof

RELATION OF LARGE-SCALE CORONAL X-RAY STRUCTURE AND COSMIC RAYS: 2. CORONAL CONTROL OF INTERPLANETARY INJECTION OF 300 keV PROTONS — SP 4-5
E. C. Roelof, R. E. Gold, S. M. Krimigis, A. S. Krieger, J. T. Nolte, P. S. McIntosh, A. J. Lazarus and J. D. Sullivan

RELATION OF LARGE-SCALE CORONAL X-RAY STRUCTURE AND COSMIC RAYS: 3. LOW-INTENSITY SOLAR PARTICLE EVENTS WITH ENHANCED $\sim$ 3 MeV HELIUM AND MEDIUM FLUXES ASSOCIATED WITH SOLAR WIND STREAMS — SP 4-6
R. E. Gold, S. M. Krimigis, E. C. Roelof, A. S. Krieger and J. T. Nolte

RELATION OF LARGE-SCALE CORONAL X-RAY STRUCTURE AND COSMIC RAYS: 4. AMPLITUDE OF THE DIURNAL VARIATION IN NEUTRON MONITORS ON INTERPLANETARY FIELD LINES ORBITING ABOVE CORONAL HOLES — MG 7-2
E. C. Roelof, R. E. Gold, A. S. Krieger, J. T. Nolte, and D. Venkatesan

RELATION OF LARGE-SCALE CORONAL X-RAY STRUCTURE AND COSMIC RAYS: 5. SOLAR WIND AND CORONAL INFLUENCE ON A FORBUSH DECREASE LASTING ONE SOLAR ROTATION — MG 5-10
R. E. Gold, E. C. Roelof, J. T. Nolte and A. S. Krieger

VARIATIONS IN THE CHARGE COMPOSITION OF THE JULY 2-12, 1974, SOLAR PARTICLE EVENT — SP 2.1-8
T. P. Armstrong and S. M. Krimigis

THE QUIET-TIME LOW ENERGY NUCLEON SPECTRUM IN THE VICINITY OF EARTH

S. M. Krimigis and J. W. Kohl
Applied Physics Laboratory, The Johns Hopkins University
Laurel, Md. 20810, USA

T. P. Armstrong
Department of Physics, University of Kansas
Lawrence, Kansas 66044, USA

The upturn in the low energy quiet-time interplanetary nucleon spectrum has previously been described as of galactic (Fan et al., 1966) or solar (Krimigis, 1970) origin. Recently Krimigis et al. (1974) have suggested that the magnetosphere may be an important source, at least at the lowest energies. Observations obtained with the JHU/APL experiment on Explorer 47 (IMP-7) during the March 9-12, 1973 period show that the magnetosphere is the dominant contributor to the quiet time interplanetary proton population in the range $0.29 \leq Ep \leq 0.5$ MeV, and suggest that it may be an important contributor up to energies of at least 2 MeV. The March 9-12 period is the quietest (on a time scale of hours) in a $\sim$ 2.5 year interval extending from September 72 through February 1975. The quiet-time energy spectrum may be represented by a power law $E^{-}(3.1 \pm 0.2)$, the H/He ratio at $\leqslant$ 2 MeV/nucleon is $\sim$ 10 and the He/Z $\geq$ 3 ratio at $\sim$ 1 MeV/nucleon is $\sim$ 8. The ratio of anti-sunward to sunward intensities is $\sim$ 2.6 and increases to $\sim$ 8.55 in a frame moving with the solar wind, i.e., the maximum intensity is coming from the direction at the bow shock. The observed intensities are factors of 3 to 10 lower than those reported by Simpson and Tuzzolino (1973), suggesting that the interpretation of the low energy gradient measurement reported by these authors needs to be revised. It is speculated that the low energy ($\leqslant$ 20 MeV) upturn in the quiet-time interplanetary proton spectrum may be related to particle emissions from planetary magnetospheres, such as that of Jupiter.

1. Introduction. It is generally agreed that the high energy ($\geqslant$ 20 MeV/nucleon) part of the interplanetary quiet-time nucleon spectrum is of galactic origin. The main reasons for this belief are (a) the well-established anticorrelation between cosmic ray intensity and solar activity and (b) a composition rich in elements which cannot be readily produced within the solar system. The shape of the energy spectrum, and the modulation due to solar activity are thought to be well understood in the context of the diffusion-convection-adiabatic energy loss model, although recent gradient results from Pioneers 10 and 11 have raised grave doubts as to the essential correctness of this model. Below $\sim$ 20 MeV, however, there is an upturn in the spectrum which has been variously described as of either galactic

(Fan et al., 1966) or solar origin (Krimigis, 1970). In addition, there is the complication of "abnormal" abundances in O,C,N and He in the range ~ 1 to ~ 20 MeV/nucleon (cf. Gloeckler, 1974).

Recently, data obtained with the Johns Hopkins University/Applied Physics Laboratory (JHU/APL) experiment on the near-circular orbiting (~ 32 by ~ 38 R_e) IMP-7 satellite suggest that the earth's magnetosphere is a significant contributor to the ambient interplanetary particle population at low energies (Krimigis et al., 1974). The present study extends the previous observations to the quietest period observed with the IMP-7 spacecraft from September 26, 1972 to February 15, 1975. It is shown that most of the observed proton intensity in the 0.3 to 0.5 MeV energy range originates from the earth's magnetosphere, and it is argued that a substantial fraction of the intensity below ~ 2 MeV must be of magnetospheric origin also. The implications of these results are discussed in the context of the possible contribution of particles accelerated in planetary magnetospheres to the low-energy interplanetary particle population.

2. Experimental. The detector used in this study has been described in detail elsewhere (Krimigis et al., 1973; Sarris et al., 1975a). Briefly, it consists of three (D1,D2,D3) solid state detectors inside an anticoincidence scintillator cup. Several differential proton, alpha particle, and $Z \geq 3$ channels are defined by onboard logic and operated in anticoincidence with the plastic scintillator. Since some of the low energy proton, alpha particle, and $Z \geq 3$ channels are one parameter (i.e., particles stopping in the D1 detector), it is necessary to make corrections to the derived intensities. Thus, the data analysis proceeds by evaluating the $Z \geq 3$ intensities and deriving an energy spectrum, which is then used to correct the He channels. Following the derivation of a He spectrum, the proton channels are appropriately corrected. In cases where these corrections could lead to substantial uncertainties, the range of possible values is included in the error bars shown. These considerations, for the most part, do not affect significantly the conclusions of this study.

3. Results. Hourly-averaged values of the IMP-7 data have been examined over the period September 26, 1972 through February 15, 1975, in order to identify those periods when the minimun counting rates were observed in the 0.3-0.5 MeV proton channel. Two such periods have been identified, January 15-17 and March 9-12, 1973. The data for the first period have already been reported (Krimigis et al., 1974) and will be referred to here. The present paper will present the data for the March 9-12 period. It is noted here that the spacecraft spends ~ 4 days of its 13-day period within the magnetotail so that, in principle, a minimum intensity period could have occurred in the interplanetary medium and have remained undetected by IMP-7. We do not consider such an occurrence very likely since (a) a low-intensity period in the interplanetary medium implies similar conditions within the magnetotail and (b) the magnetospheric burst phenomenon is global, i.e., activity within the magnetotail implies similar activity within the interplanetary medium (Sarris et al., 1975a, b). In spite of the above, we cannot exclude positively the possibility of somewhat lower intensities within the interplanetary medium than inside the magnetotail during quiescent conditions.

Figure 1 shows hourly-averaged rates of the three lowest energy proton channels and one electron channel over the period of interest. It is seen from

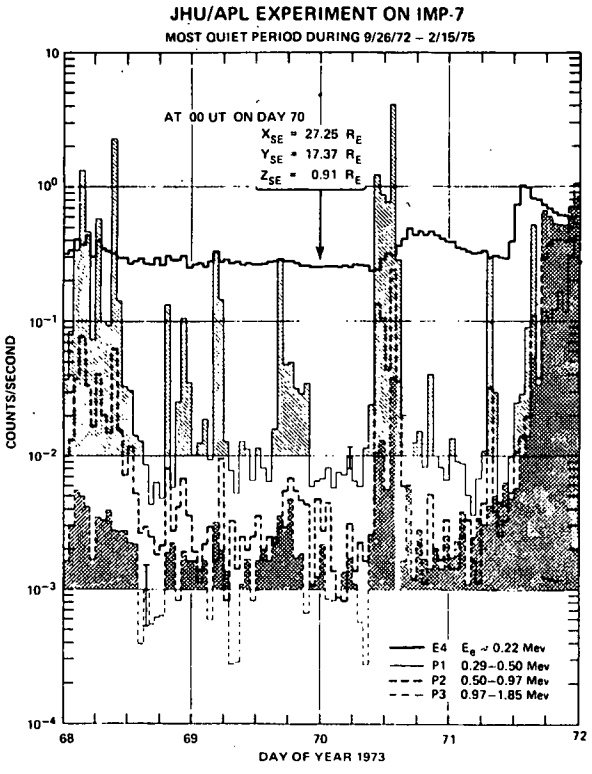

Figure 1. Hourly averages of the indicated proton channels and an integral electron channel. Note the shaded "microbursts" and the 32 "quiet-time"rates at P1 < 10^{-2} c/s. Sample error bars are shown.

$$\xi = \frac{j^+ - j^-}{j_+ + j_-}$$

where j^+, j^- represent the sunward and anti-sunward intensity, respectively, is 44% with the maximum intensity coming from ~ 220° to the earth-sun line.

It should be noted here that the anisotropy is distorted by the convective action of the solar wind which tends to generally increase the flux in the sunward direction and decrease it in the antisolar direction. A procedure for removing such a distortion from sectored data has been developed recently (Ipavich, 1974; Roelof et al., 1975) and has been applied to the present data, using the observed solar wind speed of ~ 550 km/s and a spectral exponent of 3.1 in a differential power law spectrum. The results are shown by the dashed line in the same scale. It is the figure that finite "microburst" activity is present throughout most of this period, extending to proton energies > 1 MeV, with no obvious counterpart in the 0.2 MeV electron channel. Further, for some 32 hours, out of the 3.5 day quiet-time period, the P1 count-rate is < 10^{-2} c/s, corresponding to the minimum observed intensities. It is reasonable to expect that the rates during these 32 hours represent the residual interplanetary proton population in the vicinity of earth, since there is no clearly identificable temporal character associated with these rates. We now examine in detail the angular distributions and energy spectra of protons observed during these 32 hours.

Figure 2 shows the relevant section of the IMP-7 orbit in relation to the nominal positions of the bow shock and magnetopause, during the period of observation. The P1 rates with values < 10^{-2} c/s were interspersed (among the bursts) over the shaded portion of the orbit. The counts occurring in each of eight sectors for the 32 hourly intervals have been summed and are shown on the lower left-hand corner in a polar plot. It is evident from the plot that most of the counts occur in the two sectors pointing in the general direction of the bow shock. The amplitude of the observed anisotropy given by

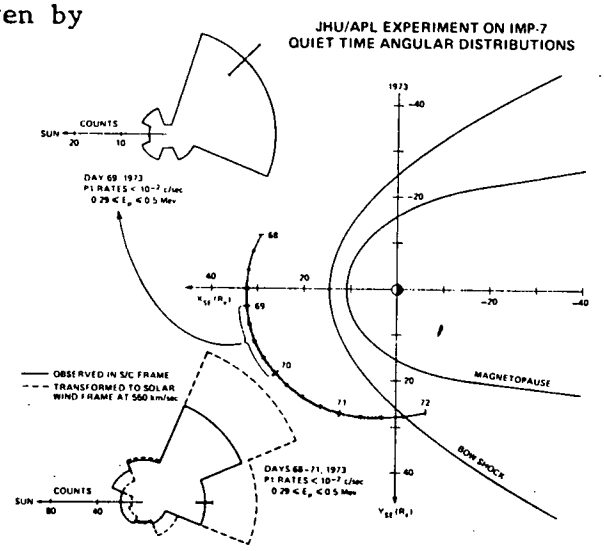

Figure 2. The angular distribution of the minimum observed intensities over the shaded portion of the IMP-7 orbit, in relation to the bow shock. Note the distortion of the distribution due to convective effect of the solar wind.

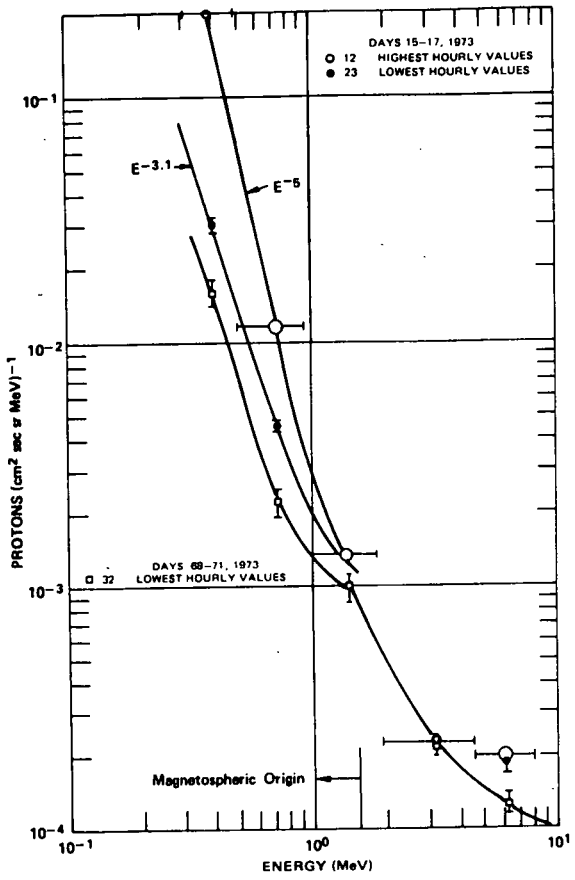

Figure 3. The proton energy spectrum for the March quiet period, compared to the January quiet period and microbursts. Note "break" point at < 2 MeV.

Figure 3 presents the proton energy spectrum during this period, as well as spectra of "microbursts" and minimum intensities observed during the January 15-17, 1973 period. It is evident that the burst spectra are very steep and generally similar to spectra of much more intense bursts (Sarris et al., 1975a). The low intensity spectra for both periods have a slope of -3.1, and all spectra appear to be converging to a common point between 1.5 and 3 MeV. Although anisotropy measurements at the higher energies are not available, it is apparent from the angular distributions at low energies (0.29-0.5 MeV), and the behavior of the spectrum that a substantial portion of the intensity below ~ 2 MeV is due to protons originating in the magnetosphere.

The spectral data presented in Figure 3 are compared with previous observations in Figure 4. It is evident that the intensity in the solar direction has decreased, while that from the general direction of the bow shock has increased markedly. The anisotropy amplitude has now increased to ~ 80%, with the solar sector intensity representing only ~ 3% of the total.

The sectored data on each day are qualitatively similar to the four-day summed data, so that the spacecraft distance from the bow shock does not appear to be a factor in influencing the anisotropy direction. As an example, the data from day 69 are shown in the upper left-hand corner, when the spacecraft was at its farthest point from the bow shock. It is again evident that the maximum intensity is coming from the direction of the magnetosphere with an amplitude of the sunward-antisunward anisotropy of 70%.

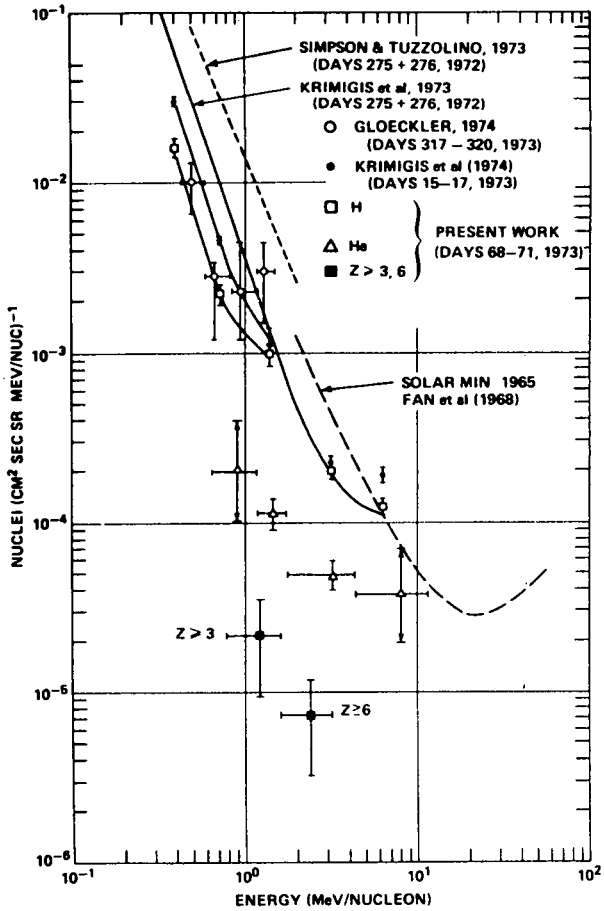

Figure 4. Comparison of present proton observations of previous ones. The 1965 solar minimum spectrum has been sketched in. The He and Z ≥ 3 spectra for this period are also shown.

that the March 73 data represent the lowest intensities at E $\leqslant$ 2 MeV which have been reported so far, either in the vicinity of earth or elsewhere in the solar system. It is important to note that the intensities are a factor 3 to 10 less than those of Simpson and Tuzzolino (1973), measured on the same spacecraft. We will comment on this discrepancy and its implications in the next section.

In addition to the proton spectra Figure 4 shows spectra of He and Z $\geq$ 3 nuclei obtained during the same March period. We shall not comment on this data, except to note that they are consistent with those of other investigators in this energy range. The H/He intensity ratio is $\sim$ 10 at E $\leqslant$ 2 MeV/nucleon and decreases to $\sim$ 4 at 3 MeV/nucleon. The He/C,N,O ratio is $\sim$ 9 at $\sim$ 2.4 MeV/nucleon, while the He/Z $\geqslant$3 ratio is $\sim$ 8 at $\sim$ 1 MeV/nucleon. These ratios are generally consistent with those of Gloeckler (1974).

4. Discussion. The data presented here and those of Krimigis et al. (1974) have introduced a new element into the discussion of the origin of the low energy component in the quiet-time interplanetary particle population. That is, the earth's magnetosphere must be considered as a possible source, in addition to the sun and the galaxy. The angular distributions have established conclusively that in the 0.3-0.5 MeV range, most of the proton intensity (i.e., at least 76%, if the 3% in the solar sector is thought to represent an isotropic component) has its origin in the earth's magnetosphere. The spectral behavior (Figure 3) and the fact that all three proton channels show enhanced counting rates during microbursts suggest that even at higher energies (i.e., < 2 MeV), the magnetosphere is a significant source, although the percentage of magnetospheric contribution may decrease as the energy increases. Even in the 2 to 20 MeV range, there is no a priori reason why the magnetosphere should not be a contributor, although the sensitivity of present-day instruments is clearly not sufficient to determine this.

It is evident from the Pioneer 10 and 11 data that the Jovian magnetosphere is probably the main source of high energy electrons ($\sim$ 0.2 to $\sim$ 40 MeV) observed in the interplanetary medium. There is the possibility that protons are also emitted from Jupiter and can be observed as much as 2 AU away (Van Allen et al., 1974). A rough calculation indicates that the Jovian magnetosphere is probably a sufficiently strong source to supply the proton fluxes observed at earth in the $\sim$ 2-20 MeV range. Any such calculation depends on a number of assumptions and the results are very much model-dependent. However, preliminary numbers are sufficiently encouraging to warrant a more detailed investigation of this source.

Comparison of the present data to those published previously provides additional insight into the problem of solar modulation and the low energy gradient: (a) The present data are probably not the modulated solar minimum spectrum of Fan et al. (1968), since those spectra were obtained by use of long-term averages in the general vicinity of earth. (b) The proton intensities in March of 73 are lower by a factor of $\sim$ 7 than those measured in the vicinity of earth by Explorer 33 in August 1967 (Krimigis, 1970). Thus, the low energy gradient and anisotropy measured during August of 67 was indeed representative of a finite solar component (Krimigis, 1970; Gleeson et al., 1971). (c) The present measurements and those for days 15-17, 1973, are lower than those of Krimigis et al. (1973) obtained with the same instrument while the spacecraft was located within the magnetotail. It is evident now that the October 72 intensities were higher and that the observed fluxes were of magnetospheric origin, since streaming away

from the earth was observed. (d) In view of the magnetospheric origin of the low energy component, the concept of measuring the radial gradient during quiet times by using earth-orbiting spacecraft as a baseline is clearly incorrect. Thus, the result reported by Simpson and Tuzzolino (1973) [(8 ± 6)% per AU for 0.5 ≤ Ep ≤ 1.8 MeV protons] cannot be viewed as a valid measure of the radial gradient, and must be reinterpreted. The present data and those of other workers (Gloeckler, 1974) point out that the Simpson and Tuzzolino (1973) earth-based intensities are quite high (by factors of 3 to 10). Thus, apart from any considerations regarding the source of the observed protons, the basic correctness of the Simpson and Tuzzolino data must be carefully reexamined.

Acknowledgements. We are indebted to R. E. Cashion, S. A. Gary and J. H. Crawford of JHU/APL for their diligent efforts in making the IMP-7 experiment a success. The efforts of the GSFC project personnel, especially those of Mr. M. A. Davis and Dr. N. Ness are acknowledged with thanks. We thank Drs. E. C. Roelof and R. E. Gold at JHU/APL for several useful discussions. Mr. J. L. Gunther of JHU/APL was instrumental in the success of the data analysis effort. This research has been supported by NASA under Task I of contract N00017-72-C-4401, between The Johns Hopkins University and the Department of the Navy.

References

Fan, C. Y., G. Gloeckler and J. A. Simpson, Proc. Inter. Conf. Cosmic Rays, London, 1, 109, 1966.

Fan, C. Y., G. Gloeckler, R. B. McKibben and J. A. Simpson, Can J. Phys., S46, 5498, 1968.

Gleeson, L. J., S. M. Krimigis and W. I. Axford, J. Geophys. Res., 76, 2228, 1971.

Gloeckler, G., Univ. of Maryland Tech. Report #74-097, 1974.

Ipavich, F. M., Geophys. Res. Lett., 1, 149, 1974.

Krimigis, S. M., Acta Physica Hungaricae, 29, Suppl. 2, 125, 1970.

Krimigis, S. M., T. P. Armstrong and J. W. Kohl, Proc. 13th Inter. Cosmic Ray Conf., 2, 1656, 1973.

Krimigis, S. M., J. W. Kohl and T. P. Armstrong, EOS, 56, 1165, 1974. (Abstract)

Roelof, E. C., E. P. Keath, C. O. Bostrom and D. J. Williams, JHU/APL Preprint (submitted to J. Geophys. Res.), 1975.

Sarris, E. T., S. M. Krimigis and T. P. Armstrong, JHU/APL Preprint (submitted to J. Geophys. Res.), 1975a.

Sarris, E. T., S. M. Krimigis and T. P. Armstrong, EOS, 56, 433, 1975b. (Abstract)

Simpson, J. A. and A. J. Tuzzolino, Ap. J., 185, L149, 1973.

Van Allen, J. A., D. N. Baker, B. A. Randall and D. D. Sentman, J. Geophys. Res., 79, 3559, 1974.

OBSERVATIONS OF QUIET-TIME INTERPLANETARY ELECTRON ENHANCEMENTS OF JOVIAN ORIGIN

S. M. Krimigis and E. T. Sarris
Applied Physics Laboratory/The Johns Hopkins University
Laurel, Md. 20810, USA

Thomas P. Armstrong
Department of Physics, University of Kansas
Lawrence, Kansas 66044, USA

A number of quiet-time enhancements in the intensity of interplanetary electrons over the range $0.22 \leqslant E \leqslant 2.5$ MeV have been observed with the JHU/APL experiment on the earth orbiting near-circular ($\sim$ 32 by 38 R_e) Explorer 47 (IMP-7) spacecraft during 1973 and 1974. These quiet-time increases last from $\sim$ 3 to $\sim$ 20 days and are observed both in the interplanetary medium and inside the magneto-tail. The main features of the observations are as follows: (a) The increases occur during the first 200 days of 1973 and from day $\sim$ 20 to $\sim$ 230 in 1974. (b) The intensity onset is relatively slow (1 to 2 days) when compared to either solar electron events or magneto-spheric electron bursts. (c) The electron energy spectrum is quite distinct from that of solar or magneto-spheric electrons and is consistent with $\gamma = 1.3 \pm 0.3$ in a differential power law spectrum. (d) Some distinct fluctuations appear in some of the intensity profiles, suggesting the presence of a periodicity. The appearance of these enhancements occurs during times when the earth could be magnetically connected to the magneto-sphere of Jupiter,assuming typical solar wind velocities. Further, the energy spectrum is not unlike that observed by Teegarden et al. (1974) on Pioneer 10 in the vicinity of Jupiter. On the basis of the above it is reasonable to suggest that the observed electrons may be of Jovian origin. The implications of these results are discussed.

1. Introduction. The low energy end (0.2 to $\sim$ 40 MeV) of the interplanetary electron population has always appeared as an add-on feature to the overall interplanetary electron spectrum (Meyer, 1969), much as the low energy ($E \leqslant 20$ MeV/nuc) nucleon component is a well-established anomaly in the overall nucleon spectrum. The prevailing explanation for the electron component has been that these electrons are secondaries (knock-ons) produced in interstellar space by higher energy nucleons. The difficulty with this hypothesis was thought to be the requirement that solar modulation be less than about a factor 5, i.e., not in accord with the diffusion-convection-adiabatic energy loss model.

Recently, following the Pioneers 10 and 11 encounters of Jupiter, it became clear that the Jovian magnetosphere is a sufficiently strong source to supply the entire low energy interplanetary electron component (e.g., Teegarden et al., 1974). In addition, it was recognized that the quiet-time interplanetary electron enhancements (3 to 21 MeV) observed over the past several years (cf., McDonald et al., 1972) may well be due to electrons of Jovian origin.

Following the Pioneer encounters of Jupiter, we began examining the electron data from the JHU/APL experiment on the IMP-7 (Explorer 47) spacecraft for evidence of quiet-time electron increases down to energies of $\sim$ 0.2 MeV. The purpose of this paper is to report the identification of a number of these increases over the 1972-1974 time interval, with good statistical accuracy and better temporal resolution than was previously possible. We find that the enhancements occur at times when connection of the interplanetary magnetic field to the Jovian magnetosphere is reasonably favorable and that the spectrum is not unlike that observed by the Pioneer spacecraft in the general vicinity of Jupiter.

2. Experimental. The JHU/APL experiment on IMP-7 has been described in detail elsewhere (Krimigis et al., 1973; Sarris et al., 1975). The channels of interest in the present study are E4, E5 and E6, which respond to electrons of $E \geqslant 0.22$, 0.5, 0.8 MeV, respectively, with an upper cutoff for all channels of $\sim$ 2.5 MeV. The efficiencies over the quoted energy ranges are not constant, so that the derivation of an energy spectrum from the counting rates is not straightforward. All channels have a 100% spin-averaged duty cycle and a time resolution of 10.24 seconds. In addition, channel E4 is sectored with a duty cycle of 38.21%. Only spin-averaged data are presented in the present report.

3. Results. Figure 1 shows a 15-day period in early 1974 containing a quiet-time electron enhancement. This period was selected in order to point out the differences in the morphology of electron increases from various sources, i.e., the sun, the earth's magnetosphere, and the interplanetary medium. The top curve shows the quantity E4-E5 in counts per second, which corresponds to the intensity in the energy range $0.22 \leqslant Ee \leqslant 0.5$ MeV. The second curve shows the quantity E5-E6, which is proportional to the intensity of $0.5 \leqslant Ee \leqslant 0.8$ MeV electrons. The lower frame shows the ratio of the two quantities, and the value represents a spectral index; large values indicate a soft spectrum while small values correspond to hard spectra.

The first observed peak on day 14 represents a typical magnetotail electron burst (Sarris et al., 1975) with a relatively soft spectrum and limited duration. The spacecraft was inside the magnetotail at this time at $\sim$ 34 R_e and moving towards the dawn magnetopause. The next three increases on days 15, 16, and 17 are solar electron events with a standard intensity profile and fairly soft energy spectrum. While the solar events are in progress, a number of superimposed magnetospheric bursts are clearly evident. By the beginning of day 16, the spacecraft was outside the magnetosphere and moving towards the subsolar point. During day 21 the beginning of an electron enhancement with a totally different intensity profile is evident. Maximum intensity is reached on day 23 with an indication of a decay early on day 25, while the spacecraft is inside the magnetotail. A long-lasting series of magnetospheric electron bursts obscures observations of the farther development of the enhancement, although data after day 30 (not shown here) suggest that the event continued through at least day 32. We note that the spectral ratio has attained its lowest values on days 21 to 26 and the highest values during the magnetospheric bursts.

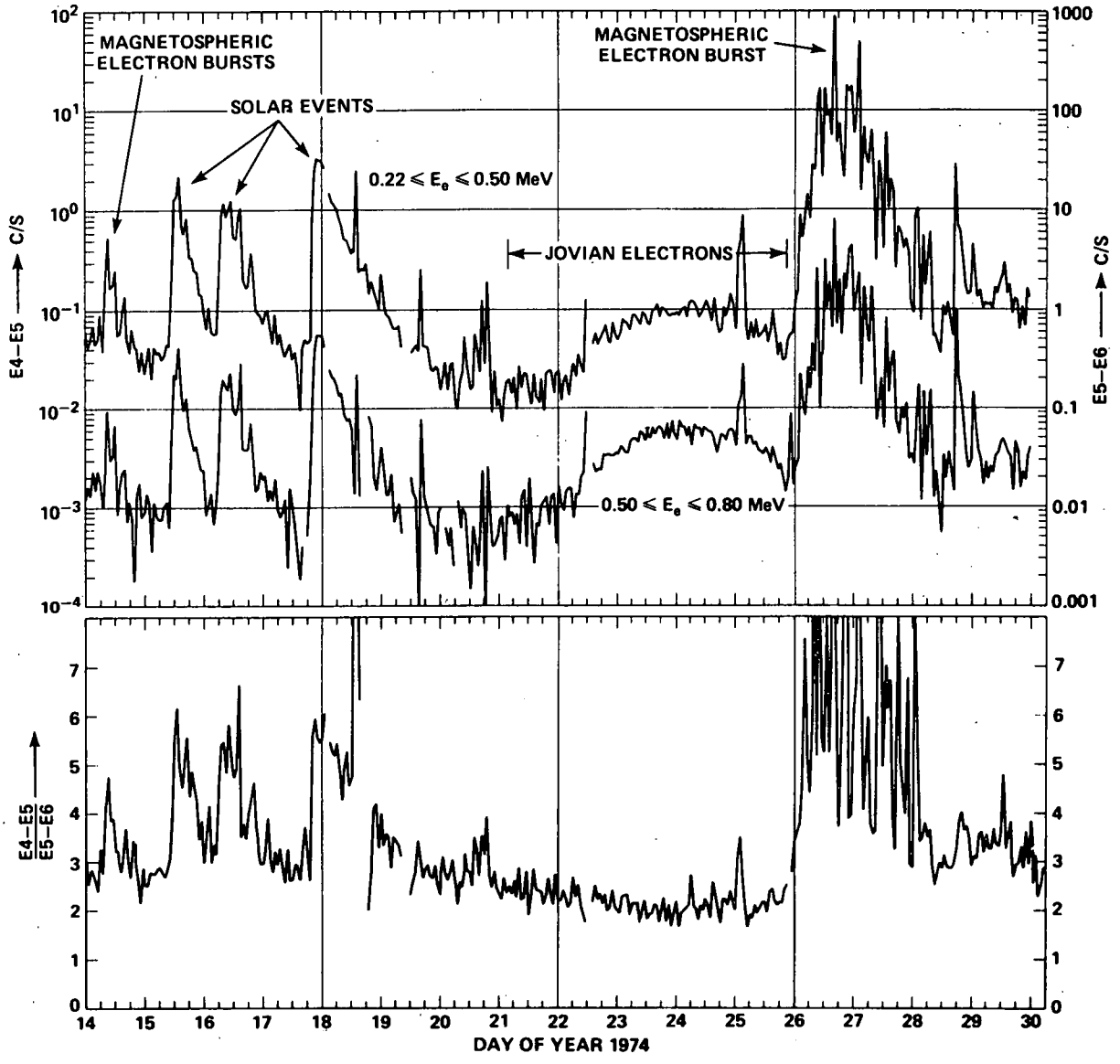

Figure 1. The full range of electron events which have been identified so far in the interplanetary medium, observed during a single time interval in the last half of January 1974. It is seen that the intensity and spectral profiles are distinctly different for magnetospheric, solar, and quiet-time increases. The statistical uncertainty is ~ 5% at rates of 10^{-1}c/s and 17% at rates of 10^{-2}c/s. The geometric factor is ~ 1.5 cm^2sr.

It is evident from the preceding that the quiet-time enhancements are clearly and easily distinguishable from electron increases of either magnetospheric or solar origin. The duration of the enhancement was at least four

days. The value of the spectral ratio at ~ 2 is consistent with $\gamma \simeq 1.3 \pm 0.3$ in a differential power law in energy spectrum, although a more thorough determination of the spectral index is presently in progress and will be reported. It is of interest to note that a regular oscillation in the data is evident (statistical uncertainty is only ~ 6%), at least for the latter part of day 22, and days 23 and 24. This oscillation is sometimes consistent with a five-hour period.

A second example of a quiet-time electron enhancement is shown in Figure 2. The onset of this enhancement occurred while the spacecraft was exiting the dusk bow shock and moving towards the subsolar point; the event was apparently over on day 159, just before the spacecraft reentered the magnetosheath, i.e., it lasted for a total of ~ 7 days. Again, a large number of magnetospheric bursts is superimposed on the quiet-time enhancement; the intensity of the bursts decreases at high energies, which explains the relative ease of observing enhancements at higher (3 to 21 MeV) energies (McDonald et al., 1972). Note that electron bursts of magnetocpheric origin are as frequent in the interplanetary medium as they are in the magnetotail. As was the case with the enhancement on days 21-25, the spectral ratio attains its minimum value during this quiet-time increase, although at a somewhat lower overall value.

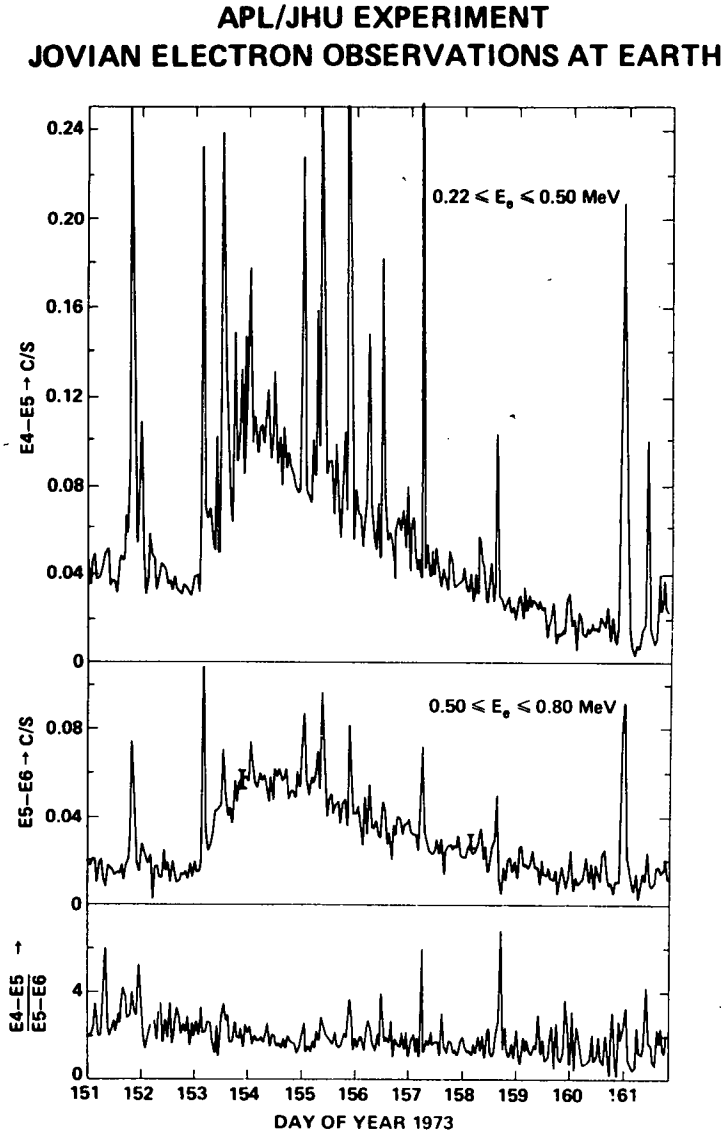

Figure 2. A quiet-time electron enhancement in mid 74 observed while the spacecraft was outside the magnetosphere for the entire duration of the event. A large number of magnetospheric electron bursts are superimposed on the quiet-time increase.

Figure 3 gives a summary of the observations of quiet-time electron enhancements over a ~ 2 year period (September 26, 1972 to December 5, 1974). The periods during which enhancements were observed are marked in at the lower part of the figure. The cross-hatched area shows the value of the solar wind velocity which is necessary to connect the earth to Jupiter at a particular time. For example, on January 3, 1973 a 600 km/s solar wind velocity is required to connect the earth to Jupiter via an interplanetary magnetic field line, while

on day 200 of the same year a 300 km/s velocity is necessary.

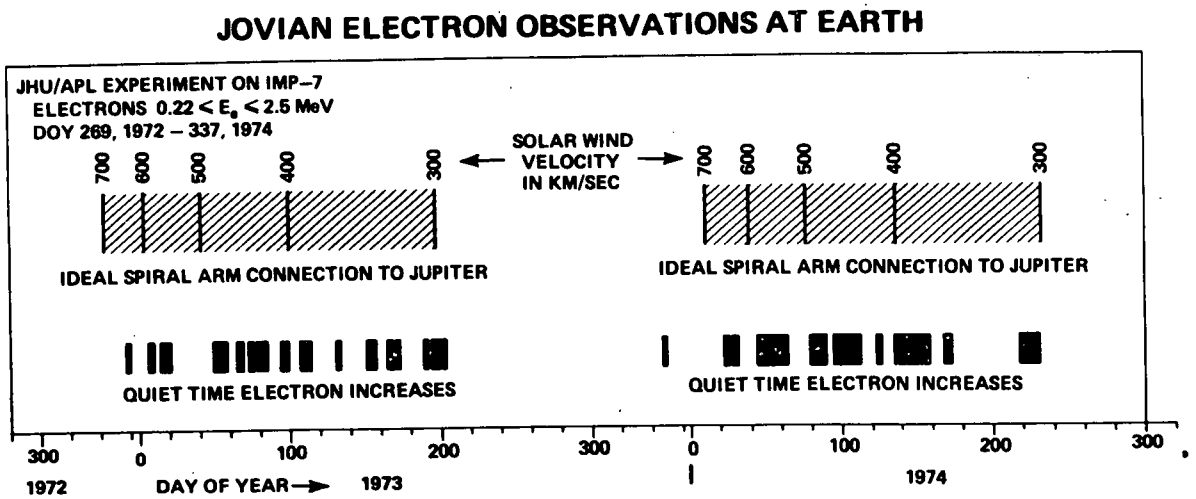

Figure 3. A summary of observations of quiet-time electron enhancements at earth. The shaded region indicates the solar wind velocity which is necessary to connect the earth to Jupiter at a given time. Note the absence of increases in the latter part of 73 and 74.

It is evident from the figure that for the first 200 days of 1973, quiet-time enhancements were observed for some 40% of the time, while virtually no enhancements were seen for the remainder of the year. A similar statement can be made for 1974. Thus, we may conclude that quiet-time increases seem to take place during that part of the year when the earth can be magnetically connected to Jupiter, if one asumes realistic values ($\sim$ 300 to $\sim$ 700 km/s) for the solar wind velocity. An inspection of observed solar wind velocities during the first part of 1973 reveals that a great deal of variability exists, with fast and slow streams being present throughout the whole period. Because of the evolution of some of the streams, however, there is a great deal of uncertainty in establishing one-to-one correspondence between solar wind connection and the presence of quiet-time electrons at earth. We shall return to this point in the discussion.

Finally, we note from Figure 3 that the duration of some of the quiet time increases is as short as three and as long as 20 days. The latter is truly remarkable, since we know that typical solar wind streams rarely last for more than 10 days, and even then they undergo considerable evolution. Thus, if quiet-time electron enhancements are somehow related to Jupiter, a mechanism must be found to explain the duration of these events by other than simple magnetic connection via the solar wind.

4. Discussion. It is clear from the data presented in Section 3 that the quiet-time electron enhancements represent a distinct class of events which are clearly different than solar electron events or magnetospheric bursts. The differences are (a) the intensity-time profile (b) the energy spectrum and (c) possible intensity fluctuations suggesting a periodicity.

It is possible to suppose that the enhancements are a different class of solar electron events consisting of continuously accelerated (or stored) electrons

which are somehow uniformly distributed over the whole solar corona. The most definitive objection to this hypothesis is the absence of such increases during the latter part of 1973 and 1974. There is no a priori reason that we can think of for expecting such a seasonal effect. The same seasonal effect may be used to reject the earth's magnetosphere as a possible source.

The arguments in favor of a Jovian origin are substantial: (a) The seasonal effect (b) Similarity of spectra observed at earth to those seen at Jupiter (c) Intensity fluctuations suggesting the periodic nature of the source. Although all of these arguments need to be examined further, it is difficult to avoid the connection with Jupiter, particularly after the Pioneer 10 encounter (Teegarden et al., 1974; Chenette et al., 1974).

As mentioned in Section 3, solar wind data in early 73 show that it is possible to magnetically connect the earth to Jupiter over the entire time of observed quiet-time enhancements. It is difficult, however, to know what the proper choice of solar wind velocity is: for, in the case of an evolving high speed stream, it will take several days before the "message" arrives at Jupiter; for a well-established stream, on the other hand, the connection is already at Jupiter and electrons should be seen as soon as the earth moves into the proper position. The more puzzling feature, as far as solar wind connection is concerned, is the duration of the enhancements (3 to 20 days). If one assumes that the Jovian magnetosphere is $\sim$ 200 R_J across, the solar wind should only connect the earth to Jupiter for only $\sim$ 10 hours. One possibility is that reconnection takes place between Jovian and interplanetary magnetic field lines, and that it continues for the entire length of the Jovian magnetotail. Thus, an event lasting for 20 days suggests a tail length of $\sim$ 4.6 AU, if a solar wind velocity of 400 km/s is assumed. We hope to pursue these ideas in a more detailed manner in a future publication.

Acknowledgements. We are indebted to R. E. Cashion, S. A. Gary, J. H. Crawford and J. W. Kohl of JHU/APL for their diligent efforts in making the IMP-7 experiment a success. The efforts of the GSFC project personnel, especially those of Mr. M. A. Davis and Dr. N. F. Ness are acknowledged with thanks. We thank Dr. A. Lazarus of MIT for making some plasma data available prior to publication. Mr.J.L. Gunther of JHU/APL was instrumental in the success of the data analysis effort. This research has been supported by NASA under Task I of contract N00017-72-C-4401, between The Johns Hopkins University and the Department of the Navy.

References:

Mayer, P., Rapporteur Papers, 12th Int. Conf. Cosmic Rays, Hobart, 235, 1971.

Teegarden, B. J., F. B. McDonald, J. H. Trainor, W. R. Webber and E. C. Roelof, J. Geophys. Res., 79, 3615, 1974.

McDonald, F. B., T. L. Cline and G. M. Simnett, J. Geophys. Res., 77, 2213, 1972.

Krimigis, S. M., T. P. Armstrong and J. W. Kohl, Proc. 13th Inter. Cosmic Ray Conf., 2, 1656, 1973.

Sarris, E. T., S. M. Krimigis and T. P. Armstrong, JHU/APL Preprint (submitted to J. Geophys. Res.), 1975a.

Chenette, D. L., T. F. Conlon and J. A. Simpson, J. Geophys. Res., 79, 3551, 1974.

SCATTER-FREE COLLIMATED CONVECTION AND COSMIC-RAY TRANSPORT AT 1 AU

Edmond C. Roelof
Applied Physics Laboratory/The Johns Hopkins University
Laurel, Md. 20810, USA

Observations of solar cosmic rays between 0.1 MeV and 1 GeV are more consistent with "scatter-free" than "diffusive" propagation near 1 AU. Since these particles also are constrained to interplanetary magnetic field lines, the parallel and transverse flow are de-coupled by "collimated convection". Local propagation is therefore more appropriately described by Liouville's equation and transport properties can be examined from the exact zeroeth and first moments of the equation averaged over all directions in momentum space. Observational results which may be explained directly without invoking local scattering include the decay of solar flare events as well as the radial gradient, diurnal and semi-diurnal variation of galactic cosmic rays.

Introduction. The early Explorer 12 observations of low-energy solar cosmic-ray anisotropies (Bryant et al, 1962) revealed that flux anisotropies were large during the rising phase of the event. Later Pioneer 6 measurements (Fan et al., 1966; McCracken and Ness, 1966; McCracken et al., 1968) showed that particles were "collimated" in their transport along interplanetary field lines, i.e., their propagation transverse to the field line was so restricted as to be negligible. This constraint could be established independently by the preservation of structures in the intensity histories measured by well-separated spacecraft (Lin et al., 1968; Krimigis et al., 1971). However, over distances $\gtrsim 0.1$ AU, the structures were not simply identifiable by "co-rotation" due to the dynamics and azimuthal variation of the solar wind speed which deformed the interplanetary field lines as they were "convected" (frozen-in) with the plasma. Therefore, Roelof and Krimigis (1973) suggested that large-scale transport of energetic particles should be described as "collimated convection", in which the net transverse motion was that of the field line itself, and the parallel motion was determined by conditions along the field line. This mode of propagation has recently been verified by Kirsch and Munch (1974) and Domingo et al. (1975).

As to what these conditions were, Roelof and Krimigis (1973) also found (as had earlier investigators) that the low-energy flux anisotropies were so strong and persistent as to imply that transport near 1 AU was closer to "scatter-free" than to the then-current "diffusion" description. Extensive examples were given by Innanen and Van Allen (1973). Lin's (1970) documentation of scatter-free propagation of > 40 keV electrons was not unexpected (due to the small gyro-radii of these particles), nor were the persistent anisotropies of ground level relativistic solar cosmic-ray events analyzed by Pomerantz and his co-workers (Duggal et al., 1971; Duggal and Pomerantz, 1972, 1973; Maurer et al., 1973), since it was known that events of the last Solar Cycle exhibited anisotropies sometimes well past the maximum of the event (Meyer et al., 1956; Carmichael, 1962; McCracken, 1962).

Therefore, if one chose to look at it, the evidence was there for propagation that was more "scatter-free" than "diffusive" at 1 AU over a range of four orders of magnitude in rigidity. It seems reasonable to ask how many aspects of cosmic-ray propagation can be explained in the approximation of no scattering near 1 AU. Then the appropriate transport equation is Liouville's equation for the phase space density $W(\underline{x}, \underline{p}, t)$.

$$\frac{\partial W}{\partial t} + \underline{v} \cdot \frac{\partial W}{\partial \underline{x}} + q \left(E + \frac{1}{c} \underline{v} \times \underline{B}\right) \cdot \frac{\partial W}{\partial \underline{p}} = Q' \tag{1}$$

Here Q' is a "source" term (Gleeson, 1969) which is left in for generality; it could also be a scattering operator as in the Boltzmann equation or quasi-linearized theory. Liouville's equation should be written in terms of the canonical momentum, but it is a property of the Lorentz force that the equation holds also for the mechanical momentum $\underline{p}$. It is understood here that in order to be consistent with negligible scattering, the $\underline{E}$ and $\underline{B}$ fields should be considered to be relatively "smooth" near 1 AU.

Equation (1) may of course be integrated by the method of characteristics to yield Liouville's theorem, i.e., W is a constant along a dynamical trajectory (since the characteristics are indeed the dynamical trajectory). The integral form is used in the companion paper (Nolte and Roelof, 1975), to model strongly anisotropic solar particle events, but in order to facilitate comparison with the weak-anisotropy theories now in use, let us take the zeroeth and first momentum moments of (1) with respect to direction in momentum space. This has been carried out by Gleeson (1969) using an approximate Green's theorem calculation which assumes W is nearly isotropic. The approximation is unnecessary and actually leads to the omission of several interesting terms. The moments can be calculated by expressing the operator $\partial/\partial \underline{p}$ in polar spherical coordinates, and manipulating terms by vector and dyadic analysis and integrating the differentiated terms by parts. Details of the calculation will be presented in an expanded paper. The results, in conventional notation, are

$$\dot{U} + \nabla \cdot \underline{S} + q \underline{E} \cdot \frac{\partial}{\partial T} \underline{S} = < Q > \tag{2}$$

$$m \dot{\underline{S}} + \frac{pv}{3} \nabla U + \nabla \cdot \underline{\underline{\Pi}} - q \underline{E} \left(U - \frac{1}{3} \frac{\partial}{\partial T} \alpha TU\right) + q \underline{E} \cdot \frac{\partial}{\partial T} \underline{\underline{\Pi}} - \frac{q}{c} \underline{S} \times \underline{B} = < Q\underline{p} > \tag{3}$$

Where $< Q > = (p^2/v) < Q' >$ is the source, averaged over all directions in momentum space, U and $\underline{S}$ are the differential (in kinetic energy T) particle density and current, and the traceless differential stress tensor $\underline{\underline{\Pi}}$ is defined in terms of the dyad $\underline{pv}$ and the identity tensor $\underline{\underline{1}}$

$$\frac{p^2}{v} < \underline{p} \underline{v} W > = \frac{pv}{3} U \underline{\underline{1}} + \underline{\underline{\Pi}} \tag{4}$$

The factor p^2/v comes from the relation between $< W >$ (differential in momentum) and U (differential in energy over a shell in momentum space).

$$UdT = < W > p^2 dp \tag{5}$$

The divergence of the stress tensor appears in Gleeson (1969), but not the terms involving $\underline{E} \cdot (\partial/\partial T)\, \underline{S}$ in (2) or $\underline{E} \cdot (\partial/\partial T)\, \underline{\underline{\Pi}}$ in (3). Although terms involving $\underline{\underline{\Pi}}$ could be omitted in weak anisotropy analyses, the new term in (2) should have appeared even in the weak-anisotropy approximation because of its obvious physical significance. It represents the average effect of particles being carried from one constant-energy surface in momentum space to another due to work being done at a rate $q\, \underline{E} \cdot \underline{v}$. It obviously vanishes when (2) is integrated over all energies, as it must since there is no net loss or gain of particles in momentum space due to energy changes in the electric field. That the absence of the term has not been apparent is probably because in most calculations to date $\underline{E} \cdot \underline{S} = 0$.

It is at this point that the present treatment diverges from other analyses. Previous studies have proceeded to esimate $< Q >$ and $< Q\underline{p} >$, using some form of the assumption that a scattering process produces the total current in a local frame co-moving with the plasma. The contention here is that observations near 1 AU are more consistent with no significant scattering, so we set $< Q > = < Q\underline{p} > = 0$. This then deletes terms related to adiabatic deceleration (but with no explicit dependence on the scattering parameters). For example, Gleeson and Axford (1968) invoke a Boltzmann collision integral to evaluate $< Q > = -(1/3\, \underline{V} \cdot \nabla (\partial/\partial T) \propto TU$ and identify it with energy changes due to "collisions" with moving magnetic irregularities (with their accompanying electric fields). In a scatter-free region, however, there are no collisions, and energy changes are completely accounted for by the $\underline{E} \cdot \underline{S}$ term in (2).

Now let us see how five diverse observational results are directly explained by collimated convection and scatter-free propagation, so $< Q >$ and $< Q\underline{p} >$ are dropped from (2) and (3). For simplicity, we shall assume that, in a spherical polar coordinate system (r, θ, φ), $\underline{B}$ has no θ-component and hence if $\underline{E} = -(\underline{V} \times \underline{B})/c$, $\underline{E}$ has only a θ-component. Conclusions for more general cases will be obvious.

1. Radial Gradient of Galactic Cosmic Rays. If we make the weak-anisotropy approximation and neglect the stress tensor in Equation (3) and set $\underline{S} = 0$ for the steady state, we immediately find that the radial (r) and azimuthal (φ) components of ∇U vanish (under the simple assumption that $\underline{S} \times \underline{B}$ and $\underline{E}$ have only a θ-component). Thus the small gradients reported by Pioneer 10 and 11 out to 5 AU are consistent with nearly scatter-free environment somewhat beyond the Earth's orbit.

2. Semi-diurnal Variation of Galactic Cosmic Rays. If the two stress tensor terms are re-introduced in the steady-state version of (3), it is seen that small radial and azimuthal components of ∇U will be balanced by the off-diagonal (θ,r) and (θ,φ) components of $\partial\, \underline{\underline{\Pi}}/\partial T$. The diagonal (θ,θ) element will respond to the meridional (θ) component of ∇U, as was pointed out by a different method in the theoretical treatment of the semi-diurnal variation by Quenby and Lietti (1968).

3. Cosmic Ray Flow along Magnetic Field Lines. Whenever the term $\dot{\underline{S}}$ can be neglected (e.g., when solar particle flux anisotropies are changing slowly), Equation (3) contains no information on $\underline{S}_{||}$, the flow along $\underline{B}$. This is physically most reasonable, since the parallel flow must be determined by conditions in the inner or outer solar system. Since the local variations of the magnetic field

are not sufficiently strong to significantly inhibit scatter-free propagation, the parallel flow is not controlled by the power spectrum of the field measured at 1 AU, but rather by its values well away from 1 AU. This illustrates the fundamental difference between this formulation of propagation and other formulations which demand that $\underline{S}_{||}$ is determined by local fluctuations in the magnetic field. The next two results are examples of non-local control.

4. Decay of Solar Flare Particle Intensities. Forman (1970) presented a simple model to reproduce the exponential decay observed in solar particle events. She used the equation which follows from a scattering mechanism comoving with the solar wind.

$$\underline{S} = -\underline{\underline{K}} \cdot \nabla U + \underline{V} \left(U - \frac{1}{3} \frac{\partial}{\partial T} \alpha \, TU\right) \tag{6}$$

If this equation is then substituted in the Gleeson and Axford (1968) equation of continuity and then all terms in ∇U are neglected, Forman (1970) obtained the approximate equation

$$\dot{U} + (\nabla \cdot \underline{V}) \left(U - \frac{1}{3} \frac{\partial}{\partial T} \alpha \, TU\right) = 0 \tag{7}$$

which leads to an exponential decay time for 10 MeV protons $\sim$ 14 hours. This approximate calculation was verified by a more rigorous solution of the complete equations (Forman, 1971). Now note that the same result can be obtained from (1) by simply assuming that the escape rate from the outer solar system is such that particles near 1 AU have a bulk velocity equal to $\underline{V}$ so that $\underline{S} = C\underline{V}U$, where C is the Compton-Getting factor which appears in (6). Then substitution in (1) and neglect of ∇U terms yields Forman's (1970) result. The results are the same because the terms that are neglected in the scatter-free treatment $< Q >$ and $< \underline{Q}p >$, all contain ∇U (which was neglected). Using the integral solution of Liouville's equation, Roelof (1973) obtained essentially the same result from the assumption of particle escape and showed that ∇U is indeed small, under the condition that the scattering region began $\sim$ 2 AU.

5. The Quiet-Time Diurnal Variation. There is an essential element in any theory of the flux anisotropy which causes the ordinary (quiet-time) diurnal variation in cosmic-ray intensity measured at a given station. Somehow, the gradient in cosmic-ray intensity normal to the ecliptic must be reduced from the value it would have in response to the polarization electric field $\underline{E} = -(\underline{V} \times \underline{B})/c$ present in the solar wind moving with velocity $\underline{V}$ carrying a magnetic field $\underline{B}$. For, as pointed out by Stern (1964), if all cosmic-ray trajectories to a given station mapped back out of the heliosphere (where the flux is presumably isotropic), and if the polarization field can be written as the gradient of a potential (which it can be in the approximation $\partial \underline{B}/\partial t = 0$), then Liouville's theorem (that the unidirectional intensity is a constant along a dynamical trajectory) implies that the flux at earth is isotropic. Beginning with Ahuwalia and Dessler (1962) and continuing with Parker (1964) and Axford (1965) it was assumed that cross-field diffusion would relax the cosmic-ray gradient in the $\underline{E}$-direction, and the quiet-time condition of zero radial flow would produce the apparent "corotation" of the cosmic-ray gas, giving a diurnal maximum at 1800 hours (east) asymptotic direction. However, it was also realized (Parker, 1967) that the relaxation of the gradient need not take place at 1 AU, but rather could take place outside (or inside) the Earth's orbit. This suggests the interesting possibility that the interplanetary cosmic-ray gradient in the $\underline{E}$-direction may be relaxed in the outer corona (rather than in the outer heliosphere), say

anywhere inside 20 to 50 $R_\odot$, the estimated radial range of the magnetohydrodynamic critical points (Weber and Davis, 1967). Reid (1964) and Axford (1965) pointed out the possibility of coronal transport of solar cosmic-rays $\geq$ 0.1 GeV, and recently Lanzerotti (1973), Reinhard and Roelof (1973), and Reinhard and Wibberenz (1974), have concluded that coronal transport is required to explain the onsets of solar particle events between about 10 and 100 MeV. Such transport is certainly consistent with the aforementioned ground-level flare events for $\geq$ 1 GeV protons discussed by Pomerantz and co-workers. We need consider only the θ-component from Equation (3), neglecting $\underline{S}$ and $\underline{\Pi}$.

$$\frac{pv}{3}\frac{1}{r}\frac{\partial U}{\partial \theta} - q\,E_\theta\left(U - \frac{1}{3}\frac{\partial}{\partial t}\alpha\,TU\right) - \frac{q}{c}S_\varphi B_r = 0 \qquad (8)$$

Here we have imposed the usual steady state boundary condition $S_r = 0$ (no net flow out of the solar system). Thus, if $\partial U/\partial\theta$ "relaxed" by coronal transport, $S_\varphi \leq C\,V_\varphi U$, where V_φ is the φ-component of the electric field drift velocity $c(\underline{E} \times \underline{B})/B^2$. On the other hand, if $\partial U/\partial\theta$ is "sustained" in the corona, then the interplanetary gradient is also sustained and tends to canel the electric field drift. The situation is sketched in Figures 1a and 1b. Observational evidence from the Skylab x-ray photographs of coronal structure supporting this interpretation are presented in a companion paper (Roelof et al., 1975).

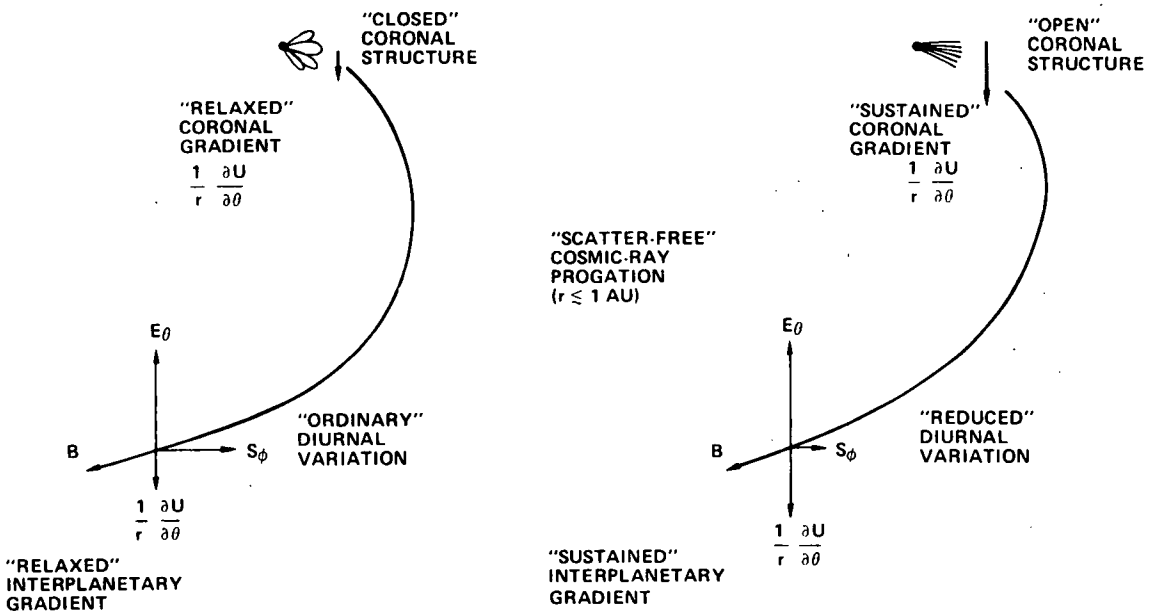

Figure 1 Vector relations for the quiet-time diurnal variation from Equation (8) in which the meridional cosmic-ray gradient is controlled by coronal magnetic structure: (a) "relaxed" by transport across "closed" structure; and (b) "sustained" by inhibited transport over "open" structure.

Acknowledgements. I am grateful for support under Air Force Cambridge Research Laboratories Contract F19628-73-C-0070 (although support does not necessarily imply endorsement) and by NASA Grant NSG7055.

References.

Ahluwalia, A.S. and J.J. Dessler, Planet. Space Sci., 9, 195, 1962.
Axford, W.I., Planet. Space Sci., 13, 115, 1965.
Bryant, D.A., T.L. Cline, U.D. Desai and F.B. McDonald, J. Geophys. Res., 67, 4983, 1962.
Carmichael, H., Space Sci., Rev. 1, 28, 1962.
Domingo, V., D.E. Page and K. -P. Wenzel, J. Geophys. Res., in press, 1975.
Duggal, S.P. and M.A. Pomerantz, Solar Phys., 27, 227, 1972.
Duggal, S.P. and M.A. Pomerantz, J. Geophys. Res., 78, 7205, 1973.
Duggal, S.P., I. Guidi and M.A. Pomerantz, Solar Phys., 19, 234, 1971.
Fan, C.Y., J.E. Lamport, J.A. Simpson and D.R. Smith, J. Geophys. Res., 71, 3289, 1966.
Forman, M.A., J. Geophys. Res., 75, 3147, 1970.
Forman, M.A., J. Geophys. Res., 76, 759, 1971.
Gleeson, L.J., Planet Space Sci., 17, 31, 1969.
Gleeson, L.J. and W.I. Axford, Astrophys. Space Sci., 2, 431, 1968.
Innanen, W.G. and J.A. Van Allen, J. Geophys. Res., 78, 1019, 1973.
Krimigis, S.M., E.C. Roelof, T.P. Armstrong and J.A. Van Allen, J. Geophys. Res., 76, 5921, 1971.
Lanzerotti, L.J., J. Geophys. Res., 78, 3942, 1973.
Lin, R.P., J. Geophys. Res., 75, 2583, 1970.
Lin, R.P., S.W. Kahler and E.C. Roelof, Solar Phys., 4, 338, 1968.
McCracken, K.G., J. Geophys. Res., 67, 423, 1962.
McCracken, K.G. and N.F. Ness, J. Geophys. Res., 71, 3315, 1966.
McCracken, K.G., U.R. Rao and N.F. Ness, J. Geophys. Res., 73, 4159, 1968.
Maurer, R.H., S.P. Duggal and M.A. Pomerantz, J. Geophys. Res., 78, 29, 1973.
Meyer, P., E.N. Parker and J.A. Simpson, Phys. Rev., 104, 768, 1956.
Nolte, J.T. and E.C. Roelof, Proc. 14th Intl. Cosmic Ray Conf. (Munich). SP 5.1-2, 1975.
Quenby, J.J. and B. Lietti, Planet. Space Sci., 16, 1209, 1968.
Parker, E.N., Planet. Space Sci., 12, 735, 1964.
Parker, E.N., Planet. Space Sci., 15, 1723, 1967.
Reid, G.C., J. Geophys. Res., 69, 2659, 1964.
Reinhard, R. and E.C. Roelof, Proc. 13th Intl. Cosmic Ray Conf., 2, 1378, 1973.
Reinhard, R. and G. Wibberenz, Solar Phys., 36, 473, 1974.
Roelof, E.C., Proc. of the Solar-Terrestrial Relations Conf., University of Calgary, Canada, 411, 1973.
Roelof, E.C. and S.M. Krimigis, J. Geophys. Res., 78, 5375, 1973.
Roelof, E. C., R. E. Gold, A. S. Krieger, J. T. Nolte and D. Venkatesan, Proc. 14th Int'l. Cosmic Ray Conference, Munich, MG 7-2, 1975.
Stern, D., Planet. Space Sci., 12, 973, 1964.
Weber, E. J. and L. Davis, Jr., Astrophys. J., 148, 217, 1967.

MATHEMATICAL FORMULATION OF SCATTER-FREE PROPAGATION OF SOLAR COSMIC RAYS

J. T. Nolte* and E. C. Roelof+
University of New Hampshire
Durham, New Hampshire 03924 U.S.A.

Abstract. The observations of strong, persistent velocity anisotropies in solar flare events demand a mathematical theory closer to the extreme of "scatter-free" (deterministic) propagation rather than diffusive (stochastic) transport, since the latter breaks down as inferred mean-free-paths exceed 0.1 AU. We have derived equations for the time-dependent phase-space density, and used Laplace transform techniques to obtain solutions under rather general conditions. The case of an Archimedean spiral field has been solved numerically, and the results compared with observations from Mariner and Explorer spacecraft of ~0.4 MeV proton intensity and anisotropy histories. These can both be replicated if the inner boundary of the modulation region is placed beyond 2 AU.

1. Introduction. At the lowest energy (~0.3 MeV) of measured proton anisotropy, both Roelof and Krimigis (1973) and Innanen and Van Allen (1973) find high anisotropies often persisting beyond the time of maximum flux. At the highest energies (> 1 GeV) at which solar protons are observed, the observation of high anistropy later than the time of maximum flux is also reported by Maurer et al. (1973). These persistent anistropies directly imply that there was negligible scattering in the inner solar system at these times. Observations of scatter-free low energy (~40 keV) electron events have been reported by Lin and Anderson (1967) and Lin (1970).

We have therefore begun a theoretical investigation of scatter-free propagation in the interplanetary medium, to determine to what extent it is possible to interpret observations of energetic solar particles without the assumption of scattering between the Sun and 1 AU. This work extends the original calculation of Roelof (1974) for a magnetic field diverging as $1/r^2$ with simplified boundary conditions, and is based in part on a thesis (Nolte, 1974), where the numerical solution of the equations in the Archimedean spiral field is discussed in detail.

2. General Theory. Let x be the distance out the field line from a convenient origin, and Θ and Φ the polar angles (in latitude and longitude) of the point where the field line passes through the reference surface S at $x=x_o$. If we can describe the space-time dependence of the magnetic field $\underline{B}$ in terms of moving field lines, then Θ and Φ determine the line and x gives the location of a point on that line. For example, field lines fixed in the photosphere are defined by Θ=const, Φ=const, regardless of their motion in interplanetary space if the reference surface S rotates with the sun (neglecting the effects of differential rotation).

*Present Address: American Science and Engineering, Inc., Cambridge, Mass. 02139 USA
+Present Address: APL/Johns Hopkins University, Silver Spring, Md. 20910 USA

The coordinates of the particle velocity ($\underline{v}$) are given in a local spherical polar system (v, θ, φ) in which the unit vector $\underline{b}$ defining the polar axis is along the local magnetic field and oriented in the sunse of increasing x. Thus $\underline{b}$ may be either parallel or anti-parallel to $\underline{B}$, depending on the polarity and degree of local distortion of the field lines. Note that $\underline{b}$ is a function of the particles position (x, Θ, Φ) and therefore infinitesmal spatial displacements in which the vector $\underline{v}$ is held constant may result in changes in θ and φ (but not v). For convenience we introduce the notation $\mu = \cos\theta$.

If we consider only electromagnetic forces on an arbitrarily fine time scale, Liouville's theorem states that the mechanical phase-space density is a constant along a dynamical trajectory.

The phase-space density (we shall how drop the term "mechanical") may be represented by a function W of the curvilinear coordinates and Liouville's theorem may be written as

$$W(x, \Phi, \Theta; v, \mu, \phi; t) = W(x', \Phi', \Theta'; v', \mu', \phi'; t') \qquad (1)$$

where the primed coordinates correspond to a point on a dynamical trajectory at time t' that passed through a point given by the unprimed coordinates at time t. As Roelof (1973) has argued, when the anistropy is strong, the streaming along the field line dominates the propagation so that the anistropy history of particles obeying guiding center motion may be obtained in the following approximations: $v' \approx V$ (neglect of electric field due to polarization of the plasma); $\Theta' = \Theta$ and $\Phi' = \Phi$ (the particle's position is equivalent to that of its guiding center and drifts due to field curvature and gradients are neglected); and $\partial W/\partial\varphi$ is negligible compared to $\partial w/\partial\mu$ (the anistropies due to transverse drifts and density gradients are negligible compared to the field-aligned streaming anistropy.

Although anistropies due to the magnetic field gradient curvature and $\underline{E}\times\underline{B}$ drifts $(\partial w/\partial\varphi)$ are neglected, it should be remembered that it is the $\underline{E}\times\underline{B}$ drift that tends to keep the particle on the same moving field line, allowing us to take $\Theta' \approx \Theta$ and $\Phi' \approx \Phi$. It should be clear therefore that the neglected anistropies must be reintroduced when the parallel streaming anistropy becomes small enough so that it is comparable to that caused by the $\underline{E}\times\underline{B}$ drift. However, the intensity history during the decay phase of solar particle events may still be discussed without including the transverse velocities (Roelof, 1973).

Suppressing the dependence on the approximate constants Θ, Φ and v and neglecting the φ-dependence, (1) becomes

$$W(x, \mu, t) = W(x', \mu', t') \qquad (2)$$

where now the pitch cosines are related to the distance out the moving field line by the conservation of the first adiabatic invariant:

$$\mu' = \frac{\mu}{|\mu|}\left[1 - \frac{B(x')}{B(x)}(1 - \mu^2)\right]^{1/2} \qquad (3)$$

The time difference for a first transit along a dynamical trajectory is then given by

$$v\tau_{ab}(\mu_a) = \int_{x_a}^{x_b} \frac{dx'}{\mu(x')} = \left|\frac{\mu_a}{\mu_a}\right| \int_{x_a}^{x_b} \frac{dx'}{\sqrt{1 - \frac{B(x')}{B(x_a)}(1 - \mu_a^2)}} \qquad (4)$$

The time to reach a mirroring point τ_m is obtained by choosing x' such that $\mu'=0$ in (3).

Propagation in interplanetary space can only be characterized as scatter-free between the outer corona and the modulation region. For the purpose of model calculations, let us take these regions to have "boundaries" at $x=x_1(\Theta,\Phi)$ and $x=x_2(\Theta,\Phi)$ respectively, as shown in Figure 1. Furthermore, let us assume that the transport process in the outer corona and modulation region is describable by "reflection" coefficients $R_1(t)$ and $R_2(t)$, respectively, such that these functions give the probability that a particle that crossed the boundary from the scatter-free region will re-enter it for the first time at t. In general, these reflection coefficients will be functions also of the entry and exit pitch-cosines. For this paper we suppress effects due to energy changes in the boundary.

We can now derive a set of relations between the density functions at the inner and outer boundaries. With $W_i^{\pm}(\mu, t) = W(x_i, \mu, t)$, for $\mu = \pm|\mu|$ (5)
for an injection beginning at time t=0

$$W_1^+(\mu_1,t) = \frac{J_1(\mu_1,t)}{v} + \int_{-1}^{0} d\mu' \int_0^t dt' R_1(\mu_1,\mu',t-t') W_1^-(\mu',t') \qquad (6)$$

$$W_2^-(\mu_2,t) = \frac{J_2(\mu_2,t)}{v} + \int_0^1 d\mu' \int_0^t dt' R_2(\mu_2,\mu',t-t') W_2^+(\mu',t') \qquad (7)$$

where J_1 and J_2 are solar and galactic unidirectional flux source functions, respectively. Neglecting energy changes in the region $x, > x > x_2$, equation (2) also implies

$$W_1(\mu_1,t) = W_2[\mu_2(\mu_1), t+\tau_{12}(\mu_1)] \qquad \mu_{12} < |\mu_2| < 1 \qquad (8)$$

$$W_2(\mu_2,t) = W_2[-\mu_2, t-2\tau_m(\mu_2)] \qquad 0 < |\mu_2| < \mu_{12} \qquad (9)$$

where $\mu_2(\mu_1)$ is determined from (3), and $\mu_{12}=\mu_2(\mu_1=0)$.

Equations (6)-(9) completely determine the functions $W(x_1,\mu,t)$ and $W(x_2,\mu,t)$ since their values are inter-related for all ranges of μ. These functions contain all the information on the propagation, since the density function $W(x,\mu,t)$ at any position $x_1<x<x_2$ and any time $t>0$ may be obtained from (2).

Because of the convolution and shift theorems, these equations are simplified considerably when we apply the Laplace transformation:

$$w_1^+(\mu_1,s) = \frac{j_1(\mu_1,s)}{v} + \int_{-1}^{0} d\mu_1' r_1(\mu_1,\mu_1',s) w_1^-(\mu_1',s) \qquad (6')$$

$$w_2^-(\mu_2,s) = \frac{j_2(\mu_1,s)}{v} + \int_o^1 d\mu_2' r_2(\mu_2,\mu_2',s) w_2^+(\mu_2',s) \tag{7'}$$

$$w_1(\mu_1,s) = e^{s\tau_{12}(\mu_1)} w_2[\mu_2(\mu_1),s] \tag{8'}$$

$$w_2(\mu_2,s) = e^{-2s\tau_m(\mu_2)} w_2(-\mu_2,s) \tag{9'}$$

Algebraic manipulation then leads to a single integral equation for $w_2^-(\mu_2, s)$:

$$w_2^-(\mu_2,s) = \frac{j_2(\mu_2,s)}{v} + \int_{\mu_{12}}^1 d\mu_2' r_2(\mu_2,\mu_2',s) e^{-s\tau_{12}(\mu_2')} \frac{j_1[\mu_1(\mu_2'),s]}{v}$$

$$+ \int_{\mu_{12}}^1 d\mu_2' r_2(\mu_2,\mu_2',s) e^{-s\tau_{12}(\mu_2')} \int_{-1}^o d\mu_1' r_1[\mu_1(\mu_2'),\mu_1',s] e^{s\tau_{12}(\mu_1')} \cdot \left\{ w_2^-[\mu_2''(\mu_1'),s] \right\}$$

$$+ \int_{-\mu_{12}}^o d\mu_2' r_2(\mu_2,-\mu_2',s) e^{2s\tau_m(\mu_2')} w_2^-(\mu_2',s) \tag{10}$$

3. Special Case Solution. So far the treatment of the basic system of equations has been quite general. However, a tremendous simplification is obtained if we make the reasonable assumptions of: (1) "diffuse reflection", where R_n is independent of the re-entrant pitch cosine; and (2), "diffuse injection" where J_n is independent of the injection pitch-cosine. Then inspection of (10) reveals that $w_2^-(\mu_2, s)=w_2^-(s)$, independent of μ_2.

Nolte (1974) used the assumptions $J_1=A_o e^{-\beta t}$, $R_1=0$, $J_2=0$ and $R_2=k_o e^{-k(t-t')}$. The integrals in (10) then reduce to integrals of exponentials of the transit times τ_m and τ_{12}, which were evaluated numerically using the Archimedean spiral field model. This resulted in an approximate expression for the inward directed distribution at the outer boundary valid at the outer boundary until approximately three times the transit time from the inner boundary.

This distribution was then transformed into a predicted detector response near 1 AU for various values of the parameters. Figure 2 shows the results of this transformation for a constant injection at the Sun, and outer boundary at 2 AU (from Nolte, 1974). This calculation is in semi-quantitative agreement with the March 21 proton observations of Innanen and Van Allen (1973), shown in Figure 3. The salient points are the initial, very high anistropy in both the calculated and actual profiles, and the decrease in anistropy nearly a full day after onset of the event, just when the particle flux begins to rise.

Quantitatively, this particular choice of parameters in the model results in an overestimate of the anistropy, (predicting a decrease of 30% compared to the observed 50% decrease) and underestimates the flux increase (the predicted increase

is 40% of the maximum, while the observed increase is 70% of the maximum flux). "Hardening" the outer boundary would increase the back-scattered component of the flux. Similarly an increase in the back-scattered component would be caused by the occurrence of some scattering between 1 and 2 AU. It seems necessary to assume that some scattering occurred within 2 AU; however, the high initial anisotropy and the semi-quantitative fit to a particular scatter-free propagation calculation indicate that scattering is not the dominant effect.

The similarity between these observations and the scatter-free predictions for constant injection at the sun would provide stronger verification of the validity of the assumption of almost negligible scattering in the inner heliosphere throughout the first two days of this event is comparable data were available from at least one other spacecraft. With data from one spacecraft only, it is not possible to determine beyond all possible doubt whether the changes in Figure 3 were due to field-aligned propagation or to a switch from one particle regime to another. However, for most such changes from one particle population to another, both the flux and anistropy change aburptly (see e.g. Roelof and Krimigis, 1973). This event is therefore a good example of one which was more nearly scatter-free than diffusive, and not strongly distorted by coronal structure.

4. Acknowledgements. This work was supported by NASA contract NGR-30-002-097 and by Research Contract F1962-73-C-0070 from Air Force Cambridge Research Laboratories, Air Force Systems Command (but does not necessarily reflect endorsement by the latter sponsor.)

5. References.

Innanen, W.G., and J.A. Van Allen, J. Geophys. Res., 78, 1019, 1973.
Lin, R.P., Solar Phys., 15, 453, 1970.
Lin, R.P., and K.A. Anderson, Solar Phys., 1, 446, 1967.
Maurer, R.H., S.P. Duggal and M.A. Momerantz, J. Geophys. Res., 78, 29, 1973.
Nolte, J.T., Ph.D. thesis, University of New Hampshire, Durham, 1974.
Roelof, E.C., Eos Trans. AGU, 55, 386, 1974.
Roelof, E.C., and S.M. Krimigis, J. Geophys. Res., 78, 5375, 1973.

RE-ENTRY
OPERATORS

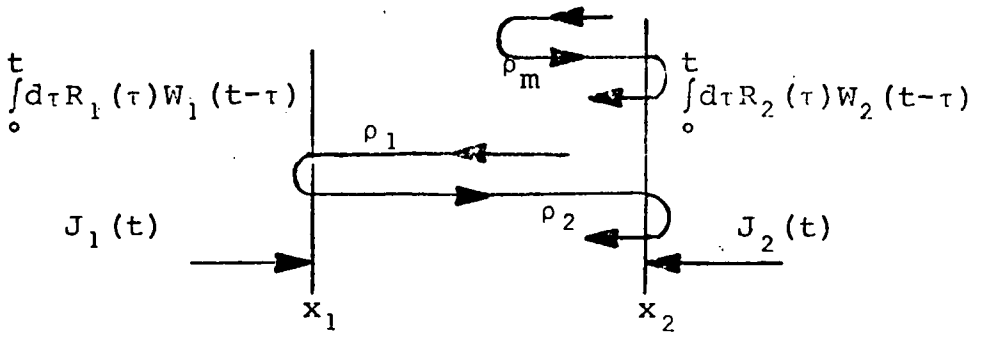

Figure 1

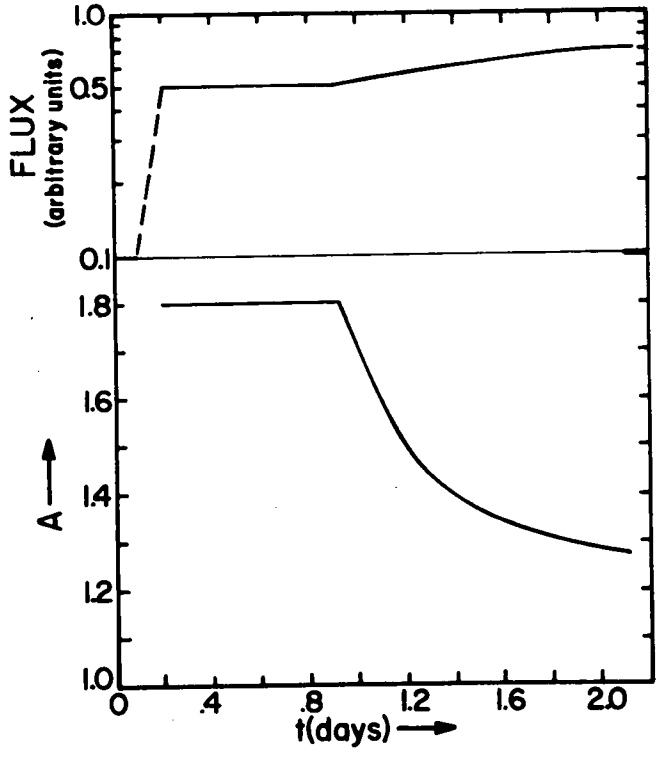

Figure 2

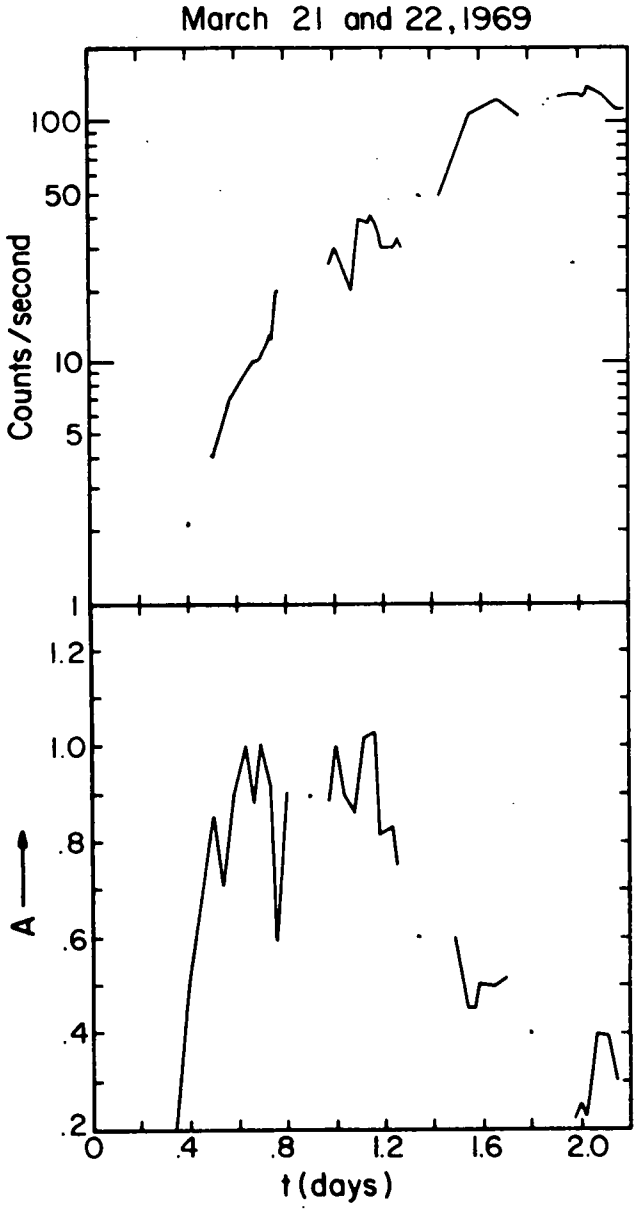

Figure 3

RELATION OF LARGE-SCALE CORONAL X-RAY STRUCTURE AND COSMIC RAYS: 1. SOURCES OF SOLAR WIND STREAMS AS DEFINED BY X-RAY EMISSION AND Hα ABSORPTION FEATURES

A. S. Krieger and J. T. Nolte
American Science and Engineering, Inc.
Cambridge, Massachusetts 02139 U. S. A.

J. D. Sullivan and A. J. Lazarus
Center for Space Research, MIT
Cambridge, Massachusetts 02139 U. S. A.

P. S. McIntosh
SEL/NOAA/ERL
Boulder, Colorado 80302 U. S. A.

R. E. Gold and E. C. Roelof
APL/Johns Hopkins University
Silver Spring, Maryland 20910 U. S. A.

Abstract. Large-scale structure of the interplanetary medium and the solar corona (as defined by recurrent high speed solar wind streams, their sources observed in soft X-rays and magnetic polarity structures) is discussed in order to present the framework in which cosmic ray propagation is investigated in subsequent papers.

1. Introduction. As a basis for studying cosmic ray propagation during the Skylab mission, we have investigated the large-scale structure of the corona and the interplanetary medium during Carrington rotations 1601-1607. In this paper we present a description of the large-scale structures which we have found to be related to cosmic ray observations. The influence of these structures on cosmic ray propagation is discussed in four related papers, also being presented at this conference (SP4-5, SP4-6, MG7-2 and MG5-10). We shall concentrate here on the recurrent high speed solar wind streams and their coronal sources, since these are of special interest to our studies.

2. Data and Discussion. Large-scale structures in the interplanetary medium can be defined in terms of high velocity streams and magnetic field polarity. In the corona, structures of interest here are identifiable in X-ray emission and in the large-scale patterns of chromospheric and photospheric magnetic polarity. We present the data used in this definition of large-scale structures in Figure 1 for reference in our related papers also. The top panel of the figure for each solar rotation is hourly averages of the solar wind velocity measured by the MIT experiment on IMP 7, plotted at the high coronal source longitude estimated using the EQRH (constant, radial velocity) approximation. We have also included sporadic measurements from Pioneers 6-9 (Solar Geophysical Data) separated up to 110° east and west of Earth to help show the temporal evolution of the streams. At the bottom of this panel we show strips of magnetic field polarity data. The top strip is polarities derived from measurements by HEOS 1 and 2 (acquired through NASA/GSFC/WDC-A), also EQRH-mapped to the high corona. The other strip is chromospheric/photospheric polarity, derived by combining the information from the Mt. Wilson magnetic field atlas (Solar Geophysical Data), individual Kitt Peak magnetograms (J. Harvey, private communication) and Hα synoptic charts (McIntosh, 1975). The bottom panel in each section is an X-ray synoptic chart, showing the low coronal emission structure. This chart was made by overlapping lunes from the centers of daily X-ray images taken by the AS&E telescope on Skylab. In the table on p. 2, the velocity and Carrington longitude of the source of all streams with peak velocity > 500 km/s. observed near Earth between days 150 and 300 in 1973 are listed. Of these, only streams A, C, D and F recur on more than one rotation. Streams A and D are associated with coronal holes (Nolte et al., 1975) while C and F originate in the high corona (20-50 $R_\odot$) over faint X-ray emission areas. However, there are also equatorial regions of faint X-ray emission without associated

high speed streams (e.g., at 290-330 on rotation 1603, and 220-250 on 1604). Resolution of this ambiguity can come only through a better understanding of the large-scale coronal structure. One effort in this direction (but not restricted to structures related to solar wind sources) is a study by McIntosh et al. (1975) of the relationship between chromospheric neutral lines and coronal X-ray structures during the last two weeks in June, 1973. Figure 2, taken from their work, shows a neutral line drawing derived from the synoptic chart overlaid onto an X-ray photograph taken on June 30, 1973. In this figure, the coronal hole which is the source of stream A on rotation 1602 is at the right, while the faint emission region near 300° on 1603 is left of center. There is evidence for a rather complicated chromospheric polarity pattern beneath this faint emission region which is not a high speed stream source; however, this figure also demonstrates that the relationship between neutral lines poorly defined in Hα structures and X-ray structures

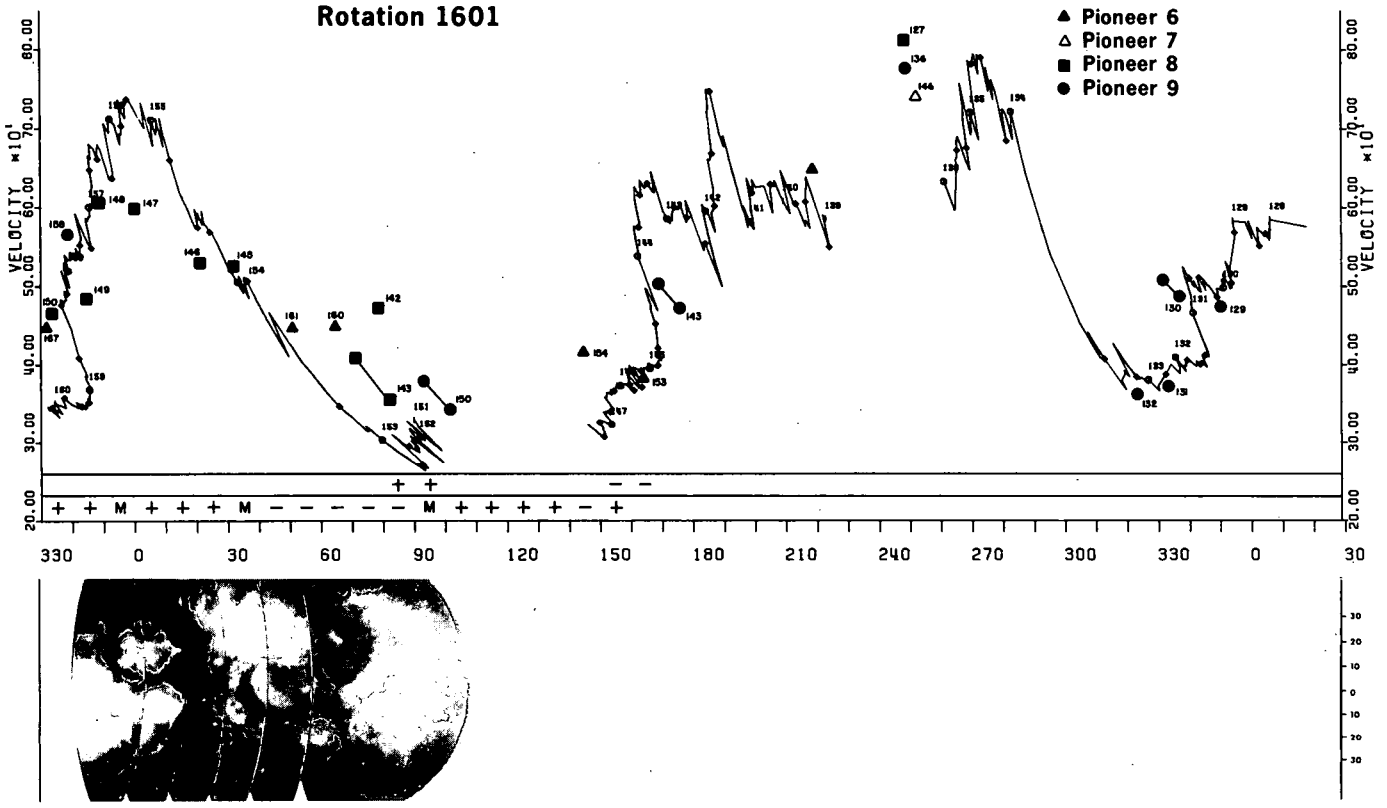
Rotation 1601
▲ Pioneer 6
△ Pioneer 7
■ Pioneer 8
● Pioneer 9
VELOCITY ×10¹
80.00
70.00
60.00
50.00
40.00
30.00
20.00
330
0
30
60
90
120
150
180
210
240
270
300
330
0
30

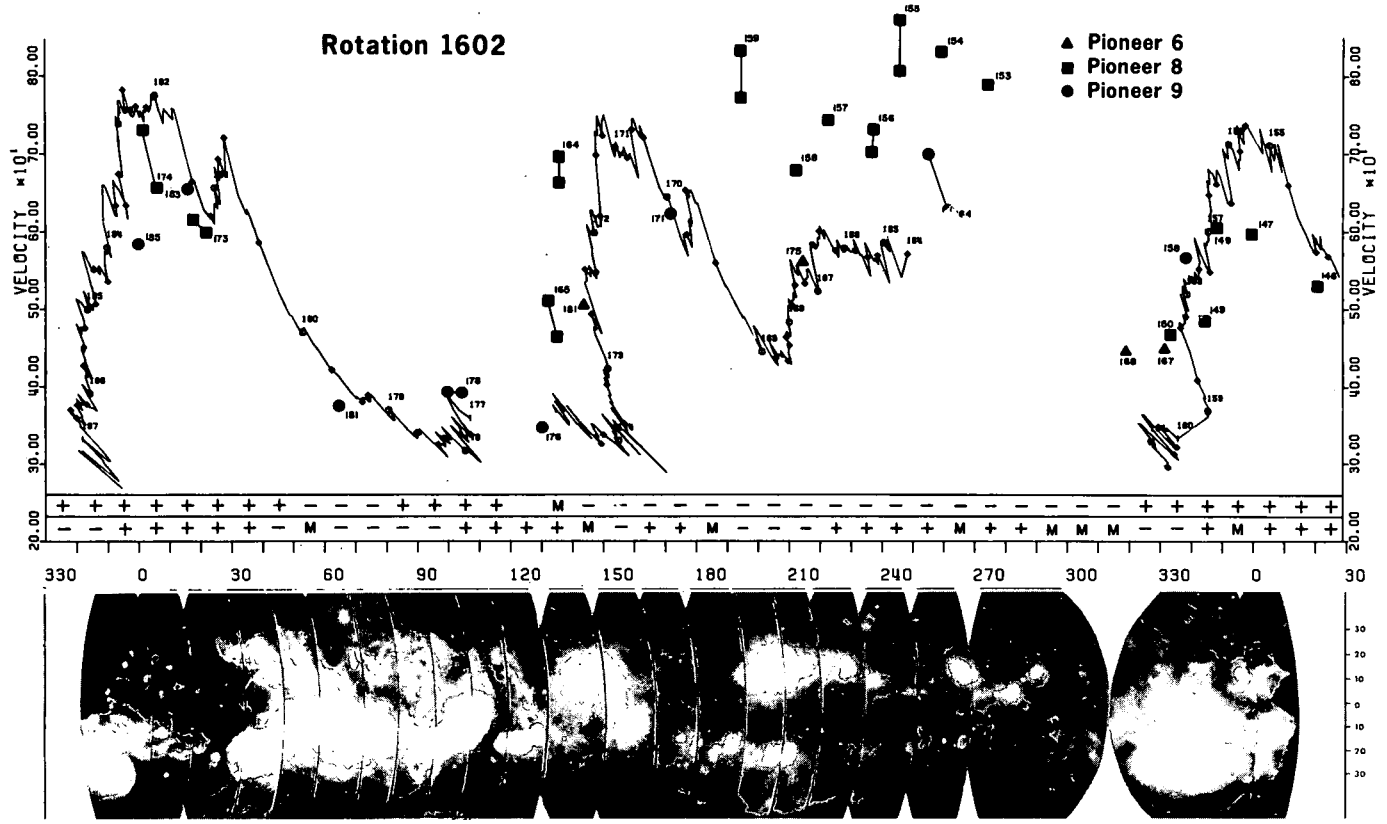
Rotation 1602
▲ Pioneer 6
■ Pioneer 8
● Pioneer 9
VELOCITY ×10¹
80.00
70.00
60.00
50.00
40.00
30.00
20.00
330
0
30
60
90
120
150
180
210
240
270
300
330
0
30

SL-0307

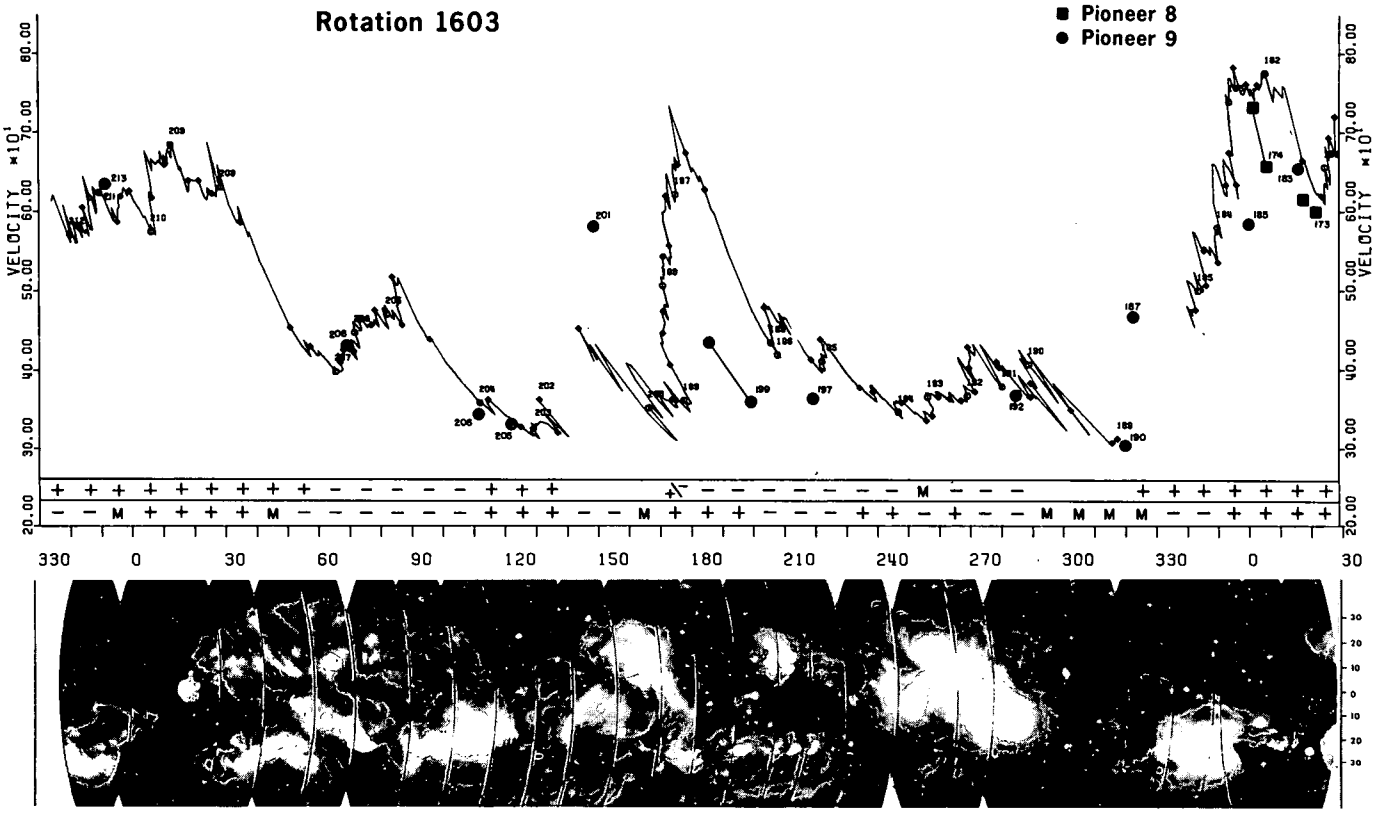
Rotation 1603
Pioneer 8
Pioneer 9
VELOCITY ×10¹
80.00
70.00
60.00
50.00
40.00
30.00
20.00
330
0
30
60
90
120
150
180
210
240
270
300
330
0
30

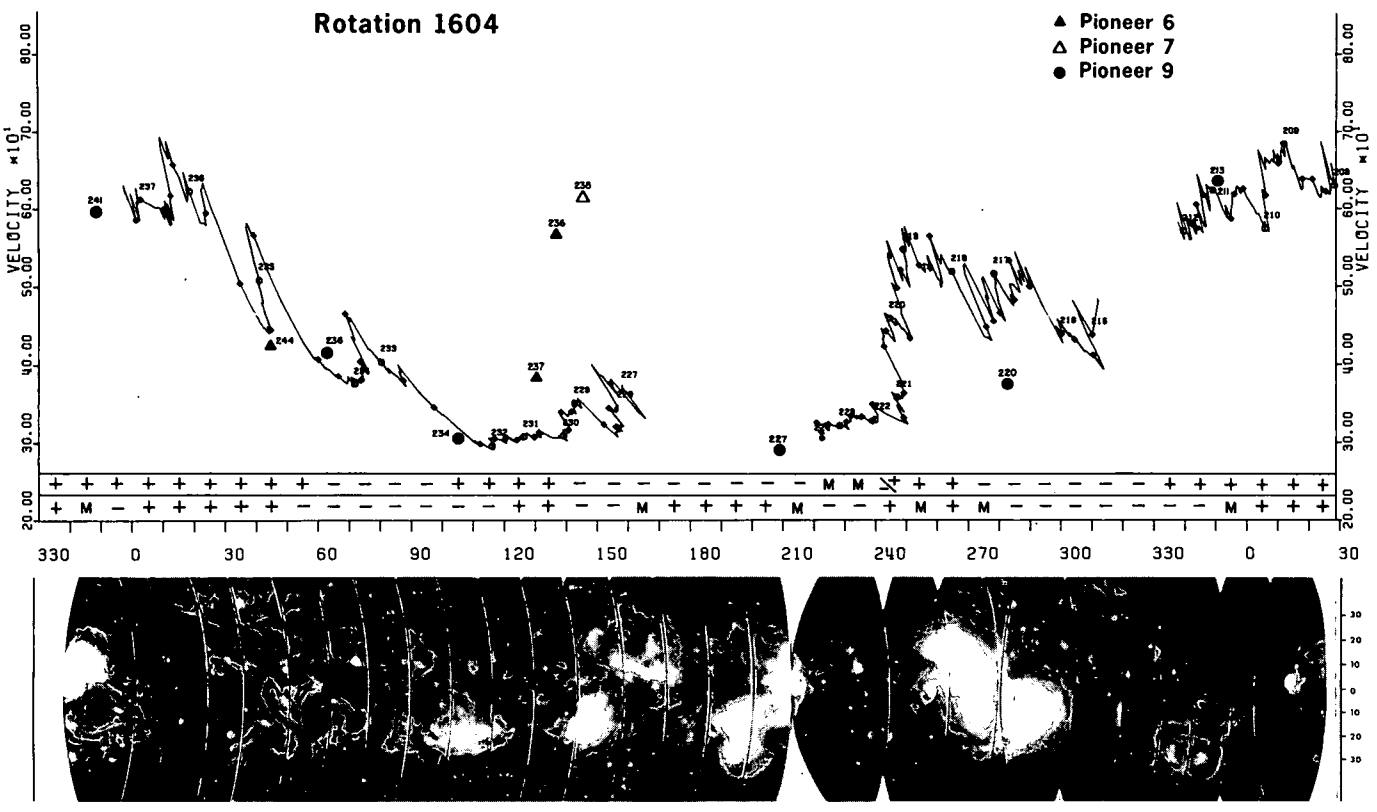
Rotation 1604
Pioneer 6
Pioneer 7
Pioneer 9
VELOCITY ×10¹
80.00
70.00
60.00
50.00
40.00
30.00
20.00
330
0
30
60
90
120
150
180
210
240
270
300
330
0
30

SL-0308

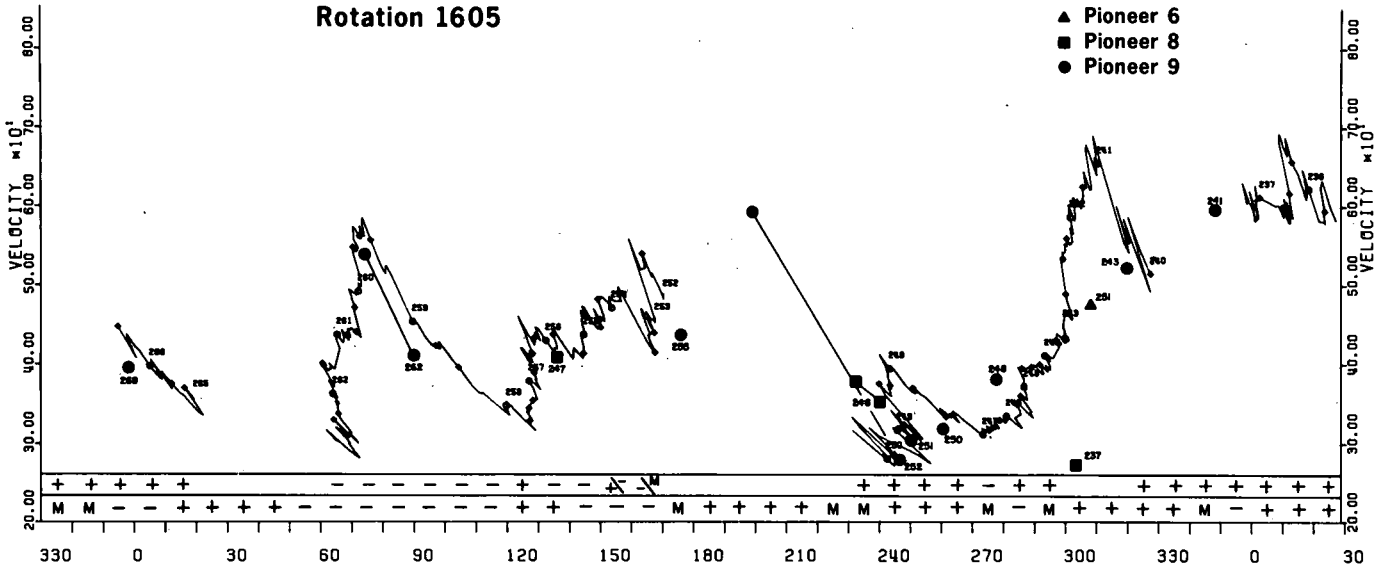
Rotation 1605
Pioneer 6
Pioneer 8
Pioneer 9
VELOCITY ×10¹
80.00
70.00
60.00
50.00
40.00
30.00
20.00
330
0
30
60
90
120
150
180
210
240
270
300
330
0
30

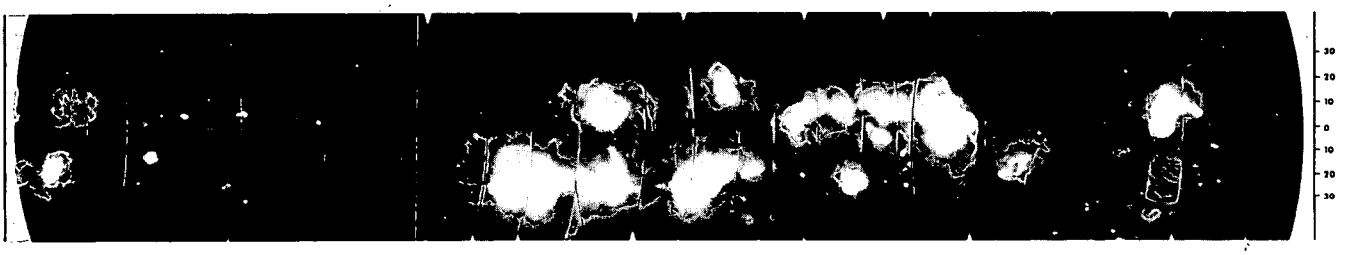

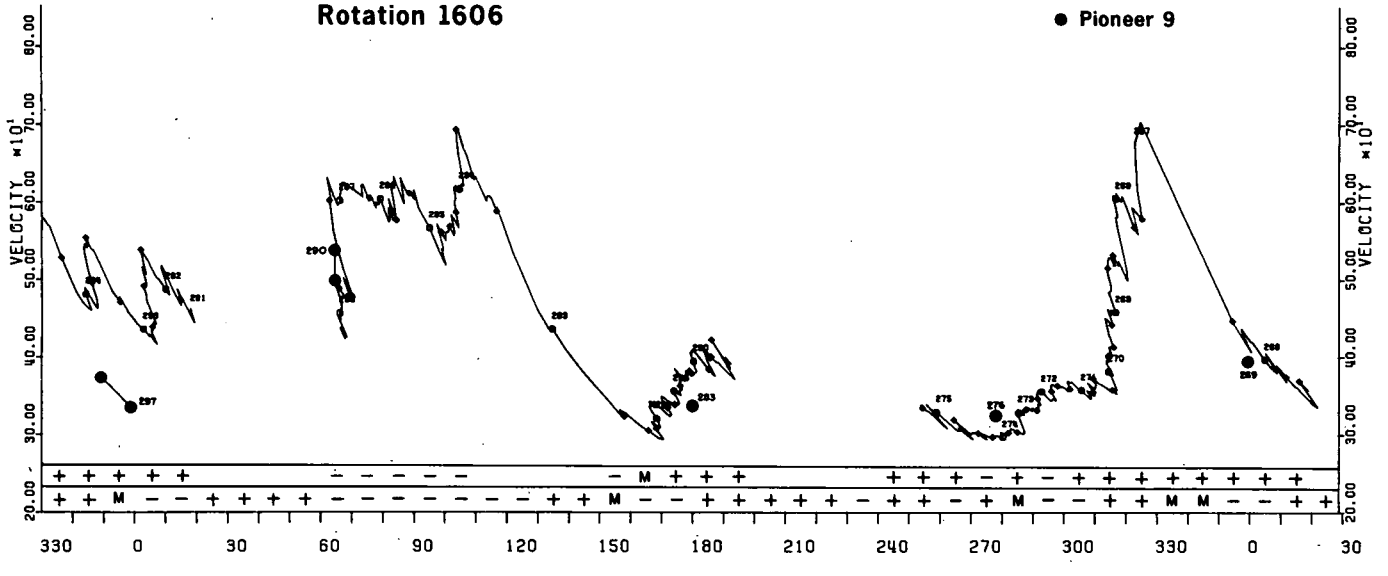
Rotation 1606
Pioneer 9
VELOCITY ×10¹
80.00
70.00
60.00
50.00
40.00
30.00
20.00
330
0
30
60
90
120
150
180
210
240
270
300
330
0
30

SL-0309

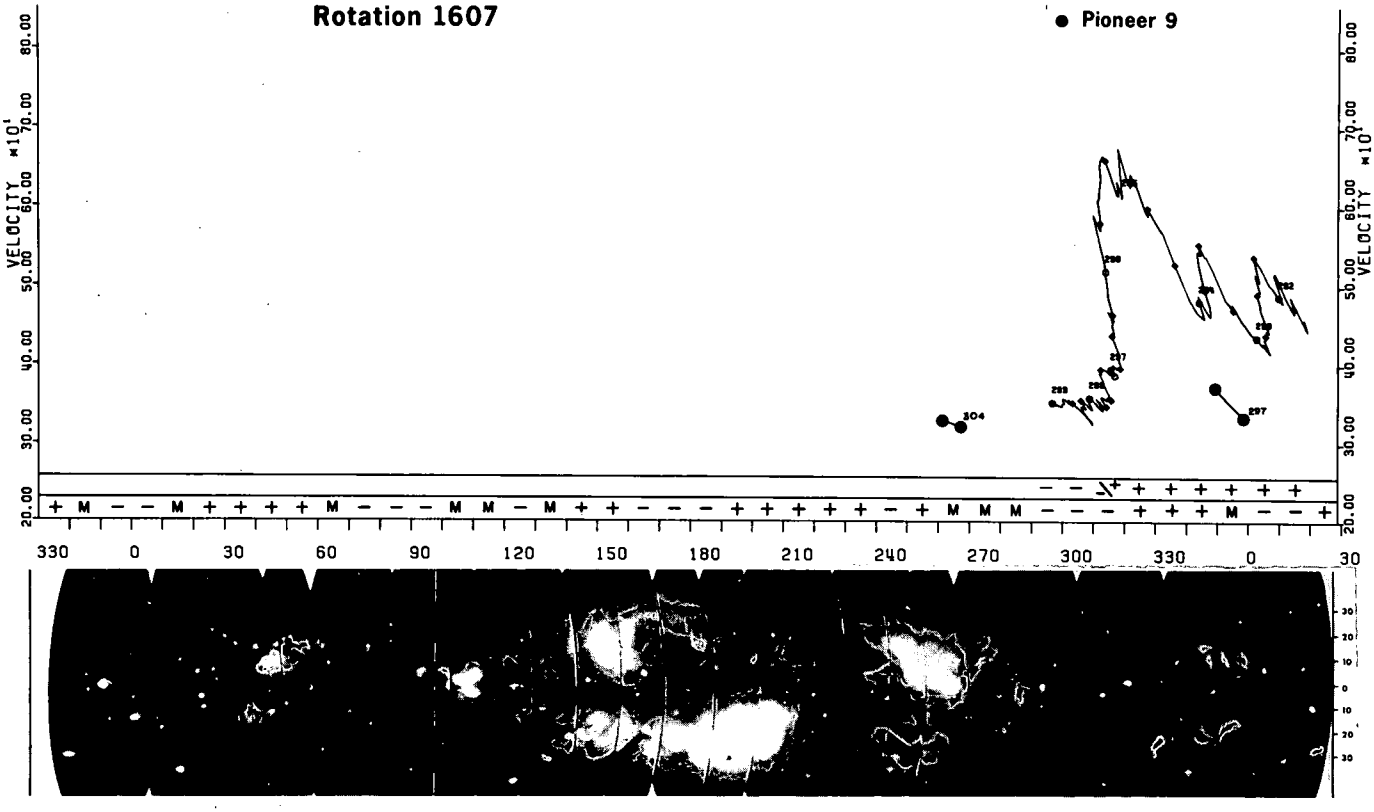
Rotation 1607
Pioneer 9
VELOCITY ×10¹
80.00
70.00
60.00
50.00
40.00
30.00
20.00
330
0
30
60
90
120
150
180
210
240
270
300
330
0
30

SL-0310

RELATION OF LARGE-SCALE CORONAL X-RAY STRUCTURE AND COSMIC RAYS: 2. CORONAL CONTROL OF INTERPLANETARY INJECTION OF 300 keV PROTONS

E. C. Roelof, R. E. Gold and S. M. Krimigis
Applied Physics Laboratory/The Johns Hopkins University
Laurel, Maryland, 20810, USA

A. S. Krieger and J. T. Nolte
American Science and Engineering, Inc.
Cambridge, Massachusetts, 02139, USA

P. S. McIntosh
Space Environment Laboratory, NOAA
Boulder, Colorado, 80302, USA

A. J. Lazarus and J. D. Sullivan
Center for Space Research, Massachusetts Institute of Technology
Cambridge, Massachusetts, 02139, USA

We report the striking coronal control of low-energy solar particles from the solar flare of September 7, 1973. The flare was at S18, W46 (Carrington longitude 188°) in McMath Plage Region 12307. We find strong intensity gradients in heliolongitude (~ 10% deg^{-1}) that are nearly identical in protons, helium, and medium nuclei at energies ~ 0.5 MeV/nuc, as well as relativistic electrons and 3 MeV protons. This pervasive gradient occurs at longitudes over bright x-ray emission structures east of the flare site which interconnect large-scale chromospheric polarity regions identifiable in Hα filtergrams.

1. Introduction. The analysis of low energy solar particle events, whether flare-associated or quasi-stationary, always leads back to the question of the magnetic structure which distributes the particles around the corona after their acceleration and before their injection into the interplanetary medium. The period spanned by the Skylab mission (May 1973-February 1974) offers an outstanding opportunity for correlative studies of coronal structures. Not only were there extensive solar observations, but the IMP 7 (and IMP 8 after October, 1973), spacecraft carried a full complement of plasma, magnetic field and energetic particle experiments.

2. Particle Observations. The particle measurements are from the APL/JHU Charged Particle Measurements Experiment (CPME), also in IMP-7. The channels of interest here all have a geometric factor of 1.51 cm^2 ster:

P1	protons	0.29-0.50 MeV
P4	protons	1.85-4.50 MeV
E4	electrons	0.22-2.50 MeV
A1	alphas	0.64-1.17 MeV/nuc
Z1	mediums ($Z \geq 3$)	~ 0.77-3.2 MeV/nuc

A complete description of the detector and the IMP 7 orbit is given in Sarris et al. (1975).

The largest particle-producing flare during Carrington Rotations 1601-1607 (May -October 1973) occurred at 1212 UT on September 7 (day-of-year 250) in McMath Plage Region (MPR) 12507 at S18°, W46° (Carrington longitude 188°). The flare was of optical importance 2B and x-ray importance C1.

Time histories of one-hour averages of the P1, P4, A1 and Z1 fluxes from day 250 to 262, 1973 are shown in Figure 1. IMP 7 was in the magnetotail on day 250, but emerged on the down side on day 253 and remained in the interplanetary medium until day 262. The similarity of the time histories is immediately apparent, and the spatial nature of the variations is made apparent by the lack of velocity dispersion of features between P1 and P4. The changes are simultaneous with a resolution of 1 hour, even though the transit times per AU differ by more than 3 hours (see, for example, the dip at ~ 0000, day 253 and the small peak ~ 2100, day 255).

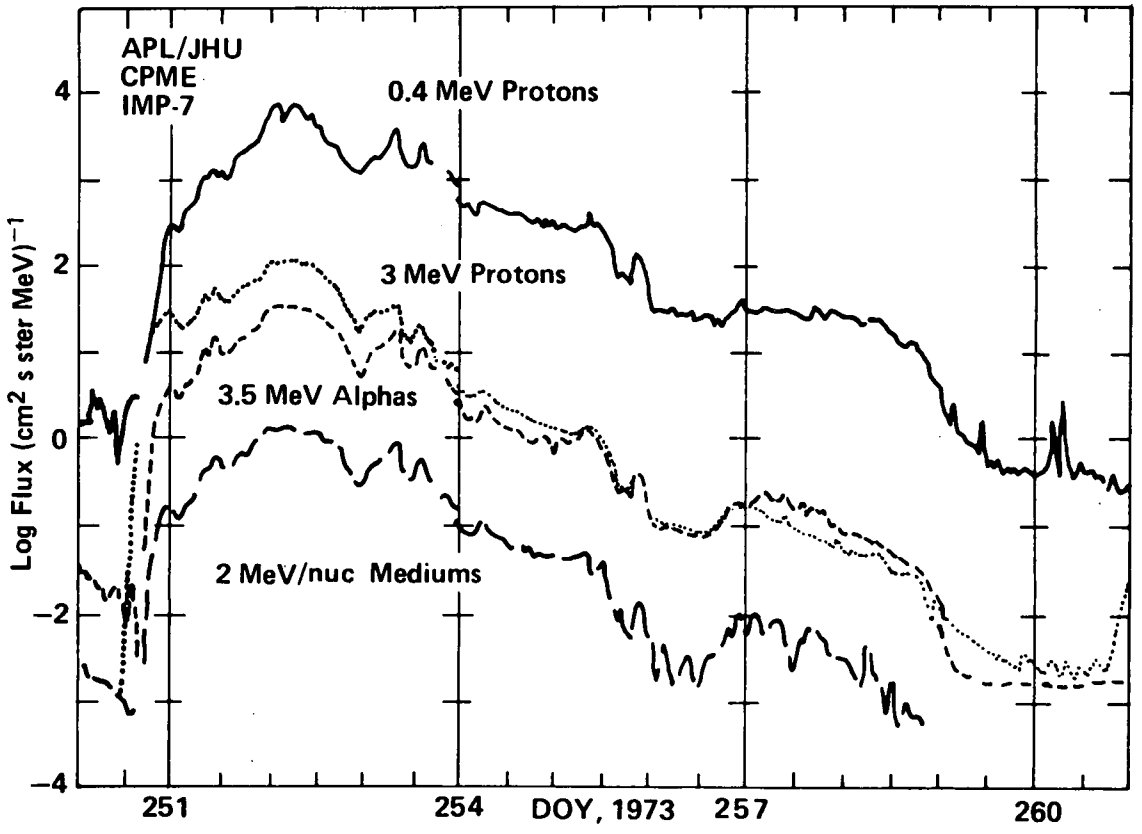

Figure 1. Time histories of particle fluxes (refer to day 251): P1 protons, 0.4 MeV (top); P4 protons, 3 MeV (second); A1 alphas, 3.5 MeV (third) Z1 mediums, ~ 2 MeV/nuc (bottom).

3. Coronal Injection Profile. Since spatial structure is indicated, we "map back" the particle fluxes to the sun using the high coronal connection longitude of the large-scale interplanetary magnetic field lines calculated from the observed solar wind velocities. The connection longitudes and solar wind velocities from the MIT plasma experiment on IMP 7 are shown and discussed in the companion paper (Krieger et al., 1975). The fluxes for P1, A1, Z1 and E4 are plotted at their connection longitudes in Figure 2 for all of Carrington Rotation 1605.

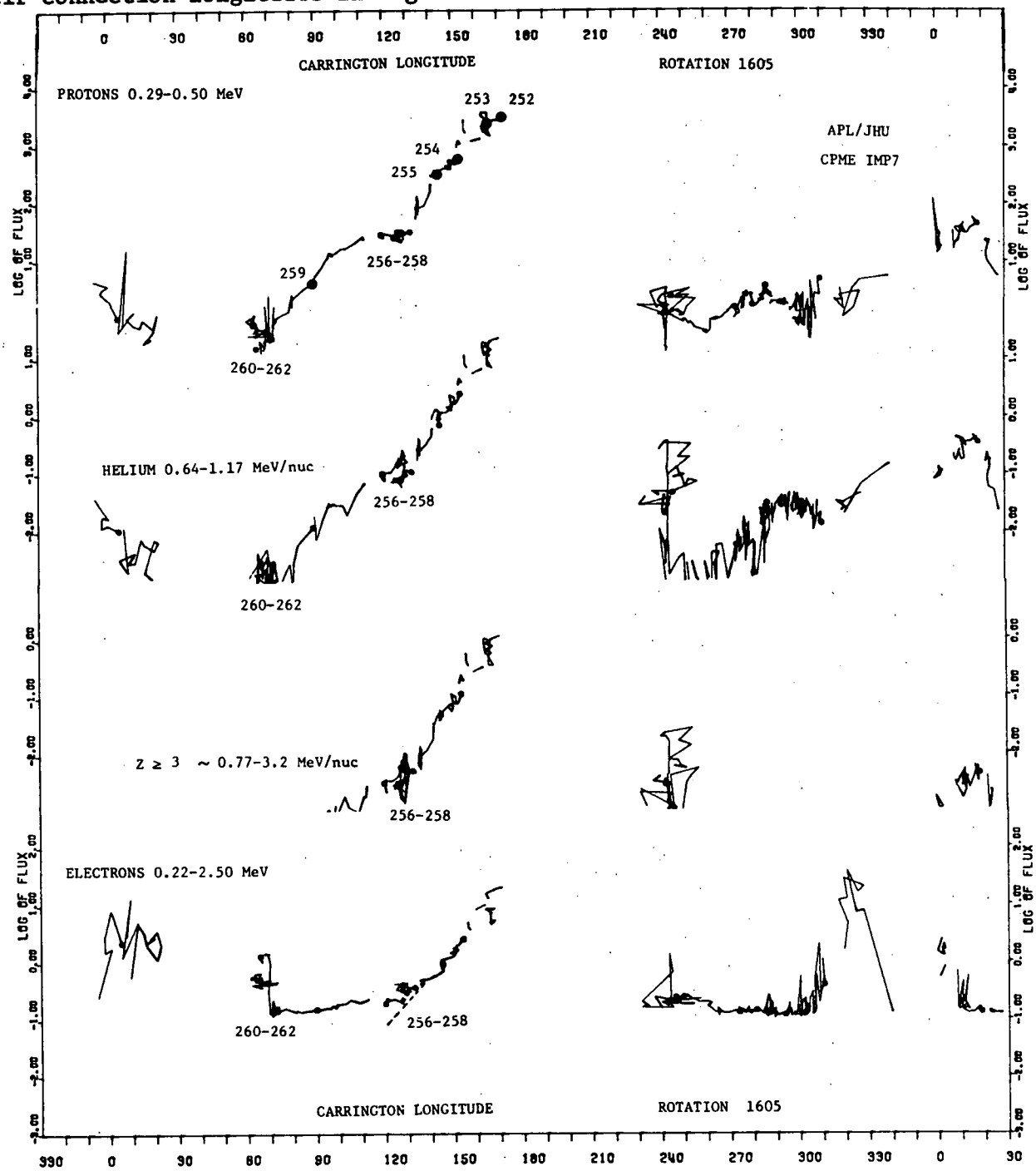

Figure 2. Coronal emission profiles of particle fluxes estimated from concurrent solar wind velocities. Day-of-observation is selectively numbered.

The result of the mapping is to transform the rather irregular time behavior of days 252-258 in Figure 1 into a closely exponential gradient in longitude from 170° to 120°. Even the relativistic electrons (not shown in Figure 1) exhibit the gradient (especially when the ambient flux $\sim 10^{-1}$ cm^{-2} s^{-1} ster^{-1} is subtracted, as indicated by the dashed line). The 3 MeV (P4) protons were not plotted in Figure 2, since their similarity to the 3 MeV (A1) alphas in Figure 1 guarantees that they have the same gradient. For all species, this gradient is about 10% per degree of longitude, covering more than two orders of magnitude in flux.

After day 256 there appear to be some temporal effects which can be seen as differences in the different curves in both Figures 1 and 2. By the same token, the temporal effects appear negligible prior to day 256 (implying continual injection of particles over at least 5 days), so we are led to a close examination of the coronal structure from 120° to 170° using our solar data.

4. Coronal Structure. Figure 3 combines the x-ray synoptic photographs from the companion paper by Krieger et al. (1975) with the Hα snyoptic chart from the Skylab atlas (McIntosh, 1975). Inferred negative magnetic polarities are shaded, Hα filaments are cross-hatched and Hα plage is stippled. MPR 12507 is easily identified at 188°, S18°. The x-ray photographs reveal that the extent of the particle gradient (170° to 120°) is essentially the same as the southern equatorial bright x-ray plages extending east of MPR 12507. There is considerable interconnection of the plages by well-defined loop structure outlined in x-ray emission. These contiguous structures (and the gradient) terminate at the western boundary of a developing coronal hole, and east of this longitude ($\sim$ 115°), the particle fluxes are at their ambient value.

5. Conclusions. The inter-connected x-ray structure is a reasonable signature in the low corona for a configuration in the outer corona that could lead to the injection profile we have found from 120° to 170°. This result is not unique, as we show in another companion paper (Gold et al., 1975), the other larger particle-producing flare of the Skylab period (July 29, 1973) also set up an injection gradient in P1, A1 and E4 as well as a spatial gradient in galactic cosmic rays which constituted the "recovery" of a Forbush decrease. The striking lack of dependence of these particle distributions on charge or rigidity suggests to us that the coronal transport mechanism may involve electric fields, since the $\underline{E}\times\underline{B}$ drift is also independent of rigidity as well as the sign or magnitude of the charge.

Acknowledgements. The research at APL/JHU was partially supported by Air Force Cambridge Laboratories Contract F19628-73-C-0070 (although support does not necessarily imply endorsement), and by NASA grant NSG7055. The research at AS&E was supported by NASA, Marshall Space Flight Center Contract NAS-8-27758, and that at MIT by NASA contract for IMP 7 data analysis.

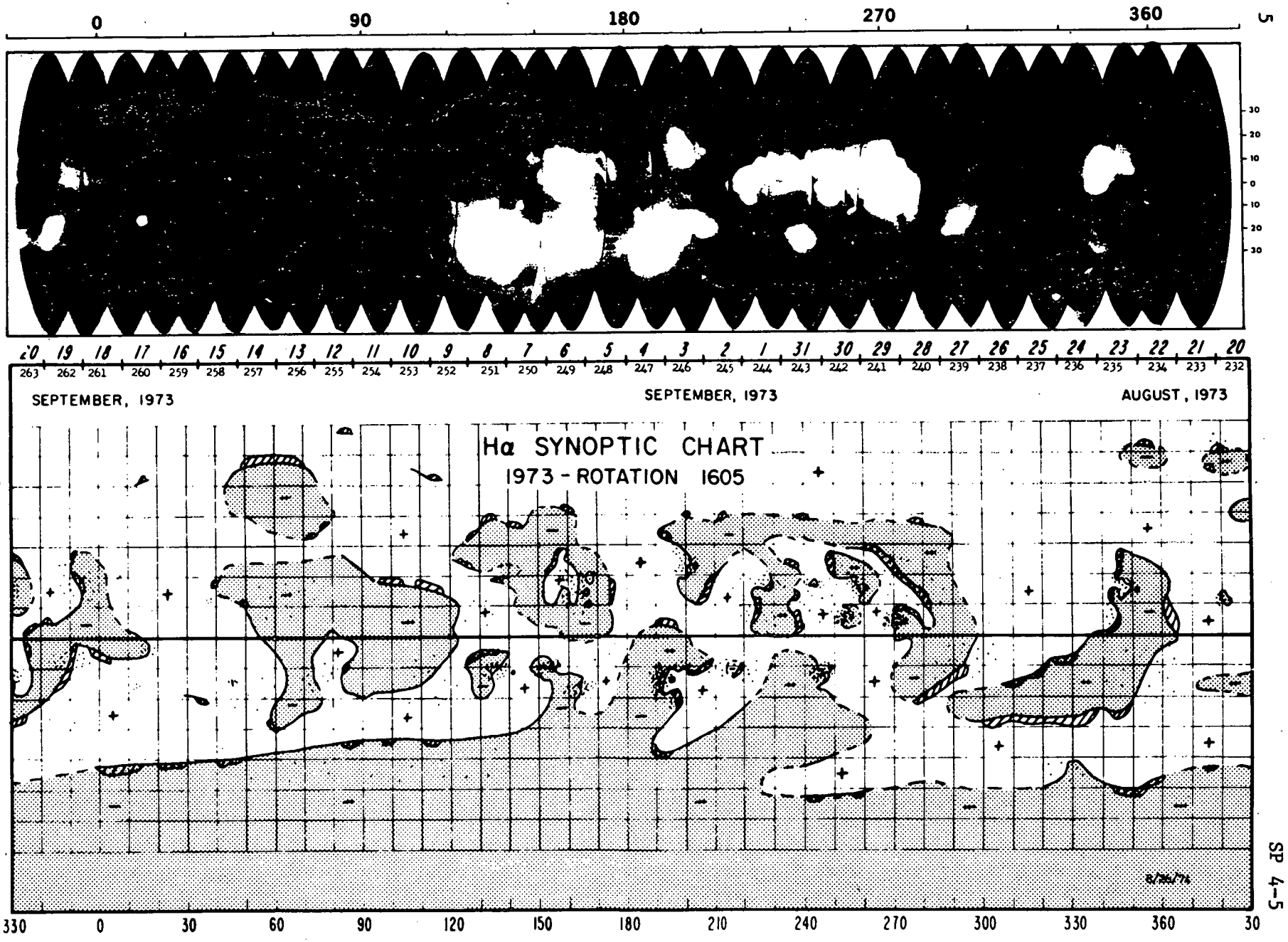

Figure 3

SP 4-5

References.

Gold, R.E., E.C. Roelof, J.T. Nolte and A.S. Krieger, "Relation of large-scale coronal x-ray structure and cosmic rays: 5. Solar wind and coronal influence on a Forbush decrease lasting one solar rotation", Proc. 14th Intl. Cosmic Ray Conf. (Munich), MG 5-10, 1975.

Krieger, A.S., J.T. Nolte, P.S. McIntosh, A.J. Lazarus, J.D. Sullivan, R.E. Gold and E.C. Roelof, "Relation of large-scale coronal x-ray structure and cosmic rays: 1. Sources of solar wind streams and Hα absorbtion features", 14th Intl. Cosmic Ray Conf. (Munich), SP 4-4, 1975.

McIntosh, P.S.,"H-alpha synoptic charts of solar activity for the period of Skylab observations May 1973-March 1974", UAG Report No. 40, Environmental Data Service, 1975.

Sarris, E.T., S.M. Krimigis and T.P. Armstrong, "Observations of magnetospheric bursts of high energy protons and electrons at ~ 35 R_e with IMP-7", J. Geophys. Res., 80, in press, 1975.

RELATION OF LARGE-SCALE CORONAL X-RAY STRUCTURE AND COSMIC RAYS: 3. LOW-INTENSITY SOLAR PARTICLE EVENTS WITH ENHANCED ~ 3 MeV HELIUM AND MEDIUM FLUXES ASSOCIATED WITH SOLAR WIND STREAMS

R. E. Gold, S. M. Krimigis and E. C. Roelof
Applied Physics Laboratory/The Johns Hopkins University
Laurel, Md. 20810, USA

A. S. Krieger and J. T. Nolte
American Science and Engineering, Inc.
Cambridge, Massachusetts, 02139, USA

The large geometric factor (1.5 cm^2 ster) of the APL/JHU particle detectors on IMP-7 and IMP-8 makes possible the measurement of Helium and Medium ($Z \geq 3$) nuclei ~ 3 MeV total energy at fluxes as low as 10^{-2} $(cm^2\ s\ ster\ MeV)^{-1}$ with statistically significant hourly averages. During the first 6 months of the Skylab mission, we have identified Helium-rich events, defined by the condition that $p/\alpha \leq 2$ at ~ 3 MeV total energy. These α events last several days each, but with fluxes seldom exceeding 1 $(cm^2\ s\ ster\ MeV)^{-1}$ and some are also rich in nuclei $Z \geq 3$. None of the events could be associated with flares of optical importance ≥ 1, and the recurrence of the α-rich events implies an influence of coronal structure on the quiet-time abundances of ~ 3 MeV solar particles.

1. Introduction. The relative abundance of Helium on the sun has fundamental astrophysical implications, as has recently been emphasized byLanzerotti and MacLennan (1973). Most studies of the solar p/α ratio have dealt with solar flare events or were limited during quiet-times to averages over ~ 1 day. None-the-less, the trend towards lower p/α ratios at lower energies ($\leq$ 1 MeV) was evident in the statistical study covering 1967-8 by Armstrong and Krimigis (1971). At the intensities measurable in that period, a p/α ratio ~ 10 (evaluated at equal energy per nucleon) was not unusual for a quiet time, but was on the low side for flare events.

We report here on Helium abundances measured at intensities sufficiently low ($< 10^{-2}$ cm^{-2} s^{-1} $ster^{-1}$ MeV^{-1}) that significant hour-averaged fluxes of solar alpha particles are measurable most of the time during May-October 1973. We find recurrent streams of Helium at intensities $\leq 10^{-1}$ $(cm^2\ s\ ster\ MeV)^{-1}$ which are exceptionally rich in alphas, with $p/\alpha < 2$ evaluated at 2.7 MeV total energy.

2. Observations. With the larger geometric factors on the detectors on current IMP spacecraft ($\geq$ 1 cm^2 ster), it is possible to obtain statistically significant hourly averages of fluxes below 10^{-2} $(cm^2\ s\ ster\ MeV)^{-1}$. We shall be discussing the measurements by the Applied Physics Laboratory/JHU Charged Particle Monitoring Experiment (CPME) on IMP-7. The lowest alpha energy channel is 0.64-1.17 MeV/nuc, while a proton spectrum is measured from the four proton channels below 4.5 MeV, with the lowest channel being 0.29-0.50 MeV. From the spectrum, the p/α ratio is calculated at a total energy (equal p and α rigidity) of 2.7 MeV. A complete description of the CPME is given by Sarris et al. (1975).

We recognized a tendency towards 27-day recurrences in the Helium fluxes which were identifiable because of the rarity of large solar particle events during this period. Consequently, we constructed the inferred coronal Helium injection profiles for the data set covering the portion of the Skylab mission for which the American Science and Engineering x-ray photographs (3-32Å and 44-54Å) were available. The method of mapping the fluxes from 1 AU back to the estimated high-coronal connection longitude of the large-scale interplanetary magnetic field lines using observed solar wind velocities has been described and justified elsewhere (Nolte and Roelof, 1973a, 1973b; Roelof and Krimigis, 1973) and is used in several companion papers (Gold et al., 1975; Krieger et al., 1975; Roelof et al., 1975).

2. Coronal Injection Profiles. The inferred Helium injection profiles (0.64-1.17 MeV/nuc) as a function of Carrington longitude are presented for Rotations 1601-8 in Figures 1 and 2, sequentially. Also indicated in the figures by cross-hatched bars are the periods in which the measured p/α ratio was less than 2 (at 2.7 MeV total energy).

It is immediately apparent that there is a recurrent, symmetrical Helium event in the vicinity of 0° for these four rotations, and moreover, that the recurrent event is Helium-rich (by our criterion). This location in the corona is the approximate eastern boundary of a recurrent coronal "hole", i.e. a region of very low x-ray and EUV emission. In a companion paper (Krieger et al., 1975), we show that this coronal hole was also closely associated with a recurrent high-velocity solar wind stream. In fact, as the equatorial extent of the coronal hole waxes and wanes until it finally closes on Rotation 1607, the solar wind stream follows suit. If we now turn to Carrington Rotations 1605-8 shown in the same format in Figure 2, we see that the Helium event also vanishes on Rotation 1607. In fact, the α-fluxes from 0°-50° longitude on the rotation are among the lowest measured during all eight rotations. However, despite this striking recurrence of the coronal hole and the Helium-rich particle stream, it is apparent from Figures 1 and 2 that there are a number of non-recurrent Helium streams and non-recurrent Helium-rich events. Just as the association of high speed solar wind streams with coronal holes is not one-to-one, the associations we discuss here are more indicative of a trend rather than an absolute realtionship.

Let us call the recurrent energetic Helium stream at ~ 0° "stream A", because there is another recurrent structure which we'll call "stream B". This stream is not as apparent as stream A. Stream B is centered over ~ 285° longitude, and although it is quite visible on Rotations 1605-8 in Figure 2, it may first have been detected as early as Rotation 1604 (Figure 1). There it appears as a deviation from the decay of one of the two flare events during this period (July 29, day 212, 1973). It is striking that stream B forms directly over the longitude of this great flare (importance 3B) which, however, produced relatively modest prompt particle fluxes, perhaps because of its location at E45°. Note also from Figure 2 that stream B is not initially Helium-rich (as is also the case with prompt flare particles), but is Helium-rich on Rotation 1608. On that rotation, a long-lived high speed stream associated with a developing coronal hole began its evolution at ~ 300° longitude.

3. Helium and Medium Stream Associations. To summarize these evolutionary pattern more concisely, we have prepared two summary charts in Figures 3a-b.

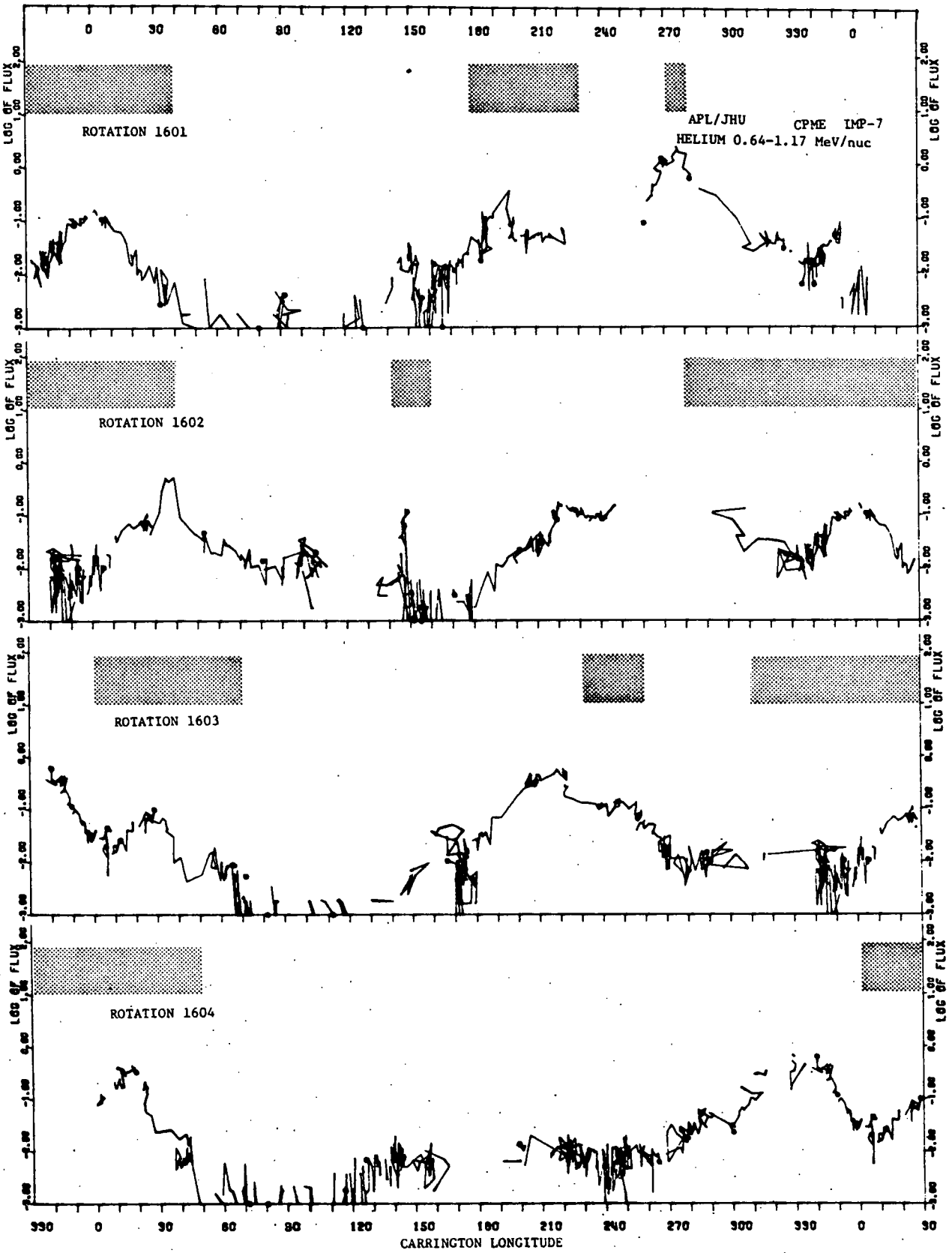

Figure 1. Inferred coronal injection Helium profiles (1601-1604). Helium-rich regions are cross-hatched.

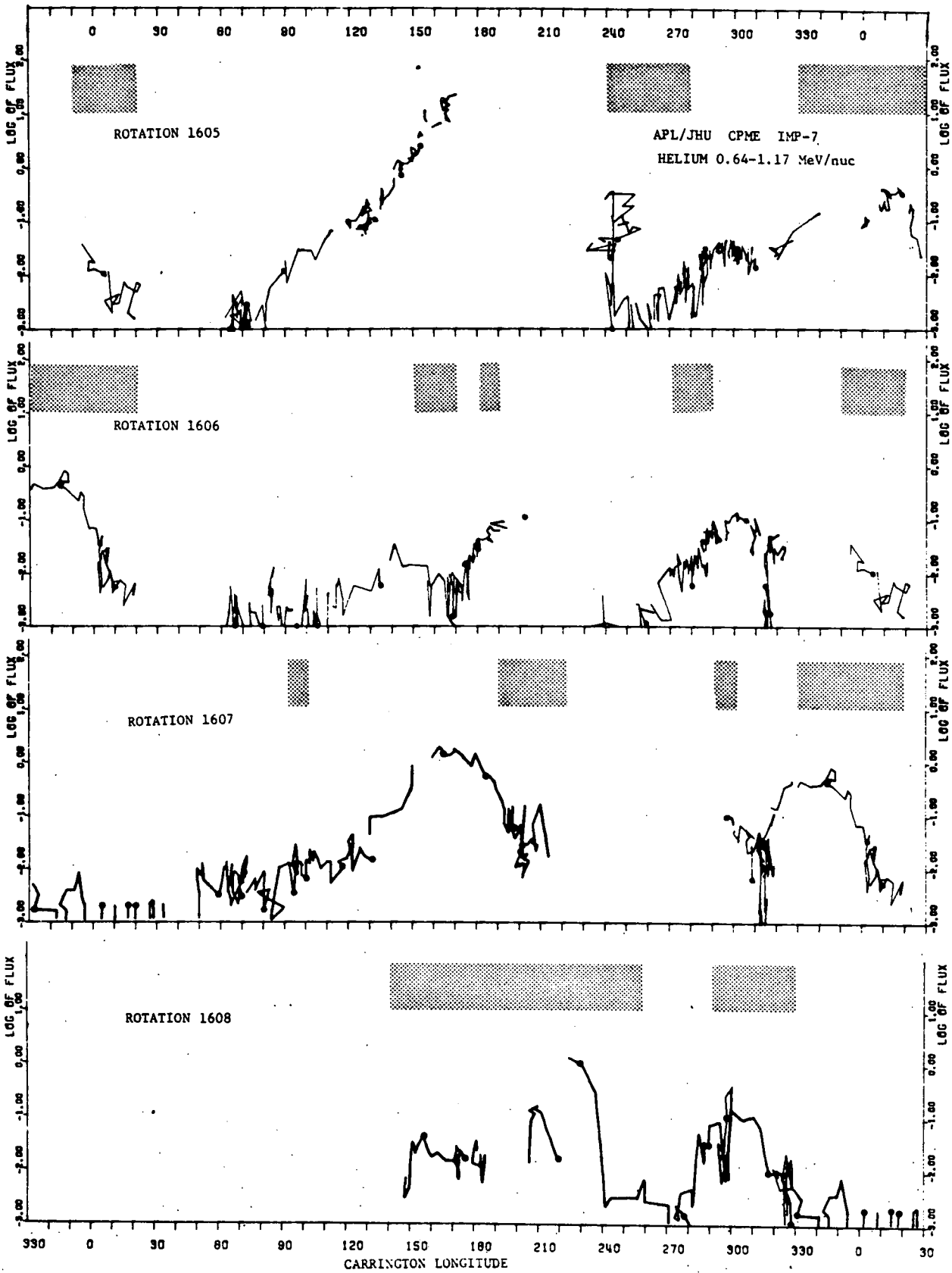

Figure 2. Inferred coronal injection Helium profiles (1605-1608). Helium-rich regions are cross-hatched.

Figure 3a (upper) shows the longitudes of the equatorial extent of coronal holes and the estimated high-coronal emission longitudes of high speed solar wind streams for each rotation (data taken from Krieger et al, 1975). Also indicated are the HEOS-2 interplanetary magnetic field polarities. From magnetograms, it is found that the polarity of the coronal hole near $\sim 0°$ is predominantly positive in the photosphere, while the developing hole (not discussed here) at $\sim 90°$ is negative in the photosphere. The interplanetary polarities show general agreement. The lower panel (Figure 3b) summarizes the observations of Helium streams A and B, with bars indicating the regions that are Helium-rich. Also shown are the CPME measurements of particles $Z \geq 3$ (0.77-3.2 MeV). It is clear that stream A is also rich in medium nuclei with intensities $> 10^{-3}$ $(cm^2\ s\ ster\ MeV/nuc)^{-1}$.

Note that as hole 1 wanes on Rotation 1607, so does stream A, but also that stream B becomes both Helium-and medium-rich on the same Rotation (1608) when the new recurrent high-speed solar wind stream begins its development. On the other hand, the solar wind stream at $\sim 90°$ which first appeared on Rotation 1603 (with what might be a negative polarity precursor $\sim 60°$ on 1602), does not develop a Helium-rich stream until four rotations later.

4. Conclusions. The associations of recurrent Helium and medium energetic particle streams with coronal structures deduced from x-ray photographs form a striking pattern, although not an exact one. None-the-less, the coronal ordering of these low-intensity, low energy nuclei suggests to us that they may be more representative of coronal "solar abundances" than flare particles, and consequently these recurrent streams should not be called "Helium-rich" compared to flare events, but rather solar flare populations should be regarded as "proton-rich" compared to these quiet-time fluxes.

5. Acknowledgments. The research at APL/JHU was partially supported by NASA grant NSG7055 and NASA contract N00017-72-C-4401, while E.C.R. was partially supported by Air Force Cambridge Research Laboratories contract F19628-73-C-0070 (although support does not necessarily imply endorsement). Research at AS&E was carried out under NASA contract NAS8-27758 from Marshall Space Flight Center. The IMP 7 solar wind data were graciously provided by A.J. Lazarus and J.D. Sullivan.

References.

Armstrong, T. P. and S. M. Krimigis, J. Geophys. Res., 76, 4230, 1971.
Gold, R. E., E. C. Roelof, J. T. Nolte and A. S. Krieger, Proc. 14th Int'l. Cosmic Ray Conf., Munich, MG 5-10, 1975.
Krieger, A. S., J. T. Nolte, P. S. McIntosh, A. J. Lazarus, J. D. Sullivan, R. E. Gold and E. C. Roelof, Proc. 14th Int'l. Cosmic Ray Conf., Munich, SP 4-4, 1975.
Lanzerotti, L. J. and C. G. Maclennan, J. Geophys. Res., 78, 3935, 1973.
Nolte, J. T. and E. C. Roelof, Solar Phys., 33, 241, 1973a.
Nolte, J. T. and E. C. Roelof, Solar Phys., 33, 483, 1973b.
Roelof, E. C. and S. M. Krimigis, J. Geophys. Res., 78, 5375, 1973.
Roelof, E. C., R. E. Gold, S. M. Krimigis, A. S. Krieger, J. T. Nolte, P. S. McIntosh, A. J. Lazarus and J. D. Sullivan, Proc. 14th Int'l. Cosmic Ray Conf., Munich, SP 4-5, 1975.
Sarris, E.T, S.M.Krimigis and T.P.Armstrong, J.Geophys.Res., 80, in press, 1975.

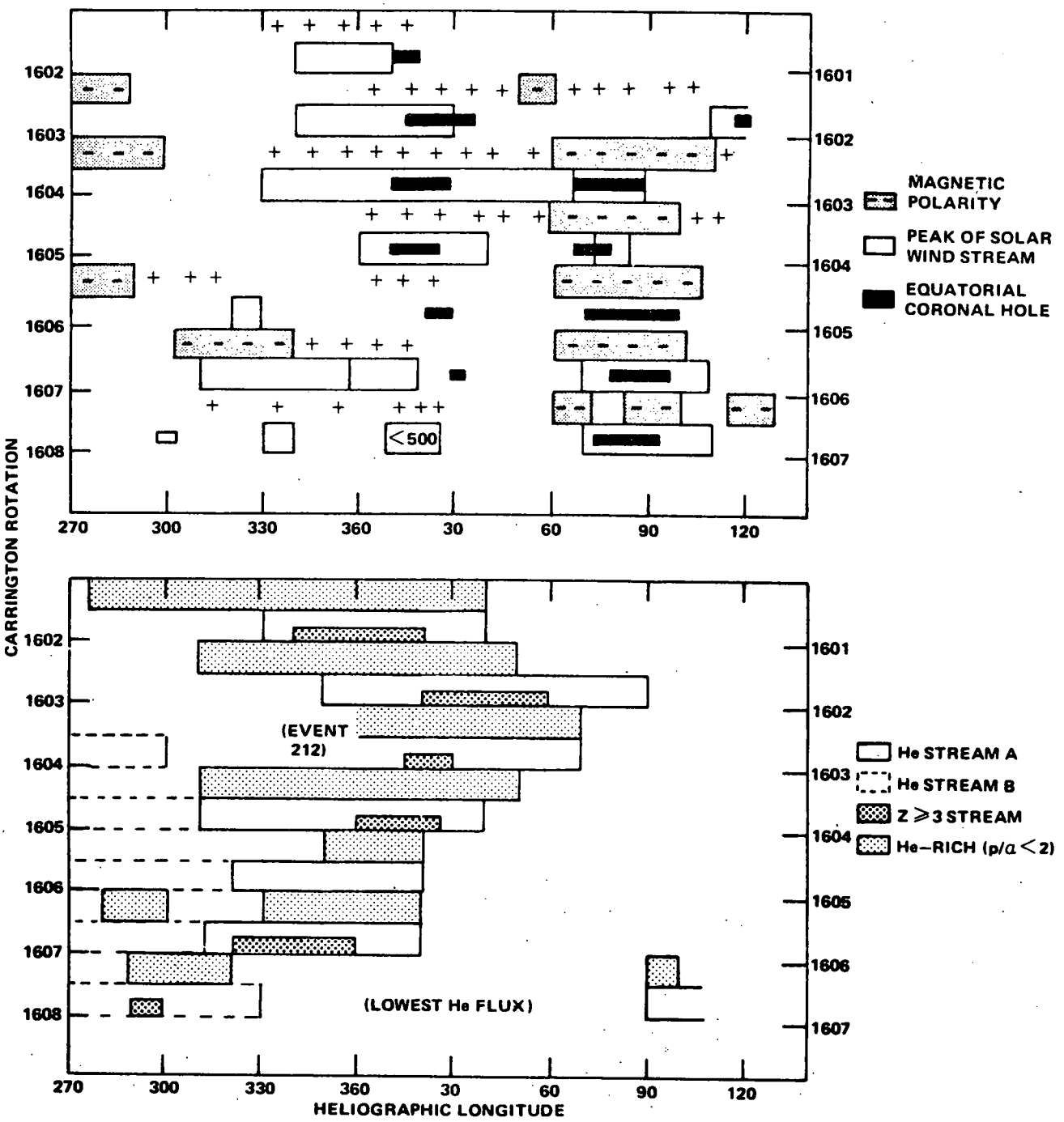

Figure 3. (a) Summary of structure and evolution solar wind streams interplanetary magnetic field polarity and equatorial extent of coronal holes (1601-1608). (b) Summary of energetic Helium streams, Helium-rich regions, and medium-rich regions (1601-1608).

RELATION OF LARGE-SCALE CORONAL X-RAY STRUCTURE AND COSMIC RAYS: 4. AMPLITUDE OF THE DIURNAL VARIATION IN NEUTRON MONITORS ON INTERPLANETARY FIELD LINES ORBITING ABOVE CORONAL HOLES

E. C. Roelof and R. E. Gold
Applied Physics Laboratory, The Johns Hopkins University
Laurel, Md. 20810, USA

A. S. Krieger and J. T. Nolte
American Science and Engineering, Inc.
Cambridge, Massachusetts, USA

D. Venkatesan
Department of Physics, University of Calgary
Calgary, Alberta, Canada

We have studied the amplitude of the diurnal variations in the Sulphur Mountain superneutron monitor as a function of the high-coronal connection longitude of the interplanetary field lines passing over Earth. The AS&E Skylab soft x-ray photographs (3-32 Å and 44-54 Å) have been scanned along an equatorial swath (N10° to S10°) for Carrington Rotations 1601-1608. Using hour-averages of solar wind velocity from the MIT experiment on IMP-7 we have estimated the high coronal connection longitude of the interplanetary magnetic lines, and find that the amplitude of the diurnal variation is biased toward below average values (< 0.4%) over coronal holes, and toward high values (> 0.4%) over bright regions. The results are consistent with the theoretical argument (Roelof 1975) that the diurnal variation is influenced by the ability of the corona to sustain a meridional cosmic ray gradient set up by the motional EMF in interplanetary space.

1. Introduction. In a comparison paper (Roelof, 1975) we argue that a substantial body of evidence implies coronal controlof cosmic-ray propagation, consequently a theory of the diurnal variation is introduced which is based on two straight forward requirements. First, Stern (1964) pointed out that in a time-independent interplanetary magnetic field, there will be no cosmic-ray anisotropy because the drift due to the motional EMF is cancelled by a meridional intensity gradient. Therefore Parker (1964) and Axford (1965a) suggested that cross-field diffusion (beyond 1 AU) "relaxed" the gradient. However, recent analyses of ground-level flare particle events (Duggal et al., 1971; Duggal and Pomerantz, 1972,1973; Maurer et al., 1973) have revealed persistent flux anisotropies that are inconsistent with significant scattering inside 1 AU, while at lower energies Lanzerotti (1973), Reinhard and Roelof (1973) and Reinhard and Wibberenz (1974) have substantiated the existence of coronal transport suggested by Reid (1964) and Axford (1965b). Therefore, why shouldn't galactic cosmic-rays experience coronal transport? If so, then at solar longitudes where coronal transport is effective, any interplanetary latitudinal gradient which the interplanetary polarization field would tend to establish could be relaxed in the corona, and the result would be the detection of a "corotating" flow as a diurnal variation when the interplanetary field lines originating above the transport region pass over the Earth. On the other hand, if transport is inhibited in a coronal region, then the interplanetary gradient can be

sustained in the corona, and if, in addition, the gradient is not relaxed beyond the Earth, no significant diurnal variation would be observed when this coronal region is magnetically connected to the Earth.

The next question is: Where is coronal cosmic-ray transport most likely to be effective, and where is it possibly inhibited? It has now been observationally established by the Skylab missions that, while bright closed loop structures observed in 3-32 Å and 44-54 Å x-rays extend a significant fraction of 1 $R_\odot$ into the low corona, there are few closed structures observed in low emission features called coronal holes (Munro and Withbroe, 1972; Krieger et al., 1973, 1974, 1975; Timothy et al., 1975). These studies have also demonstrated that the magnetic structure above coronal holes is likely to be "open" in comparison to the "closed" loop structure above active regions. It then seems that a reasonable hypothesis to test is that the observed diurnal variation should tend to be "normal" over closed magnetic structure (where coronal transport may take place via the interconnecting loop structure), while it should tend toward small amplitudes over open structure, i.e., coronal holes.

2. Observations. We have therefore taken the American Science and Engineering synoptic x-ray photographs for the Skylab period covering Carrington Rotation 1601-1608 (see Figure 1 of Krieger et al., 1975) and assigned an x-ray emissivity level to each 10° longitude bin extending from N10° to S10°. Four levels were used: (1) bright; (2) moderate; (3) weak; and (4) hole. We assigned these by eye, and the levels characterize the bins in the following sense. If a bin contains part of a bright x-ray plage or coronal hole, it was assigned the level "bright", or "hole" eventhough there may have been less intense emission levels near the plage, or more intense emission adjacent to the hole. On the other hand, the levels "moderate" and "weak" refer to the best estimate of the average intensity over the bin. Moreover, due to our growing conviction that the holes map out into diverging structures in the outer corona (Krieger et al., 1975), we also assigned a "hole" category to the bins immediately adjoining the equatorial coronal holes.

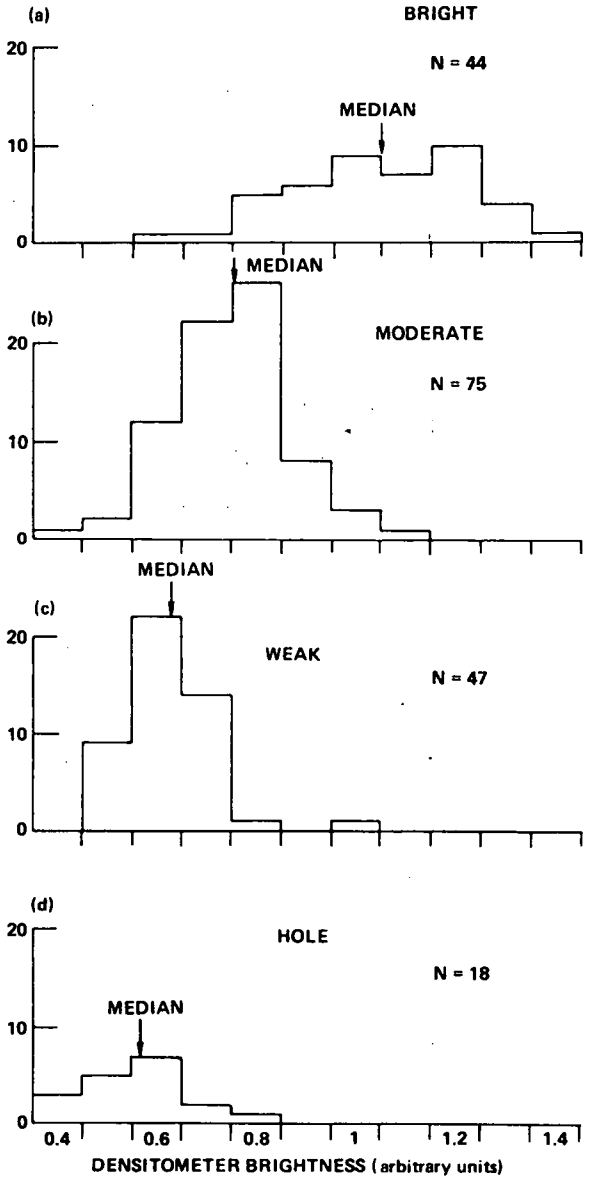

Figure 1. Comparison of four assigned x-ray intensity levels and representative densitometers reading for each 10° longitude bin.

Although we believe this procedure to yield more representative indicators of "open" or "closed" structure (i.e., hole and weak bins or moderate and bright bins, respectively), we have made a quantitative comparison of our level assignments with representative photographic densitometer measurements from the negatives of the synoptic charts (See Figure 1 of Krieger et al., 1975). Histograms of representative densitometer readings for each of the four emission level categories are shown in Figures 1a-1d. As expected, the distribution for the "bright" level is broad (since the bins usually also contain less intense emission), and the "weak" and "hole" distributions are similar (since "hole" bins often also contain weak emission). Nonetheless, the medians as well as lower and upper ranges show a clearly decreasing trend as one goes from "bright" to "hole".

The next step is to estimate the longitude of the origin of the interplanetary magnetic field line in the high corona (i.e., above the MHD critical points). In a number of studies, beginning with that of Krimigis and Roelof (1973), we have utilized a straight-forward method first suggested by Snyder and Neugebauer (1966) and justified theoretically by Nolte and Roelof (1973a, 1973b) and by multispacecraft correlations by Gold and Roelof (1975). The EQRH (extrapolated quasi-radial hypervelocity) approximation states that the high-coronal connection longitude of the large-scale interplanetary field may be calculated as if the solar wind carried out the "frozen-in" field for 1 AU at a constant velocity equal to the observed velocity. The approximation remains valid (to $\sim 10°$) because the neglected effects of plasma co-rotation (inside the critical points) and acceleration tend to cancel. Weber and Davis (1967) have estimated the altitude of these points as 20-50 $R_\odot$.

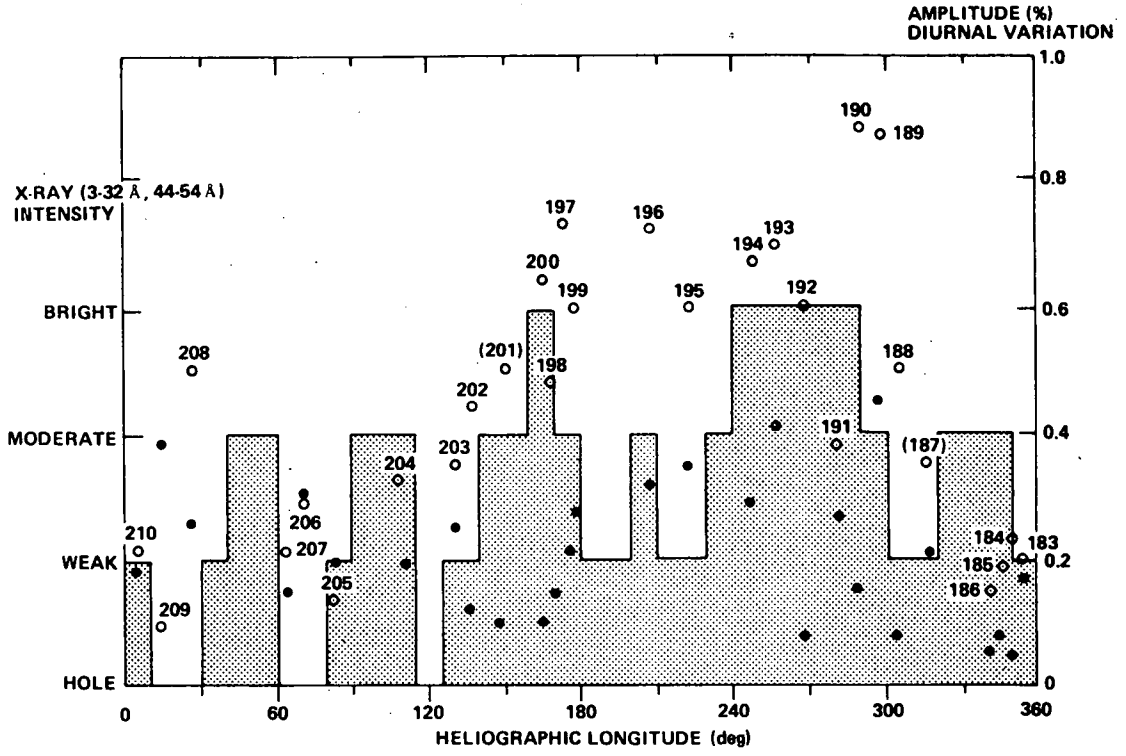

Figure 2. X-ray intensity levels and EQRH-mapped amplitudes of first (large symbols, labelled by day of observation,1975) and second harmonic of diurnal variation for Carrington Rotation 1603.

The connection longitudes at 00 UT on each day during rotation 1601-1608 were calculated from the MIT solar wind velocity measurements from IMP-7. The data set used covered days 153 to 299, 1973, corresponding to the AS&E x-ray coverage. We then associated the amplitude of the diurnal variation measured on that day by the Sulphur Mountain neutron monitor (vertical cutoff rigidity 1.09 GV) with the estimated high coronal connection longitude.

The time 00 UT was chosen since it is approximately the time of the maximum of the diurnal wave at Sulphur Mountain. A plot of the EQRH-mapped amplitudes of the first harmonic of the diurnal variation versus heliographic longitude is shown in Figure 2 for Rotation 1603 (days 182-210). Also indicated are the assigned x-ray emission levels and the amplitude of the second harmonic (provided as an indication of the purity of the diurnal wave). One easily perceives the trend on this Rotation for low diurnal amplitudes to be associated with the recurrent holes (10°-30° and 60°-80°), and conversely for high amplitudes to fall over the broad regions of moderate and bright emission. However, the relationship is not always as obvious as on this Rotation, so a statistical analysis is called for.

3. Discussion. In Figures 3a-3d, the number of occurrences of the first harmonic amplitudes in steps of 0.1% are plotted for each level of x-ray intensity in the longitude bins in which the EQRH connection longitude falls. The distributions differ significantly and systematically, as shown by both the ranges and the medians. The lack of amplitudes 0.0-0.1% is attributed to no days having perfectly constant counting rates, i.e., it is due to the minimal statistical RMS variation in the hourly counts.

Recall that the theoretically expected amplitude for pure corotation is $\simeq$ 0.7% for a mid-latitude station, and that the long-term observed average is $\simeq$ 0.4 to 0.5%. Particularly the "hole" distribution (and also the "weak" region), is rich in below-average amplitudes (0.1-0.5%) and deficient in large amplitudes, showing none above 0.7%. On the other hand, the "moderate" and "bright" regions have median amplitudes $\simeq$ 0.5%, and show extended tails above 0.7%.

Since some recurrent high-speed solar wind streams have been associated with recurrent coronal holes (Krieger et al., 1973, 1974, 1975; Timothy et al., 1975), these distributions might imply an association not between holes and small amplitudes, but rather between high speed streams and lower amplitudes. However, we can show here that this conjecture is not substantiated by the data from this period. The shaded histograms in Figures 3a-3d are the subsets of each emission level which occur in the peaks of high speed streams. Firstly, stream peaks occur over all ranges of x-ray emissions, as anticipated from the emphatic

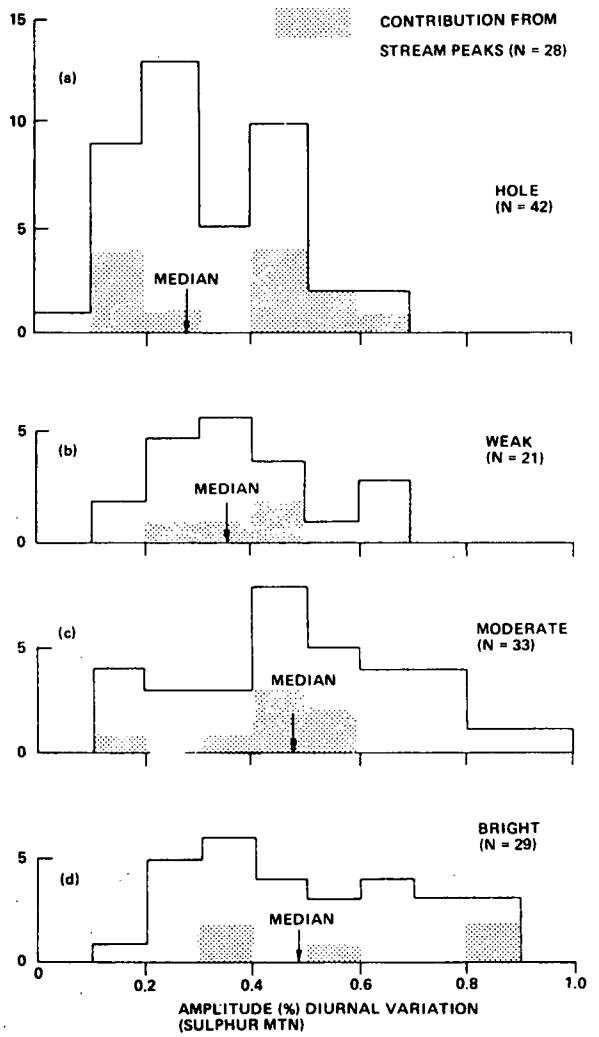

Figure 3. Distributions for 1601-1608.

statements of Krieger et al. (1974) and Timothy et al. (1975) that the relationship between holes and streams is not strictly one-to-one. Secondly, the subset histograms are a reasonably distributed sample of the main histrograms, and hence show no tendencies different from those of the main distribution.

The statistical trend is also revealed in the complementary representation of the number of occurrences of each x-ray emission level for given intervals of 0.1% in amplitude. These are shown in Figure 4 and there is a clear tendency for the association of below-average amplitude (< 0.5%) "hole" and "weak" x-ray emission, and above-average amplitudes with "moderate" and "bright" x-ray emission. Once again the contribution from stream peaks (shaded histograms) appear to be an unbiased subset of the main histograms.

4. Conclusions. We therefore conclude that the AS&E Skylab x-ray measurements of equatorial emission are consistent with the hypothesis that the amplitude of the diurnal variation is controlled, at least in part, directly by the magnetic structure of the high corona. The mechanism, in brief, is that over "closed" structures (indicated in the low corona by bright x-ray plage and closed loops), cosmic ray transport is enhanced and thereby relaxes the latitudinal interplanetary gradient that the polarization electric field tends to establish. On the other hand, over "open" structures (indicated by coronal holes and high-lying weak emission features), latitudinal cosmic-ray transport is inhibited, and the interplanetary gradient is sustained. By the arguments of Stern (1964), the latitudinal gradient in the E-direction works to cancel the "co-rotation" anisotropy (see Roelof, 1975), and hence lower amplitude diurnal waves are expected over "open" coronal structures, and conversely, higher amplitudes over "closed" structures. Since the theory only requires a mechanism for reducing the latitudinal gradient, there is no need (or inference) of transverse diffusion near 1 AU (which in any case is inconsistent with observations of relativistic solar cosmic rays).

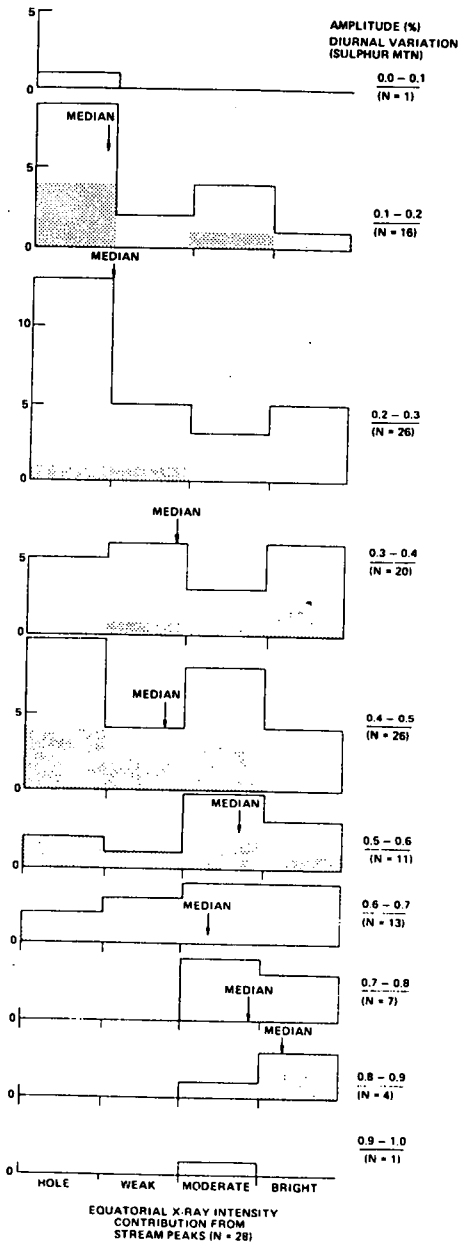

Figure 4. Comparison of frequency of occurrence of x-ray emission level for each amplitude range of diurnal variation on Rotations 1601-1608.

Of course, one could invoke some relation between weak coronal emission regions and small cross-field interplanetary diffusion beyond 1 AU (and vice versa for bright emission regions). However, the demonstrated lack of association with solar stream structure suggest to us that this is not a fruitful line of inquiry. Moreover, we see no need for invoking another (unspecified) mechanism when there is the simple mechanism at hand of coronal transport, a mechanism which is already independently implied by solar cosmic-ray transport.

Acknowledgements. The research at APL/JHU was partially supported by Air Force Cambridge Laboratories Contract F19628-73-C-0070 (although support does not necessarily imply endorsement) and by NASA grant NSG 7055, while the research at AS&E was supported by NASA, Marshall Space Flight Center Contract NAS-8-27758. The MIT solar wind data was graciously provided by A. J. Lazarus and J. D. Sullivan.

References.

Axford, W. I., Planet Space Sci, 13, 115, 1965a.
Axford, W. I., Planet Space Sci, 13,1301, 1965b.
Duggal, S. P., I. Guidi and M. A. Pomerantz, Solar Phys., 19, 234, 1971.
Duggal, S. P. and M. A. Pomerantz, Solar Phys., 27, 227, 1972.
Duggal, S. P. and M. A. Pomerantz, J. Geophys. Res., 78, 7205, 1973.
Gold, R. E. and E. C. Roelof, submitted to Solar Phys., 1975.
Krieger, A. S., A. F. Timothy and E. C. Roelof, Solar Phys., 23, 123, 1973.
Krieger, A. S., A. F. Timothy, G. S. Vaiana, A. J. Lazarus and J. D. Sullivan, Solar Wind Three, ed. C. T. Russell, Institute of Geophysics and Planetary Physics, University of California (Los Angeles), 132, 1974.
Krieger, A. S., J. T. Nolte, P. S. McIntosh, A. J. Lazarus, J. D. Sullivan, R. E. Gold and E. C. Roelof, Proc. 14th Int'l.Cosmic Rays Conf.(Munich)SP4-4,1975.
Lanzerotti, L. J., J. Geophys. Res., 78, 3942, 1973.
Maurer, R. H., S. P. Duggal and M. A. Pomerantz, J. Geophys. Res., 78, 29, 1973.
Munro, R. H. and G. L. Withbroe, Astrophys. J., 176, 511, 1972.
Nolte, J. T. and E. C. Roelof, Solar Phys., 33, 241, 1973a.
Nolte, J. T. and E. C. Roelof, Solar Phys., 33, 483, 1973b.
Parker, E. N., Planet. Space Sci., 12, 735, 1964.
Reid, G. C., J. Geophys. Res., 69, 2659, 1964.
Reinhard, R. and E. C. Roelof, Proc. 13th Int'l.Cosmic Ray Conf., 2, 1378, 1973.
Reinhard, R. and G. Wibberenz, Solar Phys.,36, 473, 1974.
Roelof, E. C., Proc. 14th Int'l.Cosmic Ray Conf.,(Munich), SP 5.1-1, 1975.
Roelof, E. C. and S. M. Krimigis, J. Geophys. Res., 78, 5375, 1973.
Snyder, C. W. and M. Neugebauer, Solar Wind (ed., R. J. Mackin and M. Neugebauer) Pergamon Press, 25, 1966.
Stern, D., Planet. Space Sci., 12, 973, 1964.
Timothy, A. F., A. S. Krieger and G. S. Vaiana, Solar Phys., in press, 1975.
Weber, E. J. and L. Davis, Jr., Astrophys. J., 148, 217, 1967.

RELATION OF LARGE-SCALE CORONAL X-RAY STRUCTURE AND COSMIC RAYS: 5. SOLAR WIND AND CORONAL INFLUENCE ON A FORBUSH DECREASE LASTING ONE SOLAR ROTATION

R. E. Gold and E. C. Roelof
Applied Physics Laboratory, The Johns Hopkins University
Laurel, Md. 20810, USA

J. T. Nolte and A. S. Krieger
American Science and Engineering, Inc.
Cambridge, Massachusetts, USA

The 3B solar flare on July 29, 1973 was the largest during the Skylab mission. Low energy solar particles and galactic cosmic rays exhibited large scale spatial gradients over 5 orders of magnitude in energy during the event decay and recovery of the associated Forbush decrease. The low energy proton gradient of ~ 2% per degree of solar longitude persisted over ~ 100°. Similar spatial gradients were observed in ≥ 0.64 MeV/nuc Helium and ≥ 0.22 MeV electrons. The spatial nature of the Forbush decrease was confirmed by Pioneer 9 observations. The lack of dependence on charge, energy or rigidity suggests an $\underline{E} \times \underline{B}$ drift. Yet comparisons with coronal x-ray photographs show no obvious associations with coronal structure.

1. Introduction. Observations of persistent anisotropies lasting well into the decay of solar events from 300 keV protons (Roelof and Krimigis, 1973; Innanen and Van Allen, 1973) to neutron monitor ground level events (Duggal et al., 1971; Duggal and Pomerantz, 1971; Maurer et al., 1973) imply that there is little interplanetary scattering of cosmic rays inside 1 AU. Scatter-free propagation (Nolte, 1974; Nolte and Roelof, 1975; Roelof, 1975) inside 1 AU means that the time intensity profiles of particles throughout this energy range are not primarily controlled by local interplanetary conditions but rather by sources and sinks where the field lines tie to the corona and outer modulating region. And since the corona very efficiently controls the distribution of low energy particles it is not unreasonable to expect some coronal influence to extend to neutron monitor energies. We have examined a solar particle event with an associated Forbush decrease that occurred during the Skylab mission and find it to be a clear example of scatter free propagation under coronal control over 5 orders of magnitude in particle energy. In this event the decay of low energy solar particles and the recovery of the Forbush decrease are predominantly spatial structures.

2. Solar Particle Observations. The first 7 solar rotations of the Skylab mission (Carrington Rotation 1601-1608; May-October 1973) produced few large solar flares and only 2 sizable solar particle events. The largest flare of the period was of $H\alpha$ importance 3B and x-ray class M7 at 1313 UT on July 29 (day 210). The flare was in the spotless McMath plage region 12461 at N14, E45. This plage region may be seen as a bright area in the northern hemisphere at 270° Carrington longitude in the American Science and Engineering "orange peel" synoptic chart of solar soft x-rays (3-32 Å and 44-54 Å) (Krieger et al., 1975) in Figure 1. The synoptic chart is constructed from central meridian lunes of the full

disk photographs and covers portions of solar rotations 1603 and 1604 from central meridian passage day 200 through 229 (July 19-August 17).

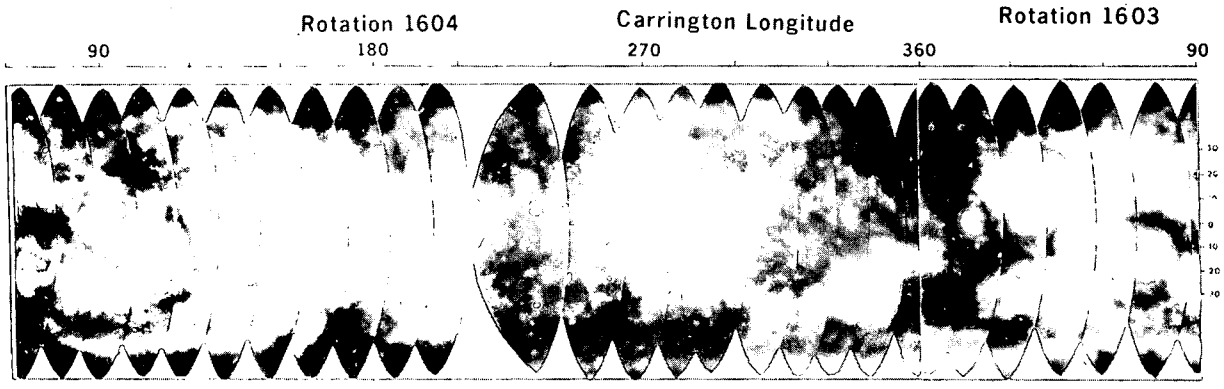

Figure 1. Snoptic chart of solar soft x-rays.

Particle observations may be related to the coronal structure revealed in the x-ray photographs by plotting the particle intensities versus their Carrington longitude injection profile in the high corona. This mapping is based on the approximation suggested by Snyder and Neugebauer (1966) that the plasma in which the magnetic field is frozen moves out radially from the sun with constant velocity. Nolte and Roelof (1973) and Gold and Roelof (1975) have shown that this approximation is probably accurate to within 10° of Carrington lontitude. Low energy solar particle fluxes observed during solar rotation 1604 by the Applied Physics Laboratory Charged Particle Monitoring Experiment (Sarris et al., 1975) on the IMP-7 spacecraft are displayed as a function of their solar connection longitude in Figure 2. The similar profiles of the three species are obivous. The bottom panel of the figure shows the 220 keV to 2.5 MeV electron onset at 1400 UT on day 210 when the spacecraft was connected at about 355°. The 0.29 to 0.50 MeV protons in the top panel and the 0.64 to 1.17 MeV alphas in the middle panel show the slower rise times normally associated with eastern hemisphere flares.

If the solar wind velocity were to decrease for a period of time at a rate that would keep the connection longitude nearly constant the observed particle flux during this "dwell" would be dominated by the temporal features of the injection. Conversely, if the solar wind velocity increased relatively quickly and the connection longitude shifted rapidly, spatial structure would predominate. Furthermore, if there were a smooth spatial gradient in the coronal injection profile but the solar wind velocity alternately increased and decreased, the observed particle time profile would resemble a staircase. The stepped time history for a similar event is shown in Figure 1 of Roelof et al. (1975). But the connection longitude mapped profile would simply replicate the smooth gradient. The solar particle fluxes observed during the decay of this event clearly display this phenomenon. From the peak of the event to the beginning of day 216 the decay may be predominantly temporal however, following this the decay is clearly spatial.

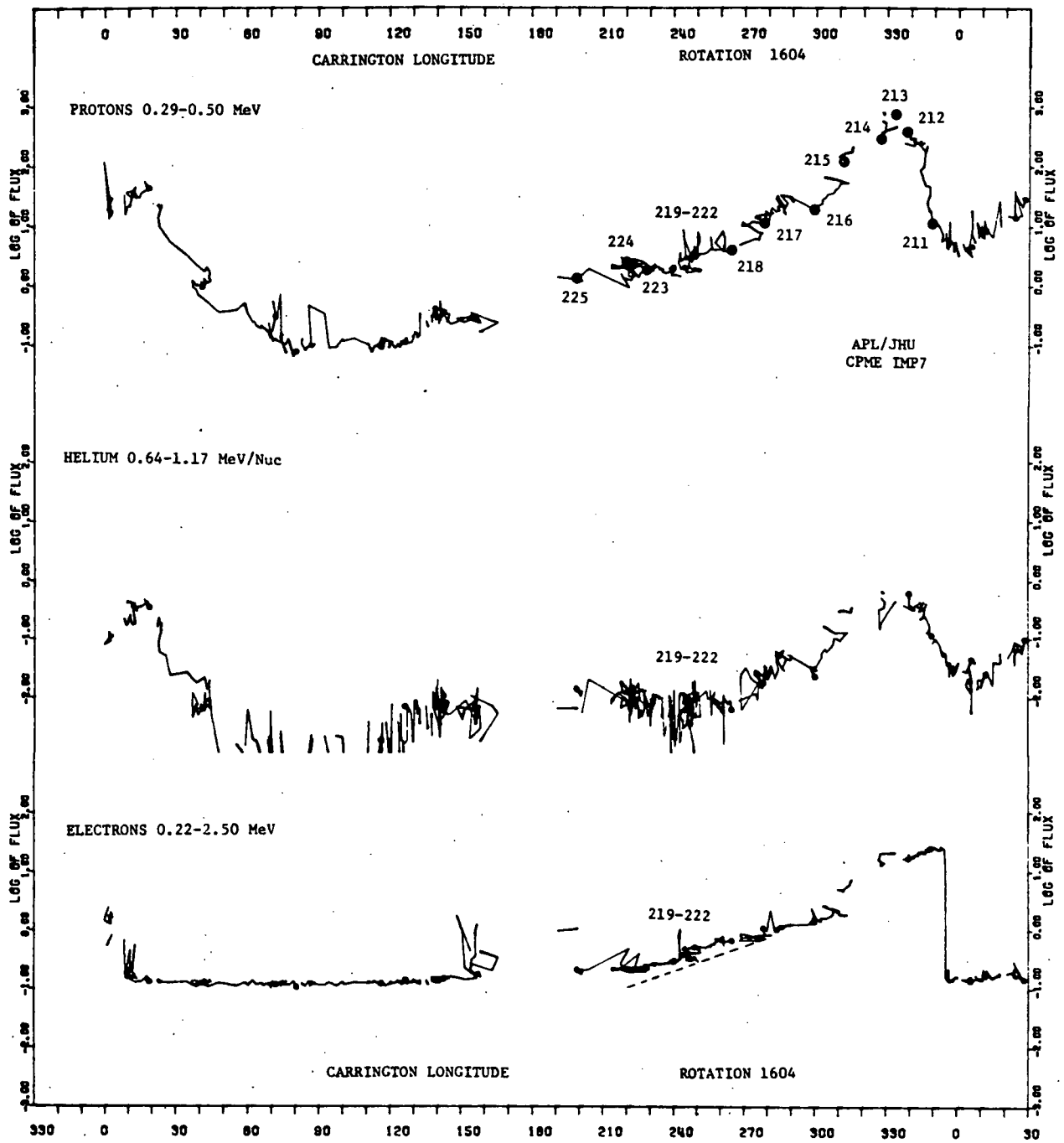

Figure 2. Coronal injection profile of low energy solar particles labelled by the day of observation.

The day numbers in Figure 2 show that the connection longitude dwelled at ~ 250° from day 219 to 222 and the observed flux was nearly constant over these three days. Yet, the injection profile is relatively smooth from day 216 to 225 indicating a coronal gradient of ~ 2% per degree in the 0.29 to 0.50 MeV protons

extending over 100% of solar longitude. The Helium and relativistic electron gradients are both strikingly similar to the protons. The dashed line in the electron fluxes in a background corrected estimate.

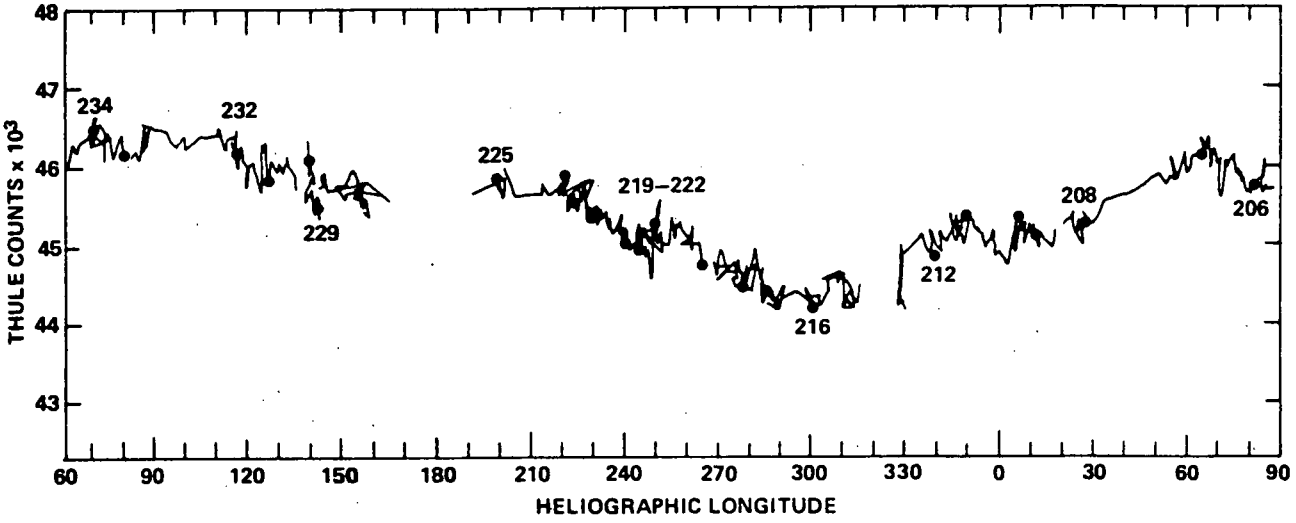

Figure 3. Thule neutron monitor counting rate plotted at its coronal connection longitude.

3. Galactic Cosmic Ray Modulation. If the galactic cosmic rays were scatter free inside 1 AU we might expect their modulation to exhibit the effects of the coronal gradient seen in the low energy solar particles. And indeed there is a spatial gradient in the recovery of the Forbush decrease as shown by the mapped Thule neutron monitor counting rates in Figure 3. This figure covers the same longitude range as the x-ray photographs in Figure 1 and the spatial gradient in the recovery of the Forbush decrease from day 216 to 225 is obvious. The figure actually starts with a broad shallow decrease on day 207 that is coincident with the sweep of a solar wind stream associated with the large coronal hole between 5 and 30°. The onset of the flare associated Forbush decrease occurred at ~ 0000 UT of day 213 and is not shown in Figure 3 since no solar wind velocity was available because IMP-7 was inside the magnetosphere.

The spatial nature of the Forbush decrease is further confirmed by limited observations available from Pioneer 9 which was about 40° west of the earth-sun line. The earth was connected to the corona at ~ 320° on day 213 at the minimum of the Forbush decrease. Yet no decrease was observed in the > 13.9 and > 40 MeV proton channels on Pioneer 9 which was connected near 0° at that time. However, a sizeable decrease was observed at Pioneer 9 on day 220 when its connection longitude had shifted to ~ 300°, near the start of the gradient seen at earth.

Prior to the onset of the Forbush decrease there was another important manifestation of scatter free propagation, the Forbush predecrease (Gold and Peacock, 1973). The predecrease resulted from a depletion of cosmic rays in a pitch angle cone $\leq 90°$ in asymptotic longitude along the magnetic field line toward the sun. The field aligned predecrease was observed at least 12 hours before the world wide Forbush decrease onset. The predecrease was most pronounced at high rigidities and was observed by equatorial neutron monitors. The Denver muon monitor has a median response of $\sim$ 55 GV. It observed a predecreases significantly larger than the Forbush decrease which followed.

4. Coronal Structure. The coronal gradient between 200 and 300° Carrington longitude on solar rotation 1604 was effective over at least five orders of magnitude in energy. This amazing structure is also nearly independent of the sign of the charge and the velocity of the particles. Roelof et al. (1975) have shown a similar phenomenon. The lack of dependence on charge, energy and velocity suggests an $\underline{E} \times \underline{B}$ drift. However, when we compare the longitude of the gradient with the underlying coronal structure revealed in the x-ray photographs in Figure 1 we find no obvious correlations since gradient extends over the magnetically closed structures signified by the bright plage of the active region as well as the whispy, relatively open structures east of the active region.

5. Acknowledgements. The authors are indebted to Dr. M. A. Pomerantz who kindly supplied the Thule data and to Dr. R. L. Chasson and Mr. T. G. Crabbe for the Denver Muon data. The solar wind data was supplied by Drs. A. Lazarus and J. D. Sullivan. The research at JHU/APL was partially supported by NASA Grant NSG 7055 and Air Force Cambridge Research Laboratories Contract F19628-73-C-0070. The research at AS&E was supported by NASA, Marshall Space Flight Center Contract NAS-8-27758.

6. References.

Duggal, S. P., I. Guidi and M. A. Pomerantz, The unusual anisctropic solar particle event of November 18, 1968, Solar Phys., 19, 234, 1971.

Duggal, S. P. and M. A. Pomerantz, Anisotropies in relativistic cosmic rays from the invisible disk of the sun, J. Geophys. Res., 78, 7205, 1973.

Gold, R. E. and E. C. Roelof, Inference of the equatorial high coronal magnetic field polarity from interplanetary measurements, submitted to Solar Phys., 1975.

Innanen, W. G. and J. A. Van Allen, Anisotropies in the interplanetary intensity of solar protons Ep > 0.3 MeV, J. Geophys. Res., 78, 1019, 1973.

Krieger, A. S., J. T. Nolte, P. S. McIntosh, A. J. Lazarus, J. D. Sullivan, R. E. Gold and E. C. Roelof, Relation of large-scale coronal x-ray structure and cosmic rays: 1. Sources of solar wind streams and Hα absorbtion features, Proc. 14th International Cosmic Ray Conference, Munich, SP 4-4, 1975.

Maurer, R. H., S.P. Duggal and M. A. Pomerantz, Pitch angle diffusion of solar flare particles in interplanetary space, J. Geophys. Res., 78, 29, 1973.

McIntosh, P. S., H-alpha synoptic charts of solar activity for the period of Skylab observations May 1973-March 1974, Upper Atmosphere Geophysics Report UAG-40, Environmental data Service, National Oceanographic and Atmospheric Administration, 1975.

Nolte, J. T. and E. C. Roelof, Large-scale structure of the interplanetary medium: 1. High coronal source longitude of the quiet-time solar wind, Solar Phys., 33, 241, 1973.

Nolte, J. T., Interrelationship of energetic particles, plasma and magnetic fields in the inner heliosphere, Ph.D. Thesis, University of New Hampshire, Durham, New Hampshire, 1974.

Nolte, J. T. and E. C. Roelof, Mathematical formulation of scatter-free propagation of solar cosmic rays, Proceedings of the 14th International Cosmic Ray Conference, Munich, SP 5.1-2, 1975.

Roelof, E. C. and S. M. Krimigis, Analysis and synthesis of coronal and interplanetary energetic particle, plasma, and magnetic field observations over three solar rotations, J. Geophys. Res., 78, 5375, 1973.

Roelof, E. C., R. E. Gold, S. M. Krimigis, A. S. Krieger, J. T. Nolte, P. S. McIntosh, A. J. Lazarus and J. D. Sullivan, Relation of large-scale coronal x-ray structure and cosmic rays: 2. Coronal control of interplanetary injection of 300 keV solar protons, Proceedings of the 14th International Cosmic Ray Conference, Munich, SP 4-5, 1975.

Roelof, E. C., Scatter-free collimated convection and cosmic ray transport at 1 AU, Proceedings of the 14th International Cosmic Rays Conference, Munich, SP 5.1-1, 1975.

Sarris, E. T., S. M. Krimigis and T. P. Armstrong, Observations of magnetospheric bursts of high energy protons and electrons at $\sim$ 35 R_e with IMP-7, submitted to J. Geophys. Res., 1975.

Snyder, C. W. and M. Neugebauer, The relation of Mariner II plasma data to solar phenomena, in Solar Wind, edited by R. J. Mackin and M. Neugebauer, pp. 25-32, Pergamon, New York, 1966.

VARIATIONS IN THE CHARGE COMPOSITION OF THE JULY 2-12, 1974, SOLAR PARTICLE EVENT

Thomas P. Armstrong
Department of Physics, University of Kansas
Lawrence, Kansas 66044, USA

Stamatios M. Krimigis
Applied Physics Laboratory/The Johns Hopkins University
Laurel, Md. 20810, USA

Large temporal and spatial variations of α, M-group and heavy nuclei have been measured with two spacecraft. SSC-associated variations of the M/H ratio are reported and discussed. Large changes in composition of solar particle fluxes in periods of a few minutes may make the interpretation of long-time averaged spectra and composition measurements very difficult.

1. Introduction. This paper is a report of simultaneous observations of the time variations of the composition of the solar particle event of July 3-6, 1974. The observations were made with two nearly identical solid-state detector telescopes in the Johns Hopkins University Applied Physics Laboratoty experiments aboard the NASA satellites Explorer 47 (IMP-7) and Explorer 50 (IMP-8). A comprehensive description of the instrumentation is available elsewhere (Sarris, Krimigis and Armstrong, 1975; Cashion et al., 1973) and only a few of the details will be given here. Table I summarizes the passbands and geometric factors for the channels we discuss here. The passbands quoted in the figures are for Explorer 47 and are nominally the same for Explorer 50; exact passbands for Explorer 50 are quoted in Table I. The design of the instrument was intended to provide good energy and composition measurements at time resolution adequate to study the fine scale interplanetary structure of particle events. As a result, we obtain measurements of proton, alpha and medium nuclei energy spectra. In addition, a single passband for heavy nuclei is monitored. The count rates are sectored as the spacecraft spin about an axis perpendicular to the ecliptic plane and angular distributions in the ecliptic plane can be obtained, although we use only the spin-averaged directional count rates and fluxes here.

The purpose of this study is to make an initial characterization of the morphology of the first relatively intense solar particle event occurring after the launch of Explorer 50 (October, 1973) so that simultaneous measurements could be made. Explorer 47 and 50 are in nominal 35 R_e low inclination circular orbits. For the period July 3-6, Explorer 50 was in the upstream interplanetary medium and Explorer 47 was passing through the dusk transition region. Explorer 47 probably did not enter the magnetopause during this period. In Section 2 we report what seem to us to be the most important of a variety of observed parameters. Section 3 gives our interpretation of the phenomena.

2. Observations. An overall summary of the interplanetary particle intensities for the period 2-7 July is given in Figure 1. Hourly averaged count rates for alphas, medium nuclei, and heavy ($Z > 20$) nuclei are shown along with the major flares and storm sudden commencements. The most active region on the sun at this time (McMath #13043, Solar-Geophysical Data #365 Pt. II) was at about E-28° central meridian distance at the beginning of this period and at about W-50°

at the end. Although several electron onsets were observed in association with flares. The period from 09:00 to 24:00 UT on July 5 was particularly scrutinized and no evidence of velocity dispersion in that flux increase was found. Representative error bars are shown for those regions of the count rate curves where statistical fluctuations are important. Note that the count rate profiles from the two spacecraft, although similar and overlapping in many places, have significant differences. Explorer 50 sees more M nuclei for the interval from the start of the available rates at 07:00 UT on July 4 until the major flux increase at 10:00 UT on July 5. Then there is a period when the M-nuclei rates are identical at the two spacecraft, followed by another interval of significant difference beginning at 18:00 UT on July 5 and persisting through the remainder of the event. There are also significant departures of the Heavy nuclei rates at the two spacecraft.

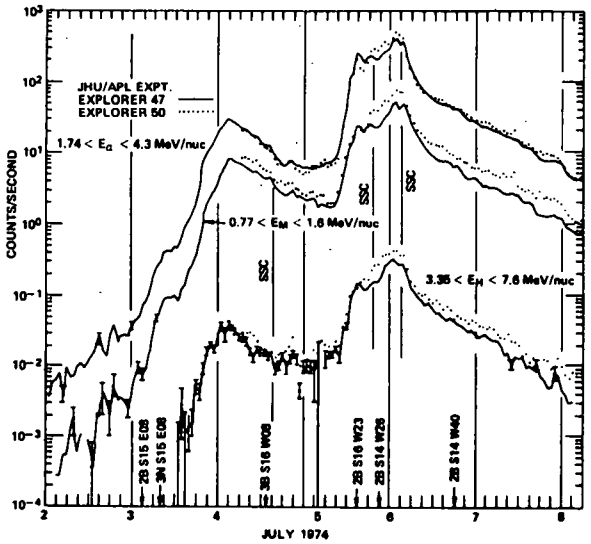

Figure 1 Hourly-averaged count rates for alphas, medium, and heavy nuclei from Explorers 47 and 50. Most important flares and SSC storm sudden commencements are shown.

An expanded, 5.5 minute averaged, version of the alpha and M-nuclei fluxes is shown in Figure 2. Here, all of the small corrections have been applied and the numbers plotted correspond to the best derivation of the differential fluxes at the specified energy/nucleon points. The salient features here are first, the fluxes at Explorer 50 are subject to much sharper temporal fluctuation than those at Explorer 47, especially in the period from 11:00-17:00 UT on July 5. During this period Explorer 50 is in the interplanetary medium while Explorer 47 is approaching the bow shock. Secondly, the occurrence of the SSC at 19:30 UT on July 5 apparently signaled the existence of conditions allowing more alphas and M-nuclei to arrive at Explorer 50 than at Explorer 47. And thirdly, the SSC at 03:20 UT on July 6 was associated with dramatically different effects at the two spacecraft. At Explorer 50, there was a modest depression of the alpha flux about 25 minutes before the terrestrial SSC but there was very little change in the M-nuclei fluxes. In contrast, at Explorer 50, there was a substantial depression of the alpha flux accompanied by a larger, velocity dependent depression of the M-nuclei flux. By inspection of Figures 1 and 2, it is evident that the composition of the radiation at the two spacecraft is neither time nor space-independent.

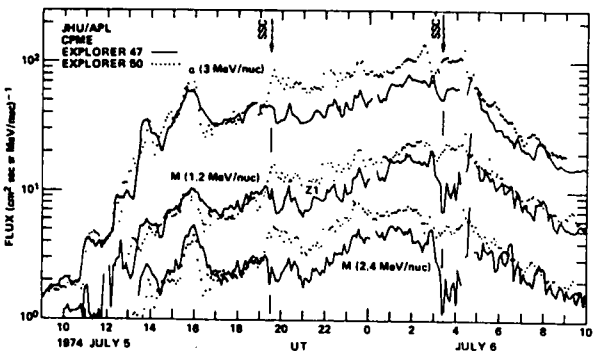

Figure 2. 5.5 minute-averaged fluxes of alphas and medium nuclei from Explorers 47 & 50.

A summary picture of the α/M abundance variation at two energy/nucleon intervals for the period July 4-6 is given in Figure 3. The statistical uncertainty of the ratios is smaller in all cases than the size of the plotted points. The

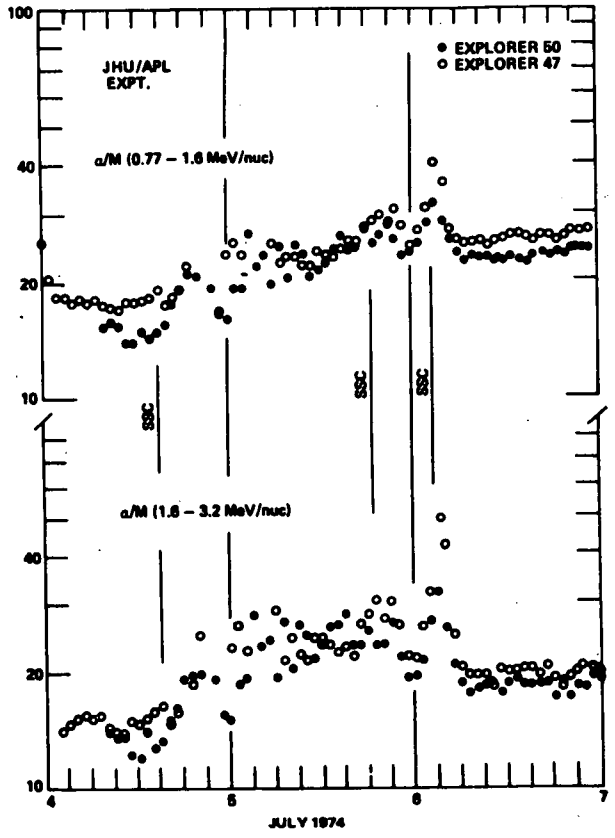

Figure 3. Hourly-averaged alpha flux/medium flux at two energies from Explorers 47 and 50.

of 03:20 on July 5 at either spacecraft. Whatever conditions that caused the observed difference in α/M ratio, therefore, are related to the M-nuclei rather than the alphas.

Figure 5 shows the ratios of hourly averaged fluxes of M-nuclei and Heavy (H) nuclei in the 3 to 8.8 MeV/nucleon range. First, note the substantial (factor of 10) variation in the ratio present at both spacecraft. Also, note the large depression in the M/H ratio observed at Explorer 47 for the SSC on July 6. Evidently, the factors which inhibited the arrival of M-nuclei were not as effective for H-nuclei; hence, the depression in M/H. In all cases the statistical uncertainties are shown when they exceed the size of the plotted points. Most of the time the M/H ratios were within one or two standard deviations at the two spacecraft. Several episodes of substantial differences were variations shown are, therefore, beyond statistics. Note the large SSC associated peak in the α/M ratio on July 6; it is larger at higher energy/nucleon. The fact that many of the points at the two spacecraft overlap suggests that the relative calibration is accurate. The fact that the ratios are generally about the same at the two energy/nucleon intervals indicates that, for this event, energy/nucleon is a good basis for comparing abundances.

An expanded view of the α/M variations around the SSC of July 5 is shown in Figure 4. It is clear that, while α/M was enhanced for the hour containing the SSC at Explorer 57, the behavior of the α/M ratio was drastically different at the two spacecraft. This difference can only be due to the different spatial locations of the two spacecraft and possibly to the effects of the nearby presence of the magnetosphere on the conditions at Explorer 47. Simultaneous observations of the p/α ratios in similar energy/nucleon intervals did not show any significant effect in association with the SSC

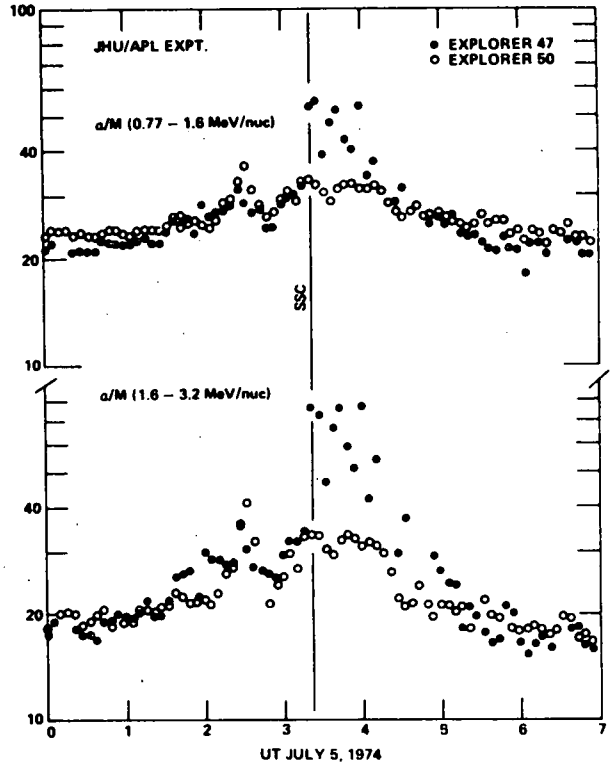

Figure 4. 5.5 minute-averaged alpha flux/medium flux at two energies for Explorers 47 & 50.

observed, suggesting the presence of spatial as well as temporal variations of the M/H abundance. For the range of M/H values observed (3.5 to 60), if the M-nuclei are assumed to be CNO in the proportion 0.49:0.116:1 (Teegarden et al., 1973) and the H nuclei as iron, the corresponding range of values of Fe/O is 0.027 to 0.46. Note, that this is the range of values that could have been obtained by sampling at various times during the event. In this case, the event-averaged Fe/O number ould lie in the lower end of the range because the most intense part of the event was characterized by that ratio.

Finally, we have made calculations using the observed spectral exponents for each of the nuclei groups observed in order to determine the effect of the changes in energy/nucleon spectra on the α/M ratios. The result of that calculation was that spectral slope changes alone are not adequate to explain the temporal variations observed in the α/M ratios.

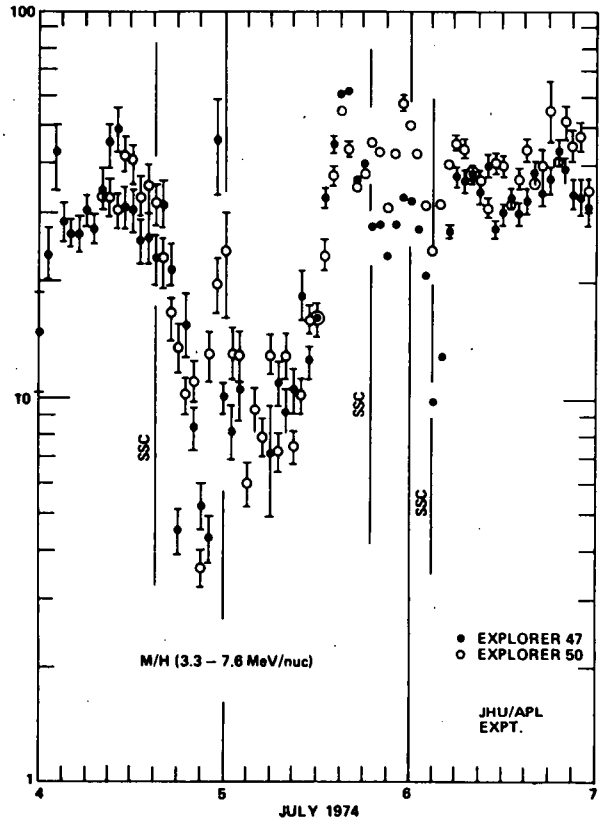

Figure 5. Hourly-averaged medium flux/heavy flux from Explorers 47 and 50.

3. Discussion and Summary. For brevity we shall simply list the remarks suggested to us by these initial simultaneous observations of the spatial and temporal structure of the composition of this event.

(1) The spatial and temporal variations of composition are large and rapid.

(2) Either a short sample or long average over the event ignores important changes in the composition. The abundance measured in a long average can contain the superposition of many different interplanetary regimes and may not be easily interpreted.

(3) The presence of the magnetosphere and transition region may have a substantial effect on measured solar particle event composition.

(4) The absence of impulsive intensity onsets while the composition measurements show substantial variations, suggest that interplanetary spatial structures in composition may exist. Possibly, these relate in some way to coronal or injection structure at the sun.

(5) The explanation of temporal and spatial variation of composition computed for equal energy/nucleon in terms of rigidity dependent interplanetary modulation of incompletely stripped nuclei is difficult to reconcile with the observation of large α/M variations simultaneous with small p/α changes.

TABLE I

PASSBANDS AND GEOMETRIC FACTOR

Species	Channel	Explorer 47 Passbands (MeV/nuc)	Flux * Evaluated at (MeV/nuc)	Explorer 50 Passbands (MeV/nuc)
Alphas	A2	$1.17 < E_\alpha < 1.74$	1.455	$1.14 < E_\alpha < 1.8$
Alphas	A3	$1.74 < E_\alpha < 4.3$	3.02	$1.8 < E_\alpha < 4.2$
Alphas	A4	$4.3 < E_\alpha < 11.5$	7.9	$4.2 < E_\alpha < 12.0$
$Z \geq 3$	Z1	$0.77 < E_M < 1.6$	1.185	$0.70 < E_M < 1.45$
$Z \geq 6$	Z2	$1.6 < E_M < 3.2$	2.4	$1.45 < E_M < 3.3$
$Z \geq 20$	Z3	$3.35 < E_H < 7.6$	5.475	$3.1 < E_H < 8.8$

Acknowledgements. This work was supported in part by NASA through Task I of contract N00017-72-C-4401 between The Johns Hopkins University and the Department of the Navy. Some of the computational work has been done at the University of Kansas Computer Center.

References.

Cashion, R. E., J. W. Kohl, S. A. Gary and D. P. Peletier, "Charged Particle Measurements Experiment for Interplanetary Monitoring Platform Missions H and J", JHU/APL #CP025, July 1973.

Sarris, E. T., S. M. Krimigis and T. P. Armstrong, "Observations of Magnetospheric Bursts of High Energy Protons and Electrons at 35 R_e with IMP-7", submitted to J. Geophys. Res., 1975.

Teegarden, B. J., T. T. vonRosenvinge and F. B. McDonald, "Satellite Measurements of the Charge Composition of Solar Cosmic Rays in the $6 \leq Z \leq 26$ Interval", Ap. J., 180, 571, 1973.

ANISOTROPY MEASUREMENTS OF ~ 50 KeV SOLAR PROTONS

R. E. Gold, C. O. Bostrom and E. C. Roelof
Applied Physics Laboratory/The Johns Hopkins University
Laurel, Md. 20810, USA

D. J. Williams
Space Environment Laboratory, NOAA
Boulder, Colorado 80203, USA

The Energetic Particles Experiment on IMP-7 measures the angular distribution of 50-200 keV solar protons in 16 sectors. The velocity of 50 keV protons may be less than 5 times that of the solar wind. A generalized non-linear Compton-Getting point transformation into the co-moving frame that contains no assumptions as to the angular distribution of either the spectrum or intensity is presented. ~ 50 keV proton data in the spacecraft frame exhibit an anisotropy ratio (J_{max}/J_{min}) that is large (≥ 5) and radial throughout the October 29, 1972 event lasting more than 9 days at this energy. This anisotropy argues against impulsive injection and diffusive decay in the inner solar system. Application of the transformation to the data reveals a long lasting residual anisotropy in the co-moving frame with protons streaming from the sun. Differences between the co-moving frame and solar wind frame velocities suggest residual electric fields upstream from the bow shock. Examination of the co-moving frame anisotropies during the post-shock spikes (Gloeckler et al., 1974) show strong maxima in the direction of the magnetosphere.

1. Introduction. One trend in the study of energetic solar protons has been to push the measurements toward continually lower energies. At these energies the protons are quite sensitive to interplanetary magnetic and electric fields and they may be used as a sensitive probe of interplanetary conditions. One channel of the NOAA/APL energetic charged particle experiment (EPE) on the IMP-7 spacecraft (1972-73A) responds to protons from 50 to 200 keV with 16 angular sectors in the ecliptic plane. The velocity of a 50 keV proton is only ~ 3000 km/sec, so the ratio of energetic proton velocity to the velocity of the solar wind may be 5 or less. At these velocity ratios we may expect the fluxes and anisotropies in the spacecraft frame to be strongly influenced by motions of the plasma in which the magnetic field lines are frozen. The approximate expressions for the Compton-Getting effect (Compton and Getting, 1935; Gleeson and Axford, 1968; Forman, 1970; Balogh et al., 1973) which relate the intensities in the spacecraft frame to those in the frame moving with the field, break down when the ratio of proton to solar wind velocity is not $\gg 1$.

In order to understand the observed anisotropies a quite general non-linear Compton-Getting transformation into the co-moving frame must be employed. Ipavich (1974) has presented a non-linear transformation that is, however, restricted by the assumption that the proton spectrum is isotropic in the co-moving

frame. However, there may not be a frame in which the spectrum is isotropic. We have developed a non-linear point transformation that contains no assumptions as to the intensity or spectral angular distributions. The only requirement is that the spectrum in each direction in the spacecraft frame be describable by a simple function. In the following development we shall assume this function to be a direction-dependent power law.

2. Generalized Non-Linear Compton-Getting Transformation. The transformation may proceed from the Lorentz invariance of the proton phase space distribution function $W(p) = W'(p')$ and its relationship to the differential energy spectrum $dJ/dE = p^2W(p)$ (Forman, 1970), where the primes signify the co-moving frame. Since the measurements are made in the spacecraft frame but we wish to describe the distribution in the co-moving frame, it is useful to express the transformation in terms of $\hat{p}$, the angle between the particle velocity and solar wind velocity and E', the particle energy in the co-moving frame.

Let the differential intensity at a given direction $\hat{p}$ in the spacecraft frame be described by a directionally dependent power law

$$dJ(\hat{p})/dE = (J_o(\hat{p})/E_o)\ (E/E_o)^{-\gamma(\hat{p})} \tag{1}$$

Since all the velocities are non-relativistic, if V is the velocity of the origin of the co-moving frame then the particle momenta are simply related by

$$\underline{p}' = \underline{p} - m\underline{V} \tag{2}$$

Taking the dot product of (2) with $\underline{p}'$ and solving for p yields

$$p = mV\cos\varphi + (p'^2 - m^2V^2 \sin^2\varphi)^{\frac{1}{2}} \tag{3}$$

where φ is the angle between $\underline{p}$ and $\underline{V}$.

Now, relating the distribution functions we see that

$$dJ'(\hat{p}')/dE' = (p'/p)^2\ dJ(\hat{p})/dE \tag{4}$$

thus the differential spectrum is a new direction p' in the co-moving frame is related to the observed spectrum by the ratio of energies in the two frames. If we evaluate the spectrum in the co-moving frame at $E' = E_o$ and express the result in terms of p and E' we find

$$dJ'\ [\hat{p}'\ (\hat{p},E')]/dE' = (J_o(\hat{p})/E_o)\ D^{-(\gamma(\hat{p})\ +\ 1)} \tag{5}$$

The quantity D^{-1} is $(p'/p)^2$ and it follows from (3) that

$$D = 1 + (2V/v')\cos\varphi' + (V/v')^2 \tag{6}$$

where v' is the velocity of the particles with energy E' and ϕ' is the angle between $\underline{p}'$ and $\underline{V}$,

$$\phi' = \phi + \sin^{-1}\left[(V/v')\sin\phi\right]. \tag{7}$$

It is apparent from (5) and (6) that for spectral slopes and solar wind velocities normally observed during solar events, large apparent amplifications of the observed flux are possible when looking in the upstream direction.

The transformation also produces large distortions in the spectrum. From (5) we see that when the spacecraft spectrum is an angle-dependent power law, the differential intensity in the co-moving frame is not a simple power law in energy. However an effective spectral slope may be calculated by taking the logarithmic derivative $d\,\ell n\, J'/d\,\ell n\, E'$ of (5). Evaluating the result at $E' = E_o$ we get

$$\gamma'(\hat{p}')_{eff} = \gamma(\hat{p}) + [(\gamma(\hat{p})+ 1)/D]\cdot[\alpha^2(1 + \sin\varphi\, \sin\varphi'(1 - \alpha^2\sin^2\varphi)^{-\frac{1}{2}}) - \alpha\cos\varphi'] \quad (8)$$

where α is the velocity ratio V/v_o'

3. 50 keV Solar Proton Data. Let us now examine some of the 50-200 keV solar proton data and see how the anisotropies are effected by convection of the magnetic field lines past the spacecraft. The IMP-7 EPE has been described by Roelof et al. (1975) and it suffices to say here that the orbit is nearly circular at $\sim 35\ R_e$ and the spacecraft spends ~ 8 days of the ~ 12 day orbital period in interplanetary space. Figure 1 shows the observed 6 minute averages for a 6 hour period from 1800 to 2400 on October 31, 1972. This was near the peak of a large solar event which has previously been described at higher energies (Armstrong and Krimigis, 1973; Krimigis and Armstrong, 1973; Hovestadt et al., 1972; Domingo et al., 1975). The density of the grey tones in the upper panel represents the ratio of the flux measured in each sector to the spin averaged flux. The display is folded with four sectors repeated on each end such that particles coming from the sunward direction are in the center of the panel and the antisolar direction appears at 1/6 the total distance in from both the top and bottom of the panel. The ideal spiral direction is 1/12 of the total distance up from the center. It is clear from the figure that the highest fluxes are coming from the sun during most of the 6 hour period and there is a relative minimum in the antisolar direction. In fact the anisotropies were dominated by the radial direction for at least 9 days, from the earliest onset through the maximum and during all of the decay until the spacecraft entered the magnetosphere on November 7. The three periods that show significant deviations from the convective anisotropy are the "post-shock" spikes which were described by Gloeckler et al. (1974) and will be discussed in the next section. The solid curve in the lower panel of Figure 1 is a log plot of the observed spin-averaged counting rate from 10^{-2} counts/sec at the bottom to 10^4 at the top. The dots in the lower panel are a log plot of the maximum to minimum sector counting rate ratio ranging from 1 at the bottom to 100 at the top. The anisotropy ratio is between 5 and 10 near the peak of the event, in Figure 2, and was > 50 near the onset and between 10 and 30 during the decay.

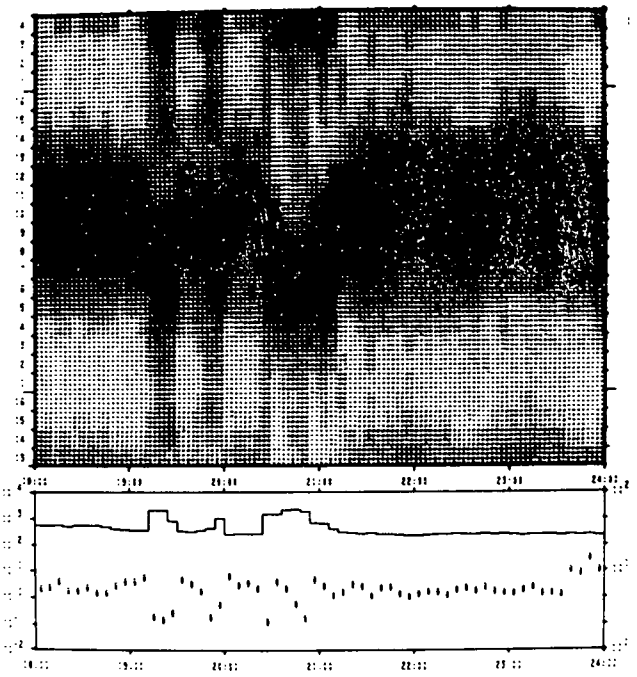

Figure 1. 50-200 keV proton data for 1800-2400 October 31, 1972.

The high radial anisotropies that were observed for 9 days during this event strongly argue against impulsive injection

followed by diffusive decay in the inner solar system at this energy range. With the high solar wind velocities observed during this event, any diffusing particle population would have been carried to beyond 3 AU by November 7 when the spacecraft entered the magnetosphere. This argument is augmented by the field aligned anisotropies in the co-moving frame as shown in the next section.

4. Anisotropies in the Co-Moving Frame. Before applying the generalized Compton-Getting transformation to the data, let us examine the spacecraft frame anisotropies during the interesting period on the right hand half of Figure 1 when the magnetic field direction twice shifted across the earth-sun line. The anisotropies on the right hand half of the upper panel of Figure 1 show a skew that first shifts above, then below, then above and finally below the darkest band along the earth-sun line. Changes in the skew are coincident with the shifts in the magnetic field direction and indicate a field-aligned component to the anisotropy in the spacecraft frame.

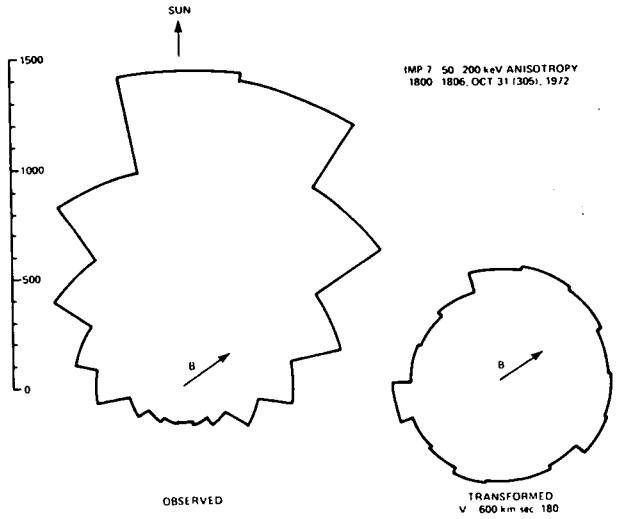

Figure 2. Observed and transformed anisotropies. The scale is Flux > 50 keV x 10^2.

Consider the first 6 minute average on the left hand edge of Figure 1 (1800 to 1806, October 31, 1972) which has an anisotropy ratio of 6 and a highly skewed distribution in the spacecraft frame as shown on the left in Figure 2. Transforming this distribution with a radial velocity of 600 km/sec results in the distribution on the right side of Figure 2. The transformed distribution is nearly symmetric about the field line direction with an anisotropy ratio of 1.3 and a flux peak along the field line coming from the sun. These field aligned residual anisotropies continue at least well into the decay.

One way that the 50 keV protons may be used to probe the interplanetary medium for residual electric fields is to compare the transformation velocity that results in a symmetric angular distribution of flux about the field line, with the observed solar wind velocity. For the case of Figure 2 this transform velocity is $\sim$ 20% less than the observed solar wind velocity. This suggests that the region upstream from the bow shock may be influenced by the presence of the magnetosphere.

It is imperative, when studying low energy solar particles in interplanetary space upstream from the magnetosphere that the possible contributions from magnetospheric protons be considered (Fan et al., 1973; Sarris et al., 1975; Roelof et al., 1975). For example, let us examine the peak of the third post-shock spike (Gloeckler et al., 1974) in the middle of Figure 1. The anisotropy peak in the spacecraft frame during this period shifted to a direction $\sim$ perpendicular to the garden hose direction, yet the field direction was within 30°

of the ideal spiral. The observed angular distribution of flux is shown on the left side of Figure 3. When this distribution is transformed using the observed solar wind velocity the resulting anisotropy peak points directly to the magnetosphere as shown on the right side of Figure 3. Similar transformed distributions are produced during the other two spikes which strongly suggests that they are of magnetospheric origin.

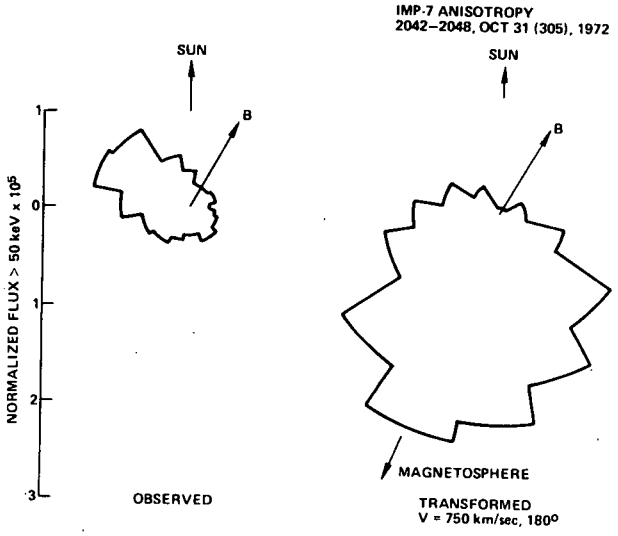

Figure 3. Observed and transformed post shock spike.

5. Acknowledgements. We are indebted to Drs. R. P. Lepping and N. F. Ness of the Goddard Space Flight Center and Drs. W. G. Feldman and S. J. Bame of the Los Alamos Scientific Laboratory for making their magnetic field and solar wind data available to us prior to publication. This work has been supported in part by NASA under Task I of Navy contract N00017-72-C-4401 and NASA contract RDJ41614 and by Air Force Cambridge Research Laboratories contract F19628-73-C-0070.

6. References.

Armstrong, T. P. and S. M. Krimigis, Time variations and angular distributions of alpha particles and medium nuclei for the October 27, 1972 solar particle event, Proceedings of 13th International Cosmic Ray Conference, Denver, 2, 1504, 1973.

Balogh, A.,S. Webb and M. A. Forman, Higher order Compton-Getting anisotropies, Planet. Space Sci., 21, 1802, 1973.

Compton, A. H. and I. A. Getting, An apparent effect of galactic rotation on the intensity of cosmic rays, Phys. Rev., 47, 817, 1935.

Domingo, V., D. E. Page and K.-P. Wenzel, October 1972 solar event-the third dimension in solar particle propagation, J. Geophys. Res., in press, 1975.

Fan, C. Y., G. Gloeckler and D. Hovestadt, Intensity oscillations of low energy solar particles observed on the IMP-7 satellite, Proceedings of 13th International Cosmic Ray Conference, Denver, 2, 1416, 1973.

Forman, M. A., The Compton-Getting effect for cosmic-ray particles and photons and the Lorentz-invariance of distribution functions, Planet. Space Sci., 18, 25, 1970.

Gleeson, L. J. and W. I. Axford, The Compton-Getting effect, Astrophys. Space Sci., 2, 431, 1968.

Gloeckler, G., F. M. Ipavich, C. Y. Fan and D. Hovestadt, Post-shock spikes: A new feature of proton and alpha enhancements associated with an interplanetary shock wave, Geophys. Res. Lett., 1, 65, 1974.

Hovestadt, D., O. Vollmer, G. Gloeckler and C. Y. Fan, Measurement of elemental abundance of very low energy solar cosmic rays, Proceedings of 13th International Cosmic Ray Conference, Denver, 2, 1498, 1973.

Ipavich, F. M., The Compton-Getting effect for low energy particles, Geophys. Res. Lett., 1, 149, 1974.

Krimigis, S. M. and T. P. Armstrong, Measurements of the relative abundances of Fe-group, He and M nuclei during the October 29, 1972 solar particle event, Proceedings of 13th International Cosmic Ray Conference, Denver, 2, 1510, 1973.

Roelof, E. C., E. P. Keath, C. O. Bostrom and D. J. Williams, Fluxes of ≥ 50 keV protons and ≥ 30 keV electrons at ~ 35 R_e: 1. Velocity anisotropies and plasma flow in the magnetotail, submitted to J. Geophys. Res., 1975.

Sarris, E. T., S. M. Krimigis and T. P. Armstrong, Observations of magnetospheric bursts of high energy protons and electrons at ~ 35 R_e with IMP-7, submitted to J. Geophys. Res., 1975.

OBSERVATION USING INTERPLANETARY SCINTILLATIONS AT 34.3 MHz OF THE EFFECT OF A SOLAR WIND DISTURBANCE ON A SOLAR ENERGETIC PARTICLE EVENT

E. C. Roelof and S. M. Krimigis
Applied Physics Laboratory/The Johns Hopkins University
Laurel, Maryland, 20810, USA

W. M. Cronyn and S. D. Shawhan
Department of Physics, University of Iowa
Iowa City, Iowa, 52242, USA

P. S. McIntosh
Space Environment Laboratory, NOAA
Boulder, Colorado, 80302, USA

Aspects of the "delayed" particle event of June 26, 1974 suggest appreciable control of particle propagation by coronal and interplanetary magnetic fields, the latter distorted by the solar wind disturbances from the parent flare some 3 days earlier. The disturbance itself was monitored using interplanetary radio scintillation observations at 34.3 MHz using the University of Iowa COCOA-Cross array at Clark Lake Radio Observatory in California. Analysis of the Hα Synoptic Chart of large-scale chromospheric magnetic polarity structure shows that the delayed particles appeared when the higher plasma velocities moved the high-coronal connection longitude of the interplanetary field lines at Earth eastward out of the complex of field structure associated with the flare region (MPR 13002).

1. Introduction. The propagation of solar cosmic rays is controlled not only by the interplanetary magnetic field, but also by coronal magnetic structure. Consequently, the development over the last decade of probing the interplanetary medium by measuring interplanetary scintillations (IPS) of radio sources offers great promise in the interpretation of solar particle events. We report here on the solar particle events of June 20-30, 1974, measured by the Applied Physics Laboratory/JHU Charged Particle Monitoring Experiment (CPME) on IMP 7 (Explorer 47). These events are of particular interest, since there were concurrent IPS observations from the University of Iowa radio array at the University of Maryland Clark Lake Radio Observatory in Borrego Springs, California. We wish to concentrate on a delayed particle event (whose onset was on June 26 although the last likely flare candidate was at ~ 0500 UT, June 23), and its relationship to the large scintillation event on June 26. The solar activity for this period will be discussed in Section 3.

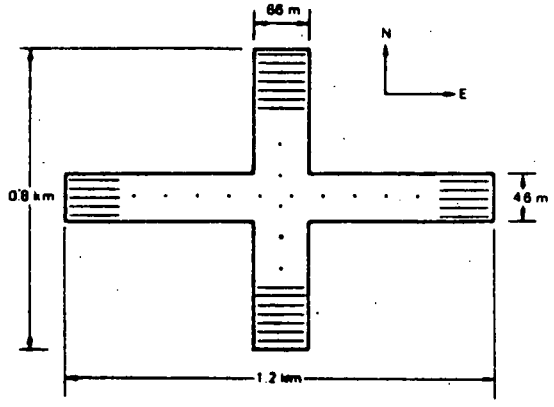

Figure 1. Overall geometry of the COCOA-Cross Array.

2. IPS Observations. In May, 1974, systematic monitoring of the interplanetary medium was undertaken using a large electronically steerable, decametric wavelength (34.3 MHz) Mills Cross radio telescope with a

collecting area of over 7×10^4 m^2 (one of the largest in the world) that was constructed as a joint undertaking by the Space Environment Laboratory of the National Oceanic and Atmospheric Administration and the Department of Physics and Astronomy of the University of Iowa. The configuration of the COCOA-Cross array is shown in Figure 1. COCOA is an acronym which stands for the individual element type (Balsey and Ecklund, 1972) which are colinear dipoles fashioned out of coaxial cable. Full details of the instrument are given in a technical report by Cronyn and Shawhan (1975). The array has been specifically designed for, and dedicated to, IPS observations at solar elongation angles ranging from 20° to 180°. It is located at the University of Maryland Clark Lake Radio Observatory south of the Santa Rosa mountains, in the eastern desert country of San Diego County, an isolated site well-suited for such sensitive studies. The extremely large collecting area and low operating frequency makes possible a unique capability of being able to observe a large number of IPS sources at source-sun elongation angles approaching 180°. We make daily observations of the activity of a grid of ~ 100 small angular diameter sources, distributed more or less at random over the sky at solar elongation angles greater than 20° and celestial declinations north of -25°. For each source, we calculate the scintillation index m during its transit from the mean intensity $\bar{I}$ and the RMS intensity fluctuation ΔI ($m = \Delta I/\bar{I}$).

A crucial question in source grid analyses is that of defining significant IPS activity. Sources vary considerably in scintillation strength due to their angular size and their solar elongation angle at the time of observation. Consequently we have made use of a non-parametric statistical definition of scintillation activity. We choose a period of about two months containing the event to be studied, and for each source, we identify the quartile (25%) of days having the highest values of m. These are called days of "high" activity. The next-ranked quartile of m-values are called "moderate" activity, and the days in the lowest two quartiles are called "low" activity. This ranking system allows non-subjective inter-comparison of sources differing widely in scintillation strength and intensity. The results for June 23-26 are plotted in Figures 2a-d in an "all-sky" format, in which solar ecliptic latitude is plotted linearly as the polar variable and solar ecloptic longitude is plotted as the azimuth. The sources are identified by their third Cambridge (3C) catalogue number. The epoch for the rank-

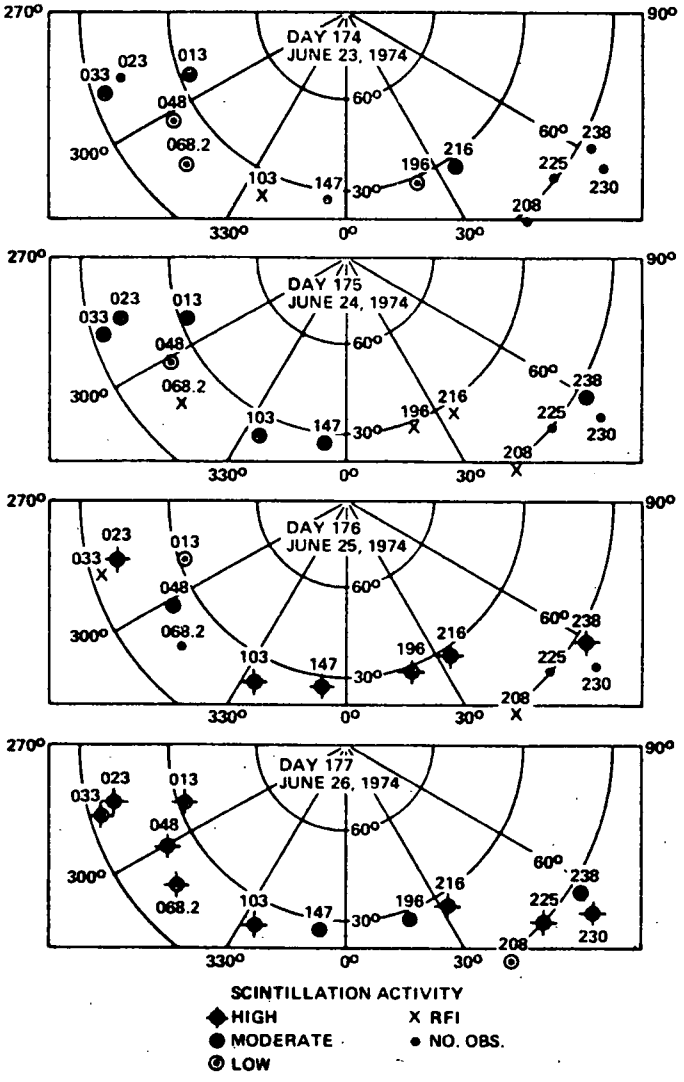

Figure 2. IPS Activity in sunward sources June 23-26 (a-d). Radio sources from 3rd Cambridge catalog.

ing analysis was day 140-day 210, 1974. The times of observations for the sources in late June ran from ~ 1400 UT for 3C13 to ~ 2400 UT for 3C238. We show only the sunward cone of elongation angles $\leq 75°$ since we will be discussing the possible identification of a flare associated disturbance.

A preliminary analysis of this IPS event was given by Cronyn et al. (1975), in which the pattern of increased scintillation of sources in the sunward cone during June 23-25 was interpreted as outward-moving disturbance initiated by the 2B flare at 0500 UT, June 23. Preliminary data from the Los Alamos Scientific Laboratories solar plasma measurement on IMP 8 (W. C. Feldman, private communication), indicate a steady rise in velocity from ~ 340 km/s at ~ 0100 UT, June 26 to ~ 800 km/s at ~ 1200 UT, June 27, interrupted by a rapid (5 minute) jump from ~ 500-600 km/s at ~ 1130 UT, June 26. The scintillation activity for eastern-looking sources (not shown here) during June 20-25 indicates a co-rotating stream that initiated a geomagnetic storm beginning 2332 UT, June 25. If we interpret the velocity jump (which was not a shock) ~ 1130 UT, June 26 as the arrival of the solar disturbance, then the interplanetary plasma near Earth on June 26 must have been extraordinarily disturbed, explaining the enhanced scintillation of practically every source monitored on June 26. We shall now discuss how these interplanetary disturbances might have produced the delayed particle event on that day.

3. Solar Particle Observation. McMath Plage Region 13002 began optical flare activity soon after its central meridian passage (CMP June 20) with small flares (< 1N) at ~ 1800 UT, June 21 and ~ 0330 UT, June 22. The only prior flares in June at this importance level had been in two other regions (12972, CMP June 3 and 12993, CMP June 14), all before June 15. The last flare $\geq$ 1N from MPR 13002 before it went over the west limb on June 26, was at ~ 1500 UT on June 24. The only other flare activity was from MPR 13002 on June 26). Therefore MPR 13002 dominated solar

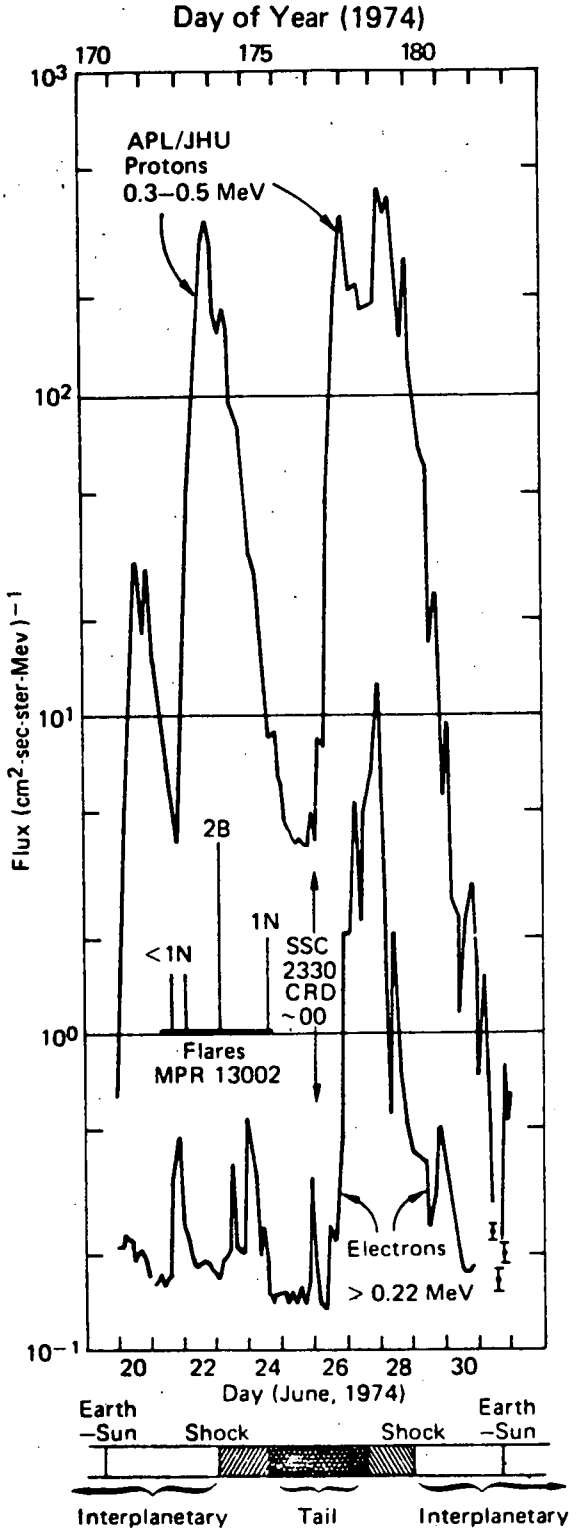

Figure 3. Solar energetic particle fluxes measured by the APL/JHU experiment on IMP-7, June 20-30, 1974. Location of the spacecraft (near-circular orbit ~34 R_e) relative to the magnetotail and Earth-sun line is shown below the figure.

activity from its CMP until its limb passage. A striking signature of this active region transit of June 20-30 is found in the 0.3-0.5 MeV proton and > 0.22 MeV electron fluxes measured by the APL/JHU experiment on IMP-7, shown in Figure 3. The times and optical importance of all flares from MPR 13002 listed in Solar-Geophysical Data (Prompt Reports) are indicated on the figure, as well as the position of IMP-7 along its ~ 34 R_e near-circular orbit relative to the magneto-tail and Earth sun line. Details of the CPME detector and IMP-7 orbit are given by Sarris et al. (1975).

The first small flare (~ 1800 UT, June 21) resulted in a prompt relativistic electron event as well as a characteristically rapid and strongly anisotropic rise in the low-energy protons. The second small flare (~ 0330 UT, June 22) produced a small electron enhancement. It therefore appears paradoxical that the larger and brighter flare (importance ~ 2B, with decimeter type III as well as meter and dekameter type II radio emission) at ~ 0500 UT, June 23 did not produce any significant prompt enhancement of either proton or electron fluxes. Nor for that matter did the 1N flare at ~ 1515 UT, June 24. It then appears that the interplanetary magnetic "connection" between the acceleration site and the earth was much "poorer" during June 23-25 than it was on June 21 and 22. This inference is strongly supported by the particle event of June 26, when it appears that the interplanetary magnetic "connection" moved to coronal regions where particle injection was greatly enhanced. It seems very unlikely that the onsets on June 26 were due to new acceleration because the relativistic electron rise is abnormally slow, and the low-energy proton rise (~ 0600) precedes that of the electrons (~ 1200) by more than 6 hours. The fact that the particle onsets did not correspond to the time of the SSC, and that the significant rises took place ~ 1200 UT, June 26, suggests that the flare plasma (which may have caused the abrupt velocity increase at that time), played an initial role in controlling the coronal connection longitude of the interplanetary field (that was later dominated by the high speed co-rotating solar wind stream).

Since complete solar wind velocity measurements are not available at the time of writing, we have made the following estimates. The period June 21-25 was very quiet geomagnetically (three-hour Kp ≤ 3), so we have assumed a velocity of 350 km/s, except for June 23 when there was a small storm ~ 0800 UT when we chose 400 km/s. Immediately after the SSC, we have used the preliminary measurements from IMP 8. It will be seen from the following discussion that the arguments will still hold even if our estimates are not too accurate.

As an indicator of coronal magnetic structure, we have chosen to use Hα Synoptic Charts, since it has been established that absorption features in solar Hα photographs (filaments, filament channels, fibril patterns, etc) delineate neutral lines for large-scale chromospheric polarity regions. Figure 4 shows a sketch derived from the preliminary (real-time) Hα Synoptic Chart for Carrington Rotation 1616 (June-July, 1974) published by P. S. McIntosh in Solar Geophysical Data (Prompt Reports) (August, 1974). Hα filaments are heavy-inked. Magnetic neutral lines are solid if inferred from Hα structure, but dashed if inferred from continuity. Sunspots are solid dots. McMath Plage Region 13002 is centered at 350° longitude ≤ 20° latitude. Magnetic polarities have been checked with solar magnetoheliograms.

The prompt low-energy protons and relativistic electrons from the June 21 flare were injected onto interplanetary field lines ~ 30° west of the flare site in MPR 13002. Even though the estimated connection longitude is over the flare site on June 23, few new particles were seen at earth. On the other hand, the onset of the "delayed" particle event of June 26 apparently was the result of the connection longitude being switched ~30° eastward (from 330° at 1200 UT, June 25 to 300° at 1200 UT, June 26) by the increased solar wind velocity associated with the IPS event. It is therefore possible that the magnetic coronal structure above the inferred neutral-line which crosses the equator ~ 295° served to "compartment" the energetic particles in the high corona, with enhanced interplanetary access for particles outside the eastern boundary of the large negative polarity region west of 270°. Similar "compartmentalization" has been found in other events by Roelof and Krimigis (1973), Gold et al. (1974) and Roelof et al (1974). In summary, the features of the Hα synoptic chart appear to order the seemingly paradoxical energetic particle observations and to reinforce this preliminary interpretation of the IPS observations of a very complicated interplanetary disturbance.

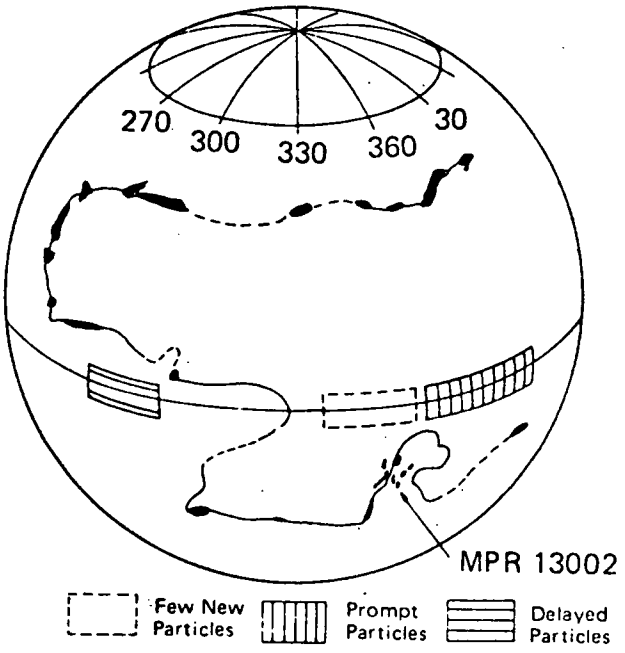

Figure 4. Large-scale Hα neutral line structure and inferred injection longitudes for energetic particles.

Acknowledgments. Research at APL/JHU was supported by NASA contract N00017-72-C-4401 and NASA grant NSG7055, and E. C. R. acknowledges support under Air Force Cambridge Research Laboratories contract F19628-73-C-0070 (although support does not necessarily imply endorsement). The COCOA-Cross array has been partially funded through NSF grant DES73-06559-A01 and by NASA grant NGL-16-001-002, with additional support from NASA/GSFC and the Space Environment Laboratory, NOAA.

References.

Balsley, B.B. and W.L. Ecklund, "A portable coaxial collinear antenna", IEEE Trans. Ant. Prop., 20, 513, 1972.

Cronyn, W.M. and S.D. Shawhan, "A decametric wavelength radio telescope for interplanetary scintillation observations", University of Iowa Department of Physics and Astronomy Report 75-12, 1975.

Cronyn, W.M., F. Erskine, S.D. Shawhan, B.L. Gotwols and E.C. Roelof, "Prediction of ionospheric effects associated with solar wind disturbances using interplanetary scintillation observations at 34.3 MHz", Proceedings of the Ionospheric Effects Symposium, (Crystal City, Virginia) (ed. J. Goodman), in press, 1975.

Gold, R.E., J.T. Nolte, E.C. Roelof and R. Reinhard, "The influence of coronal magnetic structure on low-energy solar proton events", Space Research XIV, (ed.) A.C. Strickland, Akademic Verlag, Berlin, in press, 1974.

McIntosh, P.S., "H-alpha synoptic charts of solar activity for the period of Skylab observations May 1973-March 1974", UAG Report No. 40, Environmental Data Service, 1975.

Roelof, E.C. and S.M. Krimigis, "Analysis and synthesis of coronal and interplanetary energetic particle, plasma and magnetic field observations over three solar rotations", J. Geophys. Res., 78, 5375, 1973.

Roelof, E.C., J.A. Lazniak, W.R. Webber, F.B. McDonald, B.J. Teegarden and J.H. Trainor, "Relation of coronal magnetic structure to the interplanetary proton events of August 2-9, 1972", Correlated Interplanetary and Magnetospheric Observations, (ed.) D.E. Page, D. Reidel (Dordrecht, 563, 1974.

Sarris, E.T., S.M. Krimigis and T.P. Armstrong, "Observations of magnetospheric bursts of high energy protons and electrons at $\sim$ 35 R_e with IMP-7", J. Geophys. Res., 80, in press, 1975.

OBSERVATIONS OF ENERGETIC PARTICLES NEAR INTERPLANETARY MHD DISCONTINUITIES

E. T. Sarris and S. M. Krimigis
Applied Physics Laboratory, The Johns Hopkins University
Laurel, Md. 20810, USA

T. P. Armstrong
Department of Physics, University of Kansas
Lawrence, Kansas 66044, USA

Energetic ion and electron events associated with interplanetary magnetohydrodynamic discontinuities were observed by the JHU/APL experiments on IMP-7 and 8. The measurements were made over a wide energy range extending from 0.29 to 500 MeV/nuc for the ions and from 0.22 to 2.5 MeV for the electrons and with a time resolution of 10 seconds. The following observations and conclusions are derived on the basis of the studied events: (a) Low energy (Ep < 1 MeV) proton enhancements associated with shock waves are observed mainly downstream from the shock front. Protons and alpha particles with energies between 1 < Ep < 4 MeV/nuc are piled up upstream from the shock whereas at even higher energies there is no ion enhancement but a decrease in the downstream energetic ion intensities. (b) Simultaneous particle observations by two spacecraft show that shock spikes of significantly different magnitude (by a factor of $\sim$ 6) are formed at different positions in the interplanetary medium. The formation of the spike appears to be dependent on the short term local conditions of the interplanetary medium upstream from the shock rather than a long term (hours to days) interaction of particles with the shock. (c) An enhancement in the low energy (< 2 MeV/nuc) proton and alpha particle intensities was detected for the first time in the interplanetary medium in association with a magnetic field annihilation region. (d) Tangential magnetic discontinuities act like barriers for low energy ions (E < 10 MeV/nuc). The penetration of the tangential discontinuity barrier is restricted to a region with width comparable to the ion gyrodiameters. However energetic electrons (Ee > 0.22 MeV) and high energy protons (Ep > 50 MeV) do not "see" at all the tangential magnetic discontinuity.

Observations of the interaction of energetic particles with MHD discontinuities are essential in order to understand (a) the mechanisms accelerating particles at MHD boundary layers and (b) the effects that such MHD discontinuities have on the interplanetary propagation of energetic protons.

The energization of energetic protons at interplanetary shock waves has been studied extensively both theoretically and experimentally (Armstrong et al.,

1970; Sarris and Van Allen, 1974; Chen and Armstrong, 1975; Schatzmann, 1963; Hudson, 1965; Alekseyev and Kropotkin, 1970). It has been shown that intensive acceleration of low energy protons occurs at the shock fronts when the upstream interplanetary magnetic field is "almost" parallel to the shock front. It has also been hypothesized but as yet not verified experimentally that acceleration of particles may take place in the interplanetary medium at regions of magnetic field annihilation (neutral sheets) (Levy et al., 1974).

The propagation of particles in the interplanetary medium has also been investigated in great extent (Roelof and Krimigis, 1973). One of the most crucial questions on the subject is that of the cross field motion of particles of different species and energies. Observations of particle intensity discontinuities associated with MHD tangential discontinuities are important in order to study the cross field motion of particles since there is no component of the magnetic field normal to the discontinuity surface.

From these studies it has become evident that in order to examine the nature of the boundary layer phenomena in detail we need particle observations with a time resolution τ such that $V_{SW} \cdot \tau$ is less than the gyroradii of low energy protons (few hundred KeV).

In the following we present particle observations at several distinct MHD discontinuities from the JHU/APL identical experiments on the IMP-7 and 8 spacecraft with fine time and energy resolution. The time resolution is 10 sec (5 sec for several particle channels) which allow us to sample 4 times within the gyroradius of a 300 KeV proton in a 5 γ field convected with the solar wind speed.

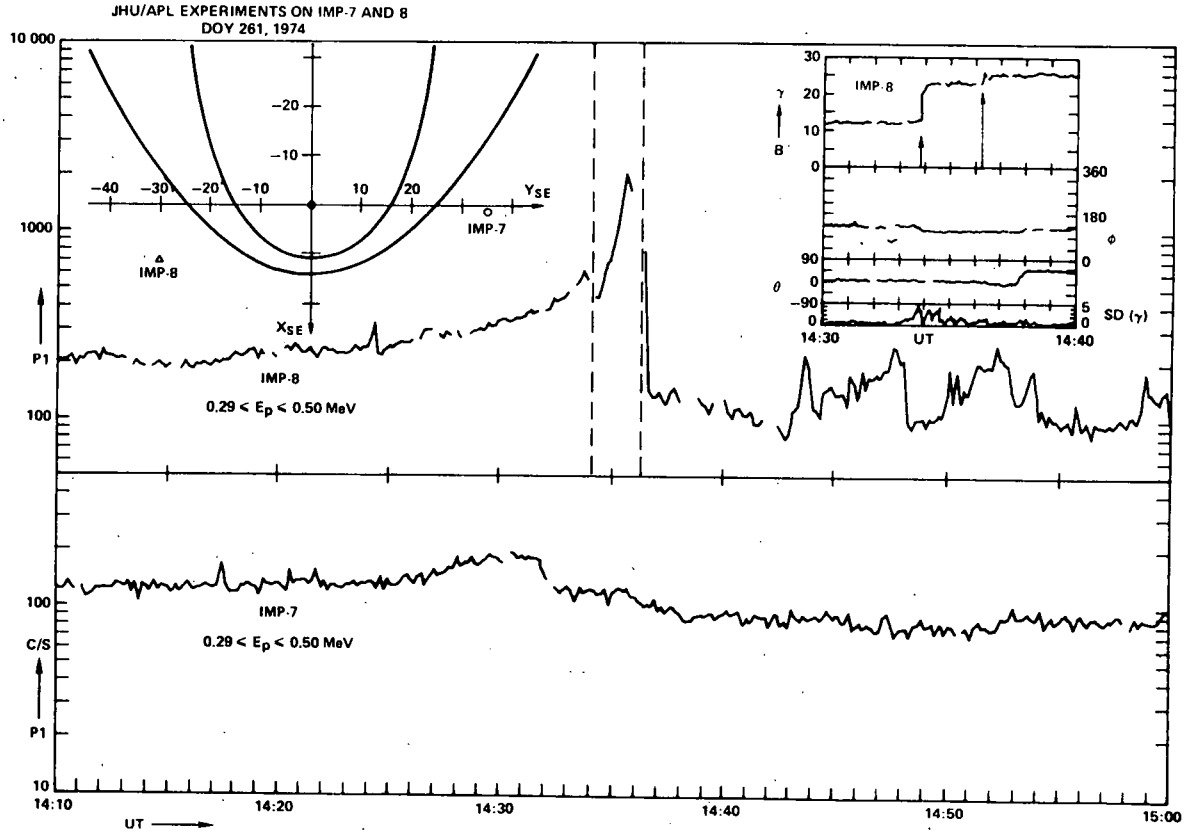

Figure 1. Simultaneous observations of low energy protons at IMP-7 and 8 during the passage of an interplanetary shock wave. (Magnetic field data courtesy of Drs. R. Lepping and N. Ness.)

The description of the experiment and data analysis is given in detail elsewhere (Sarris et al., 1975). Simultaneous magnetic field vector measurements have been obtained from the GSFC magnetometers onboard the same spacecraft.

Particle Acceleration at Interplanetary Shock Waves. Figure 1 presents simultaneous observations of low energy proton (0.29-0.50 MeV) counting rates from both IMP-7 and 8 in the interplanetary medium during the passage of a shock wave on September 18, 1974. The effect of the interplanetary shock wave on the protons at the positions of the two spacecraft is considerably different. The peak to background ratio (p/b) at IMP-7 is only ~ 1.6 whereas the proton intensity enhancements at IMP-8 show two intense peaks, a major one behind the shock wave with p/b ~ 10 and a smaller one in front of the shock with p/b ~ 3. It is noted that the major proton spike is associated with a MHD discontinuity behind the shock wave, which shows an increase in the magnetic field magnitude from 23 to 26 γ but no change in direction. This may be a perpendicular shock wave, however detailed plasma data are necessary to clearly identify it as such. The following conclusions derive from this set of simultaneous observations: (1) The shock spike is not an enhancement that was formed by a long term (hours to days) interaction of the particles with the shock. If this were the case comparable enhancements should be observed at both spacecraft irrespective of short term or local conditions. (2) The role of the earth's bow shock may be instrumental in favoring the spike formation at IMP-8 but not at IMP-7. This could happen by (a) changing the direction of the upstream magnetic field so that the angle ψ between this direction and the shock normal at IMP-8 is larger than the angle ψ at IMP-7. It is known from both analytical (Sarris and Van Allen, 1974) and numerical results (Chen and Armstrong, 1975) that the acceleration of particles at shock waves is considerably more intense for large ψ than for small ones. Unfortunately magnetometer data at IMP-7 are not available so that we cannot check the local conditions of the shock at IMP-7. (b) Multiple reflections between the advancing interplanetary shock wave and the standing bow shock. In this case the proton intensities should be essentially isotropic; however directional measurements at IMP-8 during the spikes show large field-aligned anisotropies directed away from the sun with front to back ratios ~ 3.4 for the first spike and 9.3 for the second one.

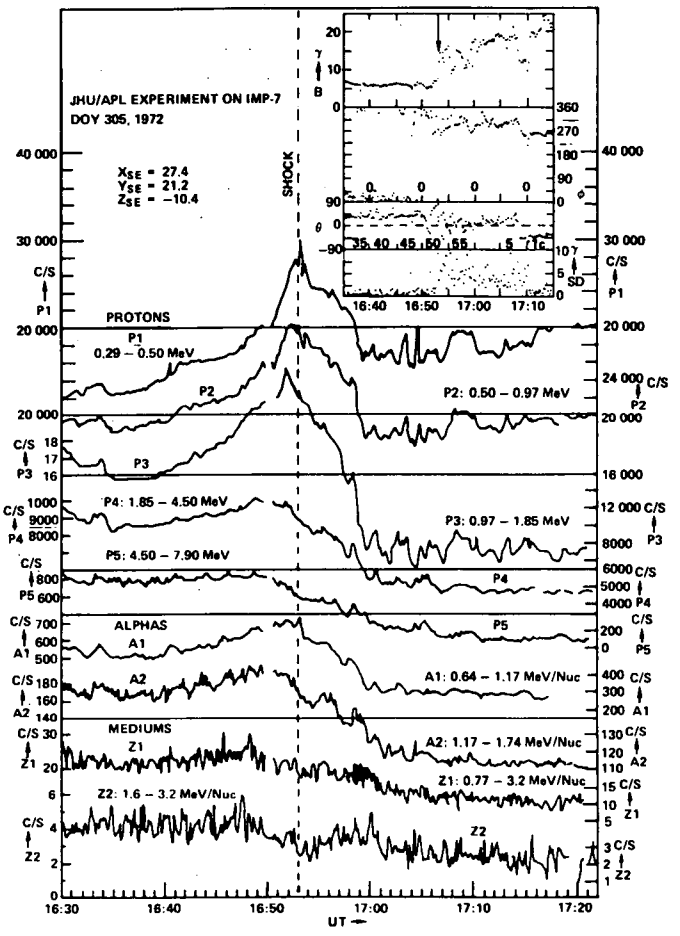

Figure 2. The responses of a series of proton, alpha and medium nuclei energy channels during the shock wave of October 31, 1972 on a 10 sec time resolution.

Figure 2 shows the responses of a series of proton, alpha and medium nuclei energy channels during the turbulent shock wave of October 31, 1972 with a 10 sec time resolution. It is seen that the effect of the shock wave on the particles is critically dependent on the particle energy. The 0.3 and 0.5 MeV proton counting rates have their maxima at the shock front whereas the bulk of the proton enhancements is concentrated behind the shock. The peak of the $\geq$ 1 MeV proton response occurs clearly upstream from the shock wave. The majority of $\sim$ 1 MeV protons are also piled up ahead of the shock. At $\sim$ 2 MeV there is only a weak proton enhancement upstream from the shock and a decrease in the proton intensities downstream. At energies $\geq$ 4.5 MeV there is no proton spike but only a decrease in the proton intensities downstream from the shock front. Alpha particles at 0.6 and 1.2 MeV/nuc show a clear enhancement upstream from the shock whereas the response of medium nuclei at 0.8 and 1.6 MeV/nuc shows no enhancement but undergoes a step decrease in the downstream region.

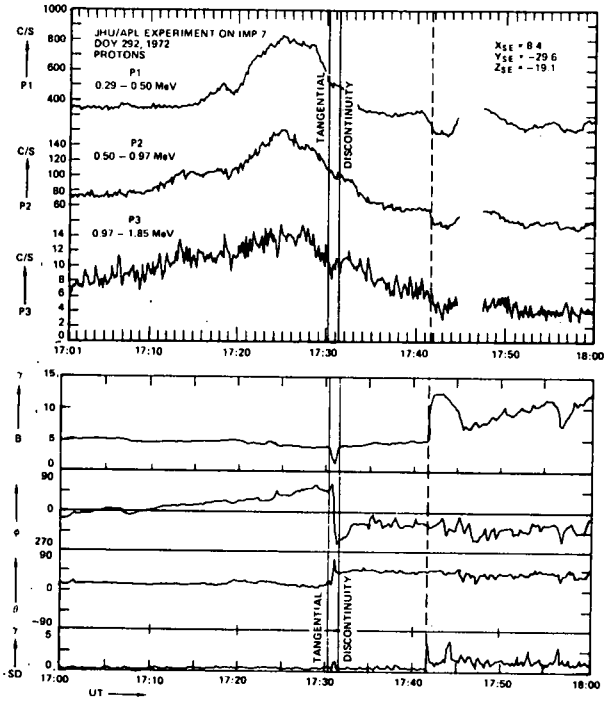

Figure 4. Simultaneous magnetic field vector and low energy proton measurements during the passage of an interplanetary magnetic annihilation region on September 18, 1972.

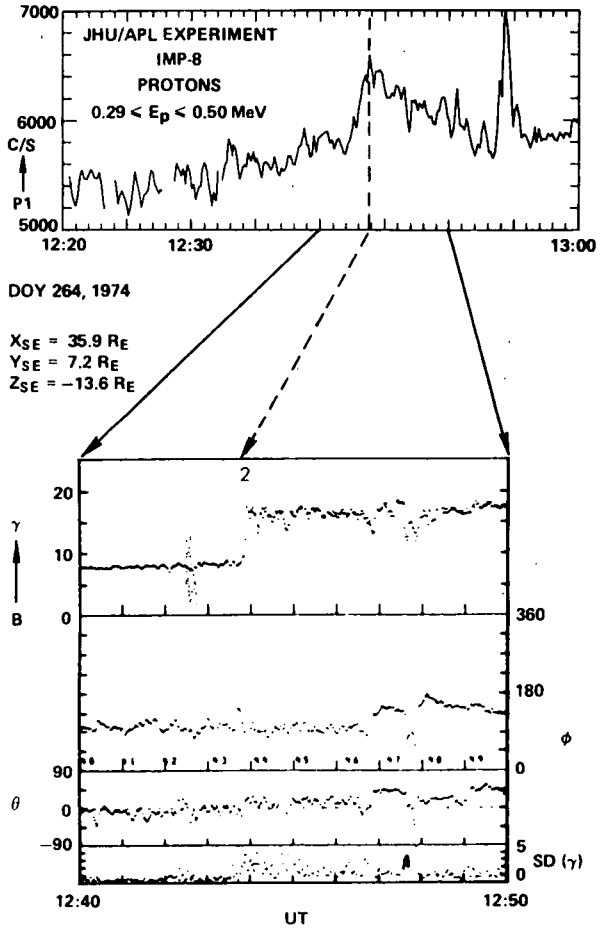

Figure 3. Simultaneous magnetic field and proton measurements around the time of the passage of a shock wave.

Figure 3 also shows the effect of an interplanetary shock on low energy protons at IMP-8 on September 21, 1974. Measurements of the magnetic field show that it is considerably turbulent in the downstream region. It is noted that the shock-associated proton (0.3 MeV) enhancement occurs mainly downstream from the shock wave and the peak intensity reaches its maximum at the shock front. The spike

at ~ 12:54 UT in the downstream region is a magnetospheric proton burst with the proton fluxes streaming away from the bow shock (Sarris et al., 1975). It is essential that observations of low energy proton (≤ 4 MeV) and electron (< 1 MeV) phenomena in the near Earth interplanetary medium take into account the sporadic occurrence of intense bursts of magnetospheric origin.

Proton Enhancement Near Interplanetary Magnetic Field Annihilation Region. Figure 4 presents simultaneous magnetic field vector and low energy proton measurements at IMP-7 on October 18, 1972 during the passage of an interplanetary magnetic field annihilation region followed about 10 min. later by a shock wave. The proton responses show an enhancement with peak over background ratio p/b ~ 2 which is clearly detached from the shock wave and occurs in association with the magnetic field annihilation region with the peak response and the bulk of the proton enhancement ahead of the tangential discontinuity.

Figure 5 presents 5.5 min. average counting rates of different channels for the same event. No distinct proton spike is detected above 1.8 MeV nor any clear electron enhancement at ~ 0.22 to 0.50 MeV. However an enhancement is present in the alpha 0.64-1.17 MeV/nuc channel. The proton fluxes during the spike are anisotropic with front to back ratio ~ 3.8 at the peak and they are field aligned and directed away from the sun.

Particle Observations at a Tangential Discontinuity. Figure 6 shows the responses of different particle channels on a 10 sec time resolution during the crossing of a tangential discontinuity on November 1, 1972 where the field direction changed by ~ 180° in azimuth (ϕ) and 90° in latitude (θ). The tangential discontinuity forms the boundary between two interplanetary magnetic sectors with different particle content. It is seen that the tangential discontinuity acts like a barrier between the proton and alpha particle population of the two regions. The width of the transition region from the high intensity to the low intensity region is shown in Figure 7 as a function of particle rigidity. The gyrodiameter of the ions in the weak field side of the discontinuity (8.5 γ) is also shown in this figure by the dashed line. The width in Km is calculated using the observed solar wind velocity

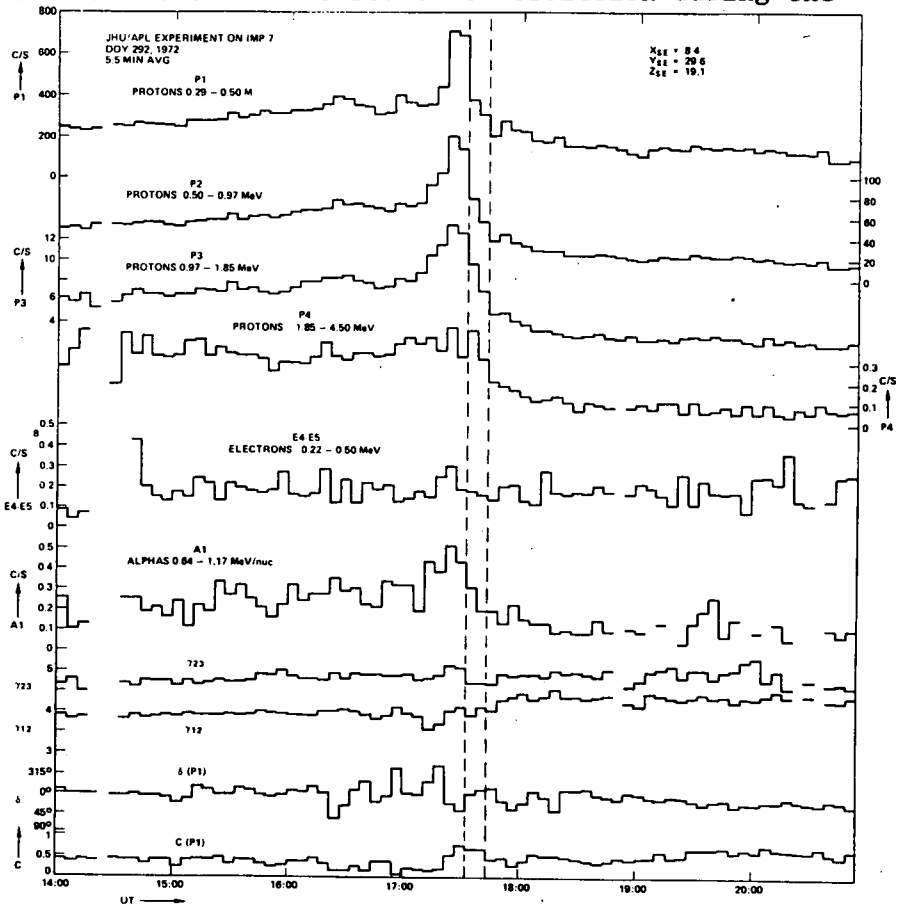

Figure 5. The 5.5 average counting rates of different particle channels, the energy spectrum index. γ and the anisotropy amplitude and direction are shown for the event of September 18, 1972.

V_{SW} = 650 km/sec. Hourly-averaged values before and after the discontinuities show that electrons and high energy ions (Ep > 50 MeV) do not "see" the tangential discontinuity whereas for low energy ions (Ep < 10 MeV/nuc) the penetration of the tangential discontinuity barrier is restricted to a region with a width comparable to the ion gyrodiameters.

Acknowledgements. Same as Paper SP 2.2-2.

References.

Alekseyev, I.I. and A. P. Kropotkin, Geomagn. and Aeronomy, 10, 755, 1970.

Armstrong, T. P., S. M. Krimigis and K. W. Behannon, J. Geophys. Res., 75, 5980, 1970.

Chen, G. and T. P. Armstrong, Proc.14th Int'l. Cosmic Ray Conf., SP 5.3-4, 1975.

Hudson, P. D., Mon. Not. R. Astr. Soc., 131, 23, 1965.

Levy, E. H., F. M. Ipavich and G. Gloeckler, Geophys. Res. Lett., 1, 145, 1974.

Roelof, E. C. and S. M. Krimigis, J. Geophys. Res., 78, 5375, 1973.

Sarris, E. T. and J. A. Van Allen, J. Geophys. Res., 79, 4157, 1974.

Sarris, E. T., S. M. Krimigis and T. P. Armstrong, JHU/APL Preprint, (submitted to J. Geophys. Res.), 1975.

Schatzmann, E., Ann. d' Astro., 26, 234, 1963.

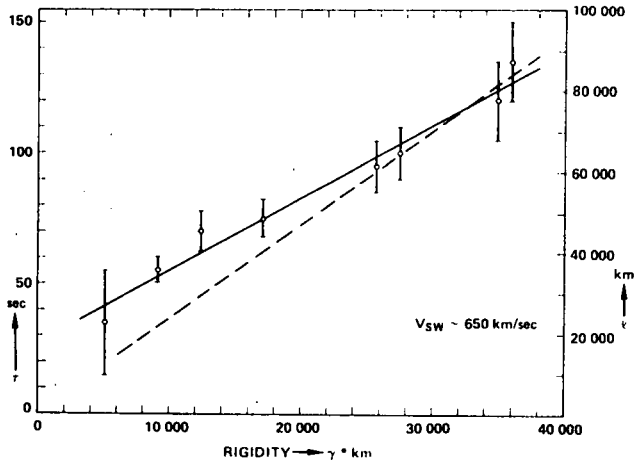

Figure 7. The width of the transition region from the high to the low particle intensity sector across the tangential discontinuity on November 1, 1972 is shown as a function of particle rigidity. The broken line shows the particle gyrodiameters as a function of rigidy.

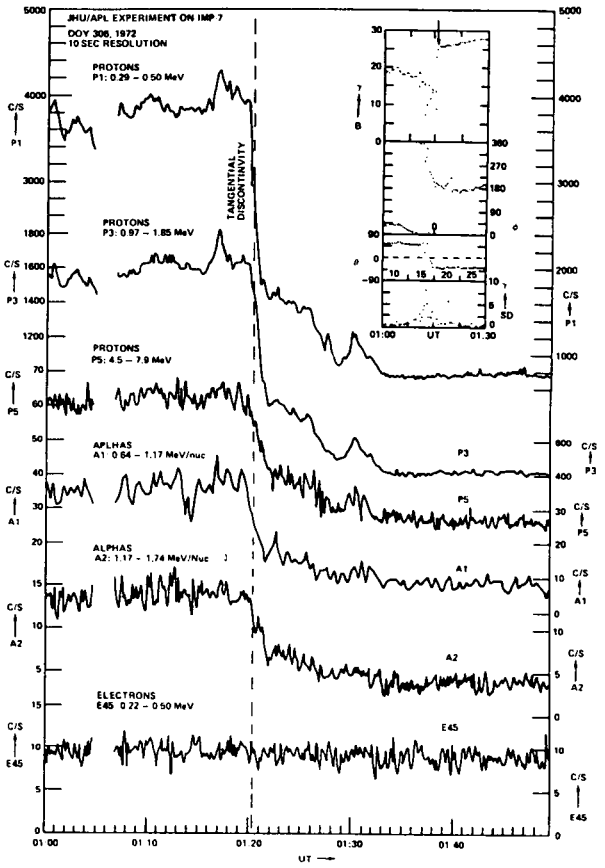

Figure 6. Simultaneous magnetic field vector and particle measurements with a 10 sec time resolution around a tangential magnetic discontinuity.

ACCELERATION OF CHARGED PARTICLES IN OBLIQUE MHD SHOCKS

G. Chen and T. P. Armstrong
Department of Physics, University of Kansas
Lawrence, Kansas 66044, USA

The motion of high energy charged particles in ideal oblique MHD shocks has been studied extensively. The orbits of charged particles can be solved exactly from Lorentz force equation. It is found that a charged particle may cross the shock front many times before it leaves the shock and it is energized during crossings. The most energetic particles are those with initial pitch and phase near the boundary between crossing and reflected particles. The reflected particles cross the shock about twice as many times as the passing particles do. The energy gain increases for larger values of shock strength and speed. If reflection occurs, the energy gain is larger for smaller angles between the field and shock surface. The introduction of scattering does not change the essential features of the process but does cause a few more higher energy particles.

1. Introduction. High energy charged particle enhancements observed near the shocks (shock spikes, ESP events, and LESP events) strongly suggest the acceleration of charged particles by propagating interplanetary shocks. Schatzman (1963) discussed charged particle motion in weak perpendicular shocks. Hudson (1965) and Quenby and Webb (1973) investigated the reflection and transmission of particles incident oblique shocks without giving the details of particle acceleration as we do here. And Sarris (1973) gave some approximate theoretical results for particle motion in oblique shocks which are in good agreement with our numerical results.

2. Model. The initial energy of charged particles to be considered here should be high enough such that the thickness of the collisionless shock is small compared to the gyroradius. Then the shock can be treated as a plane surface across which the tangential component of the magnetic field changes discontinuously. Also, we assume that contributions to the field due to high energy particle motion are negligible, energy losses due to particles' electromagnetic radiation are ignorable, and no collisions occur between particles. Particles undergo continuous motion while they interact with the shock.

Consider a plane shock moving in a direction normal to the plane of the shock. The frame of reference is the rest frame of the shock. Let $\vec{x}$ be the direction of the shock normal (Figure 1). The shock separates the space into two parts-say region I, pre-shock, and region II, postshock. The plasma in region I moves with a velocity $\vec{U}_1$ with respect to the shock and the plasma in region II has a velocity $\vec{U}_2$. $\vec{B}_1$ and $\vec{B}_2$ are the magnetic fields in pre- and post-shock regions respectively. In the matter frame we take $\vec{E}_1 = 0$, hence in the shock frame, the induced electric field $\vec{E}$ is in the $-\vec{y}$ direction and is spatially uniform and time independent. Now, the relation between the upstream and downstream $\vec{U}$, $\vec{B}$, and $\vec{E}$ can be obtained by the hydromagnetic jump conditions which include the Maxwell equations, Ohm's law for perfect conducting fluid, and the conservation equations

for mass, momentum and energy. As a result, if the shock strength is η, and if $\vec{U1} = (U_{1x},0,0)$, and $\vec{B_1} = (B_x,0,B_{1z})$, then $U_2 = (\eta U_{1x},0,U_{2x})$, $\vec{B_2} = (B_x,0,B_{2z})$ and $\vec{E} = (0,E_y,0)$, where

$$B_{2z} = \frac{\rho_1 U_{1x}^2 - \frac{B_x^2}{4\pi}}{\frac{\rho_1 U_{1x}^2}{\eta} - \frac{B_x^2}{4\pi}} B_1, \qquad U_{2z} = \frac{(1 - \frac{1}{\eta}) \frac{B_x B_{1z}}{4\pi}}{\frac{\rho_1 U_{1x}^2}{\eta} - \frac{B_x^2}{4\pi}} U_{1x}, \quad (1)$$

and

$$E_y = \frac{U_{1x} B_{1z}}{c} . \quad (2)$$

Here, ρ is the plasma density and c is the speed of light.

Since the fields are uniform, the equation of motion of a charged particle can be solved exactly from Lorentz equation in both pre- and post-shock regions. The particle spirals around the magnetic field line and its gyrocenter has a velocity $\vec{v}_{11} + \vec{v}_D$, where v_{11} is the particle's velocity parallel to the magnetic field and v_D is the electric field drift velocity in direction of $\vec{E} \times \vec{B}$. If the x-component of $\vec{v}_{11} + \vec{v}_D$ is greater than zero in region I and less than zero in region II we have the necessary and sufficient conditions for a particle to leave the shock front provided that the distance from the shock is large enough (about two gyroradi away from the shock).

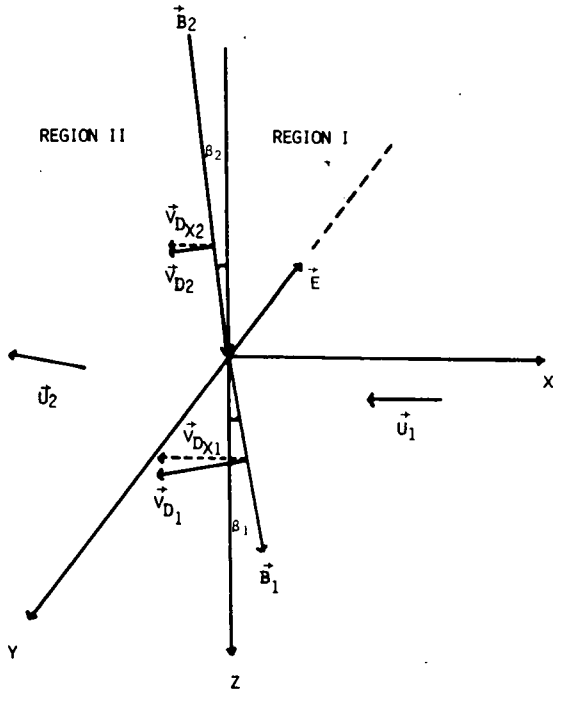

Figure 1. Geometry of shock system.

The x-component of particle orbit is a transcendental function in terms of time t. The times of crossings can be obtained by solving for the first positive root of $x(t) = 0$, although the equation may have multiple roots. To find the desired root, the extrema of x(t) are obtained so that x(t) is monotonic function between the adjacent extrema. The bisection method then is applied to the interval containing the desired root. This method is much more efficient and accurate than orbit-following or other numerical integration methods. The accuracy of the root may be as small as 10^{-8}, but for saving computer time, we used 10^{-4} and verified that our results on energies, pitch angles, and motions of particles are convergent to a few parts in a million.

We injected an ensemble of 1972 monoenergetic, isotropically distributed particles in the shock frame to obtain collective results. By running with ensembles of various sizes, we have verified that the results we discuss here are not significantly affected by sampling statistics. All particles have initial speed v_o.

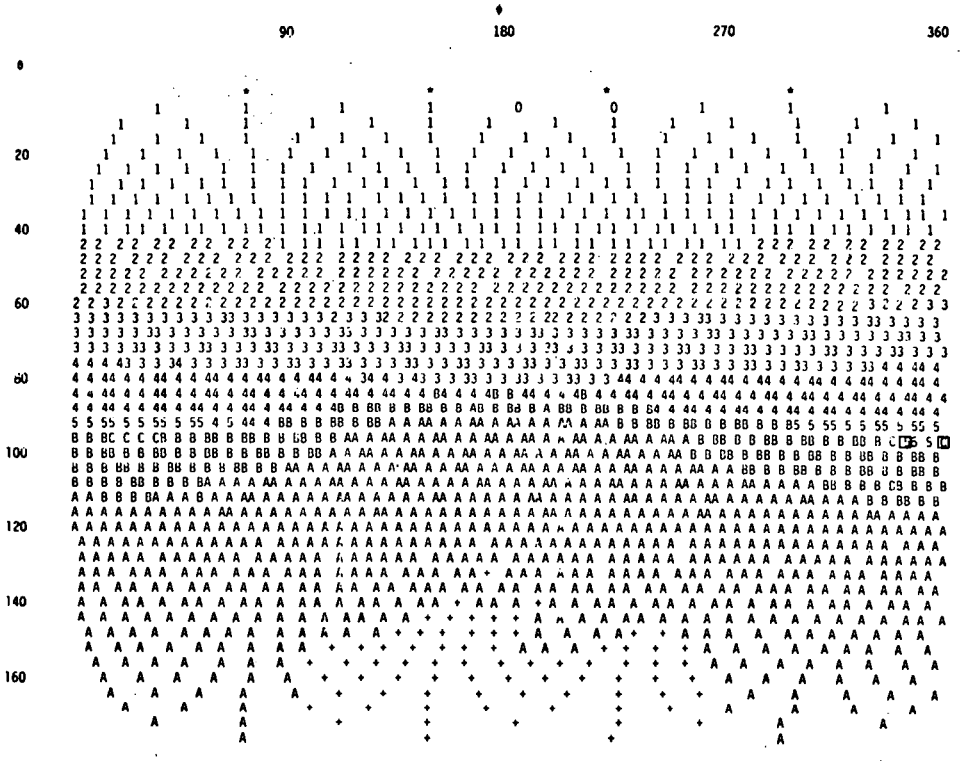

Figure 2. Distribution of final particle energies after interaction with shock versus initial pitch and phase

3. Results. One typical ensemble consisted of 1972 isotropically disturbed protons starting at (50,0,0) with speed $v_o = 10$, in a shock for $\eta = 2$ and $\tan\beta_1 = 0.1$. Afterwards, we have 4 non-interacting particles, 984 reflected and another 984 passing particles. Figure 2 displays the final energy distribution of these particles versus initial pitch and phase (Θ_i, Φ_i). Each character in Figure 2 represents one injected particle located in a rectangular grid in Θ and Φ at a point nearest its starting coordinates, given the discreteness of the printed computer page representation. The density of particles is uniform on the velocity space sphere but is non-uniform in this rectangular representation. The notation "*" represents non-interacting particles. "0","1","2",... and "+","A","B",... represent reflected particles and passing particles respectively with final relative energy E_f/E_i lying between 0 to 1, 1 to 2, 2 to 3,... etc.. It can be seen that for reflected particles the larger the pitch is,

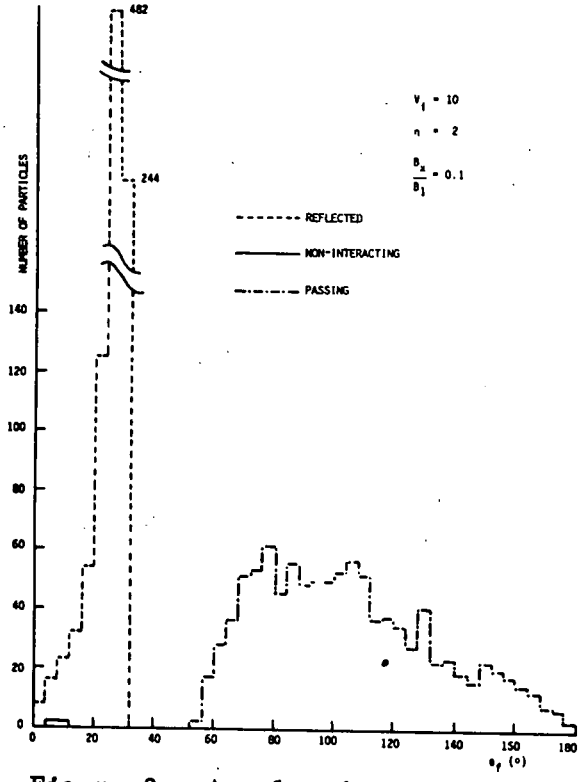

Figure 3. Angular distribution of particles after shock interaction.

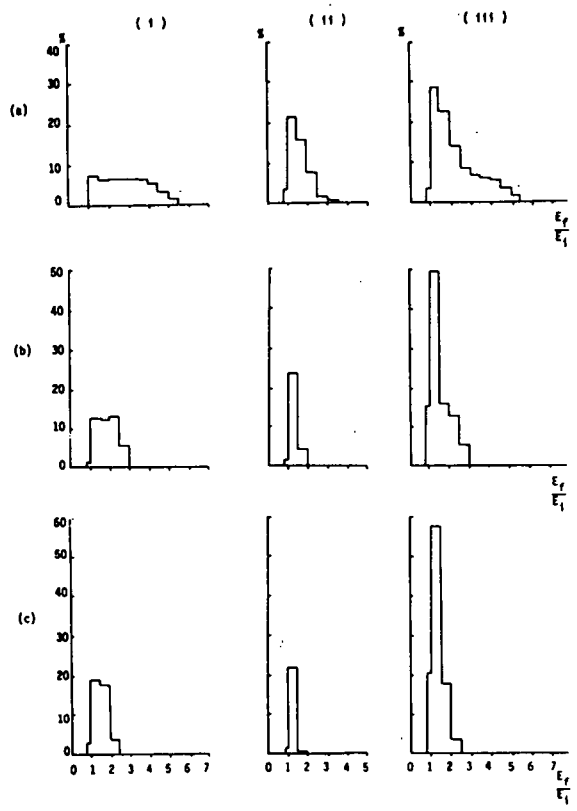

Figure 4. Distribution of final particle energies for various initial speeds.

all injected particles are shown in Figure 4 in columns (i),(ii),and (iii) respectively. Panel (a) is for $v_i = 10$, (b) for $v_i = 20$, and (c) for $v_i = 30$. Notice that the energy distribution curves for reflected particles have a plateau pattern, and those for passing particles have a rapid decay form. From the shift of the endings of the high energy tails to lower values of E_f/E_i for larger v_i, it is concluded that the relative final energies for both reflection and transmission go down if we inject with faster particles.

That the final relative energies vary inversely as v_i can be seen from Figure 5 as well. Figure 5 gives the maximum energy gains in the ensembles with various initial speeds. The curve denoted by "R" is for reflected particles, and the curve denoted by "P" is for passing particles with maximum energy gains.

the larger the number of crossings becomes and the more the energy increases. All particles are reflected up to $\Theta = 80°$. Beyond that some passing particles with larger pitches have fewer crossings and smaller energy gains. The highest energy band is the area near the boundary between reflected and passing particles (occurring at about $\Theta = 90°$ in this case).

The most energetic reflected and transmitted particles were marked out by squares in Figure 2 at $\Theta = 96°$. That reflected particle crossed the shock for 50 times in the time $t = 133.8/\omega_c$ with $E_f/E_i = 3.23$.

The final pitch angle distributions of escaping particles in the pre- and post-shock regions are given in Figure 3. A sharp peak appeared for reflected particles at 25° indicating a strong anisotropy in the pre-shock region.

In order to determine how the shock affected particles with different energies, we ran cases for ensembles with $v_i = 10,20,$ and 30 in units of shock speed in the same shock as before. The final relative energy distributions for reflected, passing, and

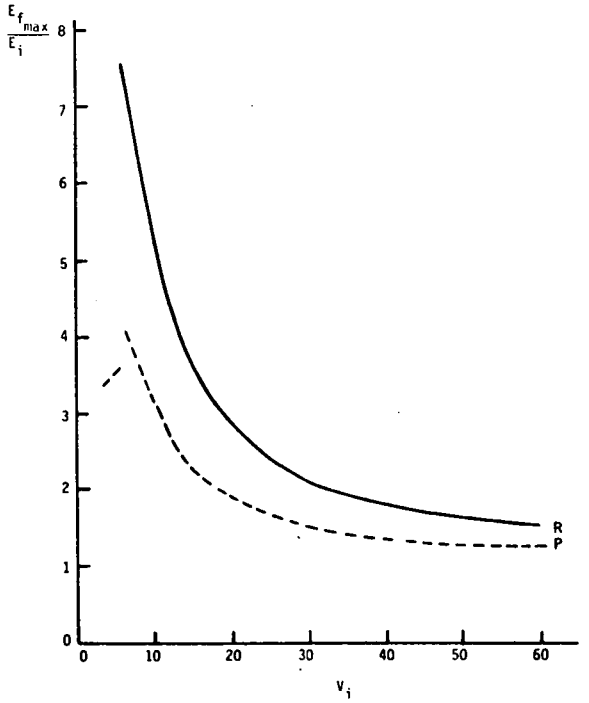

Figure 5. Dependence of maximum final energy on initial particle speed.

The dependence of final relative energy on the inclination of the magnetic field to the shock front is exhibited in Figure 6 for $v_i = 10$ and $\eta = 2$. Here, as $\tan\beta_1$ becomes less than about 0.07, i.e., $\beta_1 = 4°$, only transmission occurs; the shock acts like a perpendicular shock. As β_1 is greater than 4°, the particle is accelerated to the highest energy if it moves in a shock front with smallest β_1 for relative energies of both reflection (R_{AVE}) and transmission (P_{AVE}) are given in the same figure.

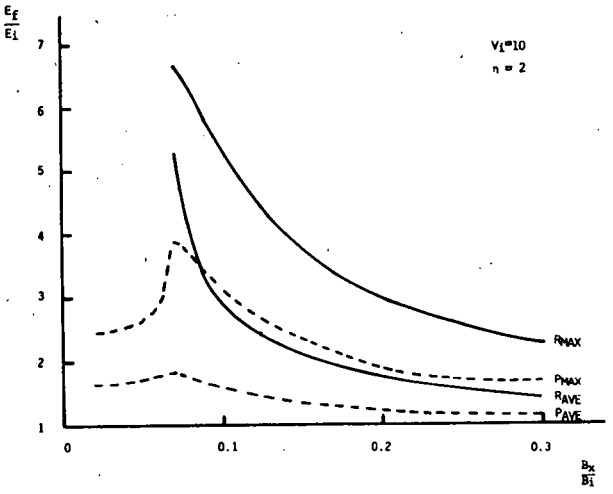

Figure 6. Dependence of final energies on shock obliquity.

Magnetic irregularities introduced into the ideal oblique shock system as scattering centers which elastically change the particle's direction or motion cause a few more high energy particles. The average features of energy distribution curves do not change much with the inclusion of scattering. Anisotropies are reduced by extensively scatterings.

4. Conclusion. From the numerical results in the last paragraphs we conclude that charged particles can gain energy by interacting with shock waves. Actually, they are speeded up only during crossings. As a particle crosses the shock from the preshock to the postshock region, the stronger magnetic field behind the shock shrinks the particle orbit, that means a shift of the gyro-center in the -y direction. The particle gains energy from the electric field. If the particle goes back to region I, the gyro-radius would be larger than the radius before crossing, thereby resulting in another shift of the gyro-center again in the -y direction. So as long as particles stay with the shock, they always gain energy from the electric field.

Particles can gain large amounts of energy only in the case of certain values of velocity (not too large compared to the shock speed) and certain values of the field inclination angles (small, but not too small to cause reflection).

Magnetic irregularities near the shock front may enhance or abate the particle energy either by increasing or decreasing number of crossings or by shifting the gyro-center in the +y or -y direction.

Acknowledgements. We would like to thank the Kansas University Computation Center where all the computing work has been done. Financial support is due in part to the NASA IMP-7 and 8 program and to a University of Kansas General Research Grant.

References:

Chen, G., Numerical Simulation of the Interactions of Charged Particles with Oblique Magnetohydrodynamic Shocks, Thesis, University of Kansas, 1975.

Hudson, P. D., Reflection of Charged Particles by Plasma Shocks, Mon. Not. R. Astr. Soc., 131, 23, 1965.

Quenby, J. J. and S. Webb, Numerical Studies of the Interaction of Energetic Particles with Interplanetary Field Discontinuities, 13th International Cosmic Ray Conference Papers, Vol. 2, 1343, 1973.

Schatzman, E., On the Acceleration of Particles in Shock Fronts, Ann. Astrophys., 26, 234, 1963.

A PRELIMINARY IDEALIZED NETWORK OF NEUTRON MONITORS FOR THE STUDY OF SOLAR MODULATION

R. E. Gold
Applied Physics Laboratory, The Johns Hopkins University
Laurel, Md. 20810, USA

M. A. Shea and D. F. Smart
Air Force Cambridge Research Laboratories
Hanscom AFB, Massachusetts 01731, USA

An idealized network of neutron monitors has been developed with asymptotic cones optimized for the study of solar modulation of cosmic rays. The network is constructed such that the asymptotic cones form horizontal and veritcal chains. This network will permit efficient separation of spatial, temporal and spectral features of a modulation event. The horizontal chains can distinguish between longitudinal and temporal structures. The vertical chains separate latitudinal and spectral structures. The network is based on a world grid of cosmic ray trajectories using the International Geomagnetic Reference Field for epoch 1975.0.

1. Concept of an Idealized Network. Neutron monitors have been measuring the intensity of the nucleonic component of galactic cosmic rays for nearly thirty years. And, with the advent of a large number of superneutron monitors during the 1960's, detailed studies of the spectral and spatial structure of even small amplitude and relatively rapid modulations became possible. These studies require a network of neutron monitors with a wide range of cutoff rigidities and asymptotic cones of acceptance (Rao et al., 1963) in order to separate temporal spatial and rigidity dependences. Unfortunately, economic and practical necessities have dominated in most neutron monitor site selections with the result that most monitors are concentrated in relatively small geographic areas.

An idealized network of neutron monitors is one in which the monitor locations are chosen for their asymptotic cones and cutoffs without regard for geographic locations. A network for studying time variations on the scale of a few hours or less, would have a sufficient number of stations located so that a "snapshot" of the event by the monitors in the network could define its spectral and spatial characteristics.

Idealized networks could be designed for the study of individual cosmic ray phenomena and networks for the study of ground-level events and solar modulations would be highly desirable. The ground-level event network would have cutoff regidities that covered the critical range up to 2 GV in order to obtain good spectral resolution and it would have asymptotic cones that would cover a wide range of pitch angle so that anisotropy time histories and therefore solar particle propagation models could be studied.

The design of a ground-level event network is severely limited, however, by the effects of external magnetic fields on the trajectories of cosmic rays with rigidities less than $\sim$ 2 GV. These external field effects would result in diurnal

variations in both the asymptotic cones and cutoffs of stations in the network. Since present geomagnetic field models are not sufficiently developed to produce an accurate description of these effects, an idealized network optimized for the study of ground level events can not be designed at this time.

2. Use of an Idealized Network. An idealized network that would enable spatial, spectral and temporal separation of solar modulation effects on cosmic rays may be constructed from two series of chains of cosmic ray monitors. First, "horizontal" chains with asymptotic cones spaced evenly around the world at a constant latitude could easily separate the temporal development of a modulation transient from its longitudinal structure since the full longitudinal profile would be measured at all times.

The second series of neutron monitor chains would have their asymptotic cones arranged "vertically" at the same asymptotic longitude. The monitors in these chains may be divided into the polar and the equatorial branches using the stations with magnetic cutoff rigidities near the atmospheric cutoff ($\sim$ 1 GV) as the dividing line. The stations in the polar branch, therefore, all have the same effective cutoff rigidity (atmospheric) and view the same longitude but their asymptotic cones are centered at different latitudes ranging from approximately equatorial to true polar. The polar branches may thus be used to deduce the latitude dependence of the modulation.

The stations in the equatorial branch have cutoff rigidities that range from about 1 GV up to the equatorial cutoff, which may vary from $\sim$ 13 GV to $\sim$ 17.5 GV depending on their longitude. Yet their asymptotic cones are all centered within $\sim$ 20° of the equator at the same longitude. Since they are viewing the same region of the celestial sphere this range of cutoff rigidities may be used with variational coefficients (Rao et al., 1963; McCracken et al., 1965; Shea et al., 1968; Gold et al., 1974) to deduce the rigidity spectrum of the modulation.

3. Network Design Considerations. The starting point for the design of this idealized network was a five by fifteen degree world grid of asymptotic directions and cutoff rigidities calculated using the International Geomagnetic Reference Field for Epoch 1975.0 (Shea and Smart, 1975). Station locations for the horizontal and vertical chains were derived by interpolation from the world grid.

The concept of horizontal and vertical chains of compact asymptotic acceptance cones is itself highly idealized. Asymptotic cones in the real geomagnetic field are rarely compact and often quite distorted. Yet, there is a general trend for asymptotic cones to gradually shift from the small latitude spread and large longitude spread of equatorial stations to the large latitude spread and narrow longitude spread of high latitude stations. Because of the variety in asymptotic cone sizes a network has to be carefully designed to give the best compromise of cone shapes over the desired rigidity range. The relationships between cutoff rigidity and asymptotic directions are also complex in the geomagnetic field. Thus idealized network design is, in the last anslysis, reduced to a tedius set of interpolations and iterations to arrive at the best station locations with the desired asymptotic coordinates and cutoff rigidities.

The solar modulation idealized network was designed with four vertical chains since most of the phenomena of research interest have spatial or temporal scales equivalent to $\geq$ 6 hours observing time. More vertical chains could be

added but the longitude spread of the asymptotic cones of equatorial stations would partially defeat this attempt at greater resolution. Two horizontal chains, one each in the Northern and Southern Hemispheres, permit temporal and longitudinal separation to a scale equivalent to 3 hours.

The four vertical chains were chosen with asymptotic cones separated at 90° longitude intervals and placed such that stations on their northern ends would have a good chance of falling on land masses. The resulting asymptotic longitudes are 60, 150, 240 and 330 degrees. However, since the station locations are chosen for their asymptotic direction and cutoff rigidity, a large fraction must fall in the oceans.

The defining rigidity band chosen for the solar modulation network was 5 to 20 GV since less than 10% of the response of a high latitude neutron monitor to a rigidity independent modulation mechanism occurs below 5 GV. The region below 5 GV is also generally spread over a wide range of asymptotic longitude which would further reduce the response to a spatially localized modulation. More than 50% of the response to a rigidity independent modulation lies below 20 GV and for modulation mechanisms proportional to the inverse of rigidity, $\geq$ 95% of the response lies below 20 GV. The 5 to 20 GV range of this design is certainly not sufficient for all solar modulations. For example it would be inadequate for the study of modulations with positive rigidity exponents since the majority of the response to these modulations may be above 20 GV.

The vertical chains in the idealized network each have 19 stations of 10 types characterized by asymptotic latitude and cutoff rigidity as shown in Table I. For this preliminary network the longitude alignment of the asymptotic cones were optimized near the effective center of the 5 to 20 GV rigidity band. In most cases the resulting location is very close to that which would result from optimization over the entire rigidity band. These defining rigidities are also listed in Table I.

TABLE I

Station Type	Defining Characteristics	Defining Rigidity
1	True polar stations at latitude $\leq$ 80° with asymptotic latitudes $\geq$ 65° at 10 GV	10
2	Near polar with asymptotic latitude $\simeq$ 60°	10
3	Asymptotic latitude $\simeq$ 45°, Cutoff rigidity $\leq$ 1 GV	10
4	Asymptotic latitude $\simeq$ 20°, Cutoff rigidity $\leq$ 1 GV	10
5	Cutoff rigidity $\simeq$ 1 GV	10
6	Cutoff rigidity $\simeq$ 2 GV	13
7	Cutoff rigidity $\simeq$ 5 GV	13
8	Cutoff rigidity $\simeq$ 10 GV	15
9	Cutoff rigidity $\simeq$ 12 GV	16
10	Equatorial station with maximum cutoff rigidity	20

The two horizontal chains are composed of the eight stations with 1 GV cutoff. They utilize the 1 GV stations of the vertical chains plus eight additional 1 GV cutoff stations with asymptotic cones centered between those of the vertical chains.

A world map showing the locations of all the stations in the idealized network is presented in Figure 1. The horizontal chains are designated by stars and the vertical chains with asymptotic longitudes at 60, 150, 240 and 330 degrees are designated by dots, triangles, squares and diamonds respectively. All of the chains have fewer than 19 stations since some of the defining characteristics are incompatible with the real geomagnetic field. For example, there is no location that yields an asymptotic cone centered at 240° longitude and 20° latitude that has a cutoff less than 1 GV.

The idealized network presented here is a preliminary design for the study of solar modulation. It is in no sense a final recommendation of neutron monitor placement but primarily a presentation of the idealized network concept.

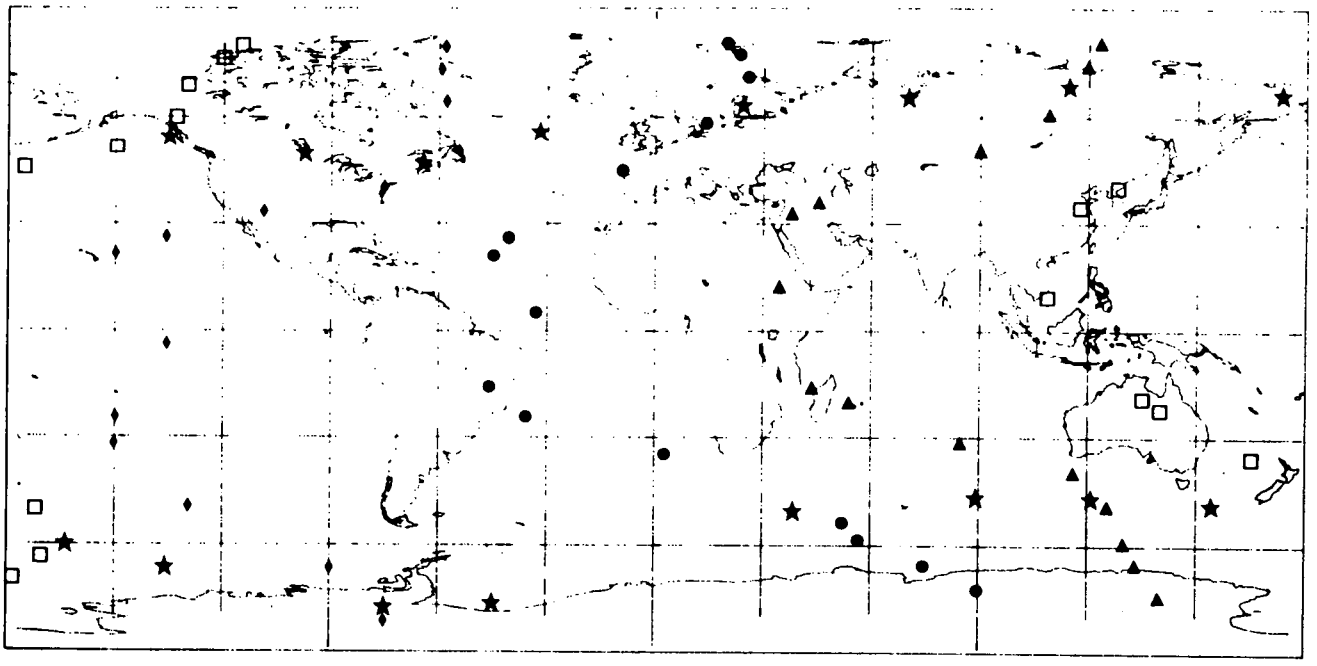

Figure 1. Neutron monitor locations in an idealized network for the study of solar modulation.

4. Acknowledgements. This work has been supported in part by Air Force Cambridge Research Laboratories under Contract F19628-73-C-0070.

5. References.

Gold, R. E., D. S. Peacock, M. A. Shea and D. F. Smart, An extended set of cosmic-ray variational coefficients, Air Force Cambridge Research Laboratories, AFCRL-TR-74-0063, Special Reports, No. 173, 1974.

McCracken, K. G., U. R. Rao, B. C. Fowler, M. A. Shea and D. F. Smart, Cosmic Ray Tables, IQSY Instruction Manual No. 10, IQSY Committee, London, 1965.

Rao, U. R., K. G. McCracken and D. Venkatesan, Asymptotic cones of acceptance and their use in the study of the daily variation of cosmic radiation, J. Geophys. Res., 68, 345, 1963.

Shea, M. A., D. F. Smart, K. G. McCracken and U. R. Rao, Supplement to IQSY Instruction Manual No. 10, Cosmic Ray Tables, Air Force Cambridge Research Laboratories, AFCRL-68-0030, 1968.

Shea, M. A. and D. F. Smart, Tables of asymptotic directions and vertical cutoff rigidities for a five degree by fifteen degree world grid as calculated using the International Geomagnetic Reference Field for Epoch 1975.0, Air Force Cambridge Research Laboratory Environmental Research Paper No. 510, AFCRL-TR-75-0247, 1975.